

# **Stratigraphy of the Upper Miocene Volcanic Rocks of the Island of Kos, Greece: Geodynamic Implications**

By

Nikolaos Tsoukalas

A Thesis Submitted in Partial Fulfillment of the  
Requirements for the Degree of Master of Science

In

The Faculty of Graduate Studies

Department of Geology, Saint Mary's University

Halifax, Nova Scotia, Canada



Library and  
Archives Canada

Bibliothèque et  
Archives Canada

Published Heritage  
Branch

Direction du  
Patrimoine de l'édition

395 Wellington Street  
Ottawa ON K1A 0N4  
Canada

395, rue Wellington  
Ottawa ON K1A 0N4  
Canada

*Your file    Votre référence*  
*ISBN: 978-0-494-44668-3*  
*Our file    Notre référence*  
*ISBN: 978-0-494-44668-3*

**NOTICE:**

The author has granted a non-exclusive license allowing Library and Archives Canada to reproduce, publish, archive, preserve, conserve, communicate to the public by telecommunication or on the Internet, loan, distribute and sell theses worldwide, for commercial or non-commercial purposes, in microform, paper, electronic and/or any other formats.

The author retains copyright ownership and moral rights in this thesis. Neither the thesis nor substantial extracts from it may be printed or otherwise reproduced without the author's permission.

**AVIS:**

L'auteur a accordé une licence non exclusive permettant à la Bibliothèque et Archives Canada de reproduire, publier, archiver, sauvegarder, conserver, transmettre au public par télécommunication ou par l'Internet, prêter, distribuer et vendre des thèses partout dans le monde, à des fins commerciales ou autres, sur support microforme, papier, électronique et/ou autres formats.

L'auteur conserve la propriété du droit d'auteur et des droits moraux qui protègent cette thèse. Ni la thèse ni des extraits substantiels de celle-ci ne doivent être imprimés ou autrement reproduits sans son autorisation.

---

In compliance with the Canadian Privacy Act some supporting forms may have been removed from this thesis.

Conformément à la loi canadienne sur la protection de la vie privée, quelques formulaires secondaires ont été enlevés de cette thèse.

While these forms may be included in the document page count, their removal does not represent any loss of content from the thesis.

Bien que ces formulaires aient inclus dans la pagination, il n'y aura aucun contenu manquant.

  
**Canada**

# Certification

Stratigraphy of the Upper Miocene Volcanic Rocks of the Island of Kos, Greece:

Geodynamic Implications

by

Nikolaos Tsoukalas

A Thesis Submitted to Saint Mary's University, Halifax, Nova Scotia  
in Partial Fulfillment of the Requirements for the  
Degree of Master of Science in Applied Science.

May 2<sup>nd</sup>, 2008, Halifax, Nova Scotia

© Nikolaos Tsoukalas, 2008

## Examining Committee:

- Approved: Dr. Marcos Zentilli, External Examiner  
Department of Earth Sciences, Dalhousie University
- Approved: Dr. Georgia Pe-Piper, Senior Supervisor  
Department of Geology
- Approved: Dr. David Piper, Supervisory Committee Member  
Geological Survey of Canada - Atlantic
- Approved: Dr. Victor Owen, Supervisory Committee Member  
Department of Geology
- Approved: Dr. Cristian Suteanu, Supervisory Committee Member  
Department of Geography
- Approved: Dr. Andrew MacRae, Program Representative
- Approved: Dr. Kevin Vessey, Dean of Graduate Studies

## **ABSTRACT**

### **Stratigraphy of the Upper Miocene Volcanic Rocks of the Island of Kos, Greece: Geodynamic Implications**

**by Nikolaos Tsoukalas**

Kos is one of several localities (Samos, Patmos, Bodrum) in the southeast Aegean Sea with Upper Miocene volcanic rocks. The stratigraphic succession of flows, ignimbrites and interbedded sediments was studied in the field in order to better understand the age, distribution, source and tectonic setting of Upper Miocene volcanic rocks of Kos. Previous radiometric dating shows that the age of the volcanism is about 10 Ma.

In northern Kos, thin andesite flows and dacite domes are overlain by thin pyroclastic rocks near Profitis Ilias and at Tripa; north of Agios Fokas, a thin pyroclastic succession includes lahars. In southern Kos, pyroclastic successions totalling 80 m in thickness are interbedded with Miocene clastic sediments and marls at Agios Fokas and Agios Stefanos.

The results on the basis of petrography and geochemistry suggest correlations between Agios Stefanos and Agios Fokas pyroclastic rocks and affinity to the minor andesite-dacite volcanism at Profitis Ilias and Tripa. Paleocurrent indicators in ignimbrites suggest that the Agios Stefanos section was derived from a source to the southeast and Agios Fokas from a source to the south, most probably from a Miocene precursor of the modern volcanic centre of Yali-Nisyros.

May, 2008

## ACKNOWLEDGEMENTS

*For the fulfillment of my graduate degree requirements, I was assigned to write the present graduate thesis. This project would not have been completed without the contribution and support of particular persons and foundations.*

*From this position I feel the need to express my most sincere thanks to my academic teachers, Georgia Pe-Piper and David J.W. Piper, for giving me the opportunity to study abroad. Their advice, encouragement and continual interest at all stages of this work were inexhaustible. Besides this, their assistance has been crucial for the gradual development of my scientific thought and geological education in multiple stages of this research, during the field and laboratory work as well as the writing part. I will also never forget their support during the first few months through the rough times – even when I thought that there was no light at the end of the tunnel, they never stopped believing in me and encouraging me. Once again, many, many thanks for everything!*

*Thank you to the committee members Drs. Victor Owen and Cristian Suteanu, as well as the external examiner Dr. Marcos Zentilli, for their time and patience during the thesis corrections and reviews and of course for the constructive comments.*

*Thanks to NSERC for the Discovery Grant to Georgia Pe-Piper, and consequently the financial support for the field and laboratory work, I was also supported by this Discovery Grant, in addition to receiving both a fellowship and graduate award from the Faculty of Graduate Studies and Research, Saint Mary's University.*

*I also acknowledge the Alexander S. Onassis Public Benefit Foundation in Greece for the scholarship provided to me in a critical point of my master's degree.*

*I would like to thank Greg Baker and Randy Corney for the lab assistance they provided any time I wanted, as well as the geology department faculty, staff and fellow students for their support all these years, and the nice time we had together. I shall be grateful to my teachers in TESL Centre who helped me to learn English. Without you, I would have never accomplished what I have.*

*I am profoundly grateful to my parents Spyridon and Anastasia who supported me not only financially, but mostly emotionally. I owe special thanks to my brother Ioannis for his help in many ways and mostly to the field assistance he provided to me during the June, 2006 field work. Yanni, you are now a lawyer specialised in volcanic rocks! Many, many thanks go also to relatives and friends in Canada, USA and Greece for their support and encouragement all these years.*

## TABLE OF CONTENTS

<b>Title</b> .....	i
<b>Certification</b> .....	ii
<b>Abstract</b> .....	iii
<b>Acknowledgments</b> .....	iv
<b>Table of Contents</b> .....	vi
<b>List of Tables</b> .....	ix
<b>List of Figures</b> .....	x
<b><u>1. Introduction</u></b> .....	<b>1</b>
1.2 General Geology of Greece and adjacent areas .....	1
1.3 Geology of Kos .....	3
1.3.1 Individual lithological units .....	4
• Pre-Alpine basement .....	4
• Alpine Rocks .....	4
• Neogene Sedimentary Rocks .....	5
• Neogene Plutonic Rocks .....	6
• Neogene Volcanic Rocks .....	8
1.4 Objectives .....	10
<b><u>2. Upper Miocene volcanology and pyroclastic stratigraphy</u></b> .....	<b>12</b>
2.1 Introduction .....	12
2.2 Methods .....	12
2.2.1 Field Equipment .....	13
2.2.2 Field work .....	14
2.3 Volcanic stratigraphy of Tripa .....	16
2.4 Volcanic stratigraphy of Prof. Ilias .....	23
2.5 Volcanic stratigraphy of Ag. Stefanos .....	30
2.5.1 “North of Club Mediterranee” .....	30
Lower Sedimentary Unit .....	30
Lower Pyroclastic Unit .....	36
Middle Sedimentary Unit .....	37
2.5.2 “North of Kastri – Cape Tigani” .....	38
Middle Pyroclastic Unit .....	38
Upper Sedimentary Unit .....	41
Upper Pyroclastic Unit .....	42
2.6 Volcanic stratigraphy of Ag. Fokas .....	50
2.6.1 “Ag. Fokas” .....	50
Lower Sedimentary Unit .....	50
Pyroclastic Unit .....	55
Upper Sedimentary Unit .....	63

2.6.2 “North of Ag. Fokas” .....	64
<b>3. Petrography</b> .....	<b>67</b>
3.1 Introduction .....	67
3.2 Methods .....	68
3.2.1 Macroscopic division of lithic clasts .....	68
3.2.2 Thin section preparation .....	68
3.3 Petrographical description of lithic clasts .....	69
3.3.1 Type A1 .....	69
3.3.2 Type A2 .....	70
3.3.3 Type A3 .....	71
3.3.4 Type A4 .....	72
3.3.5 Type B1 .....	73
3.3.6 Type B2 .....	73
3.3.7 Type C .....	74
3.3.8 Type D .....	76
3.3.9 Type E .....	77
3.3.10 Type F .....	78
3.3.11 Type G .....	80
3.4 Petrographical description of lava flows .....	80
3.4.1 Tripa volcanic rocks .....	80
3.4.2 Prof. Ilias volcanic rocks .....	81
3.4.3 Comparisons between lavas and lithic clasts .....	84
3.5 Comparative results from petrographical study .....	85
<b>4. Geochemistry</b> .....	<b>93</b>
4.1 Introduction .....	93
4.2 Analytical sample preparation .....	94
4.3 Rock Nomenclature .....	94
4.4 Major Element variation .....	101
4.5 Trace Element variation .....	101
4.6 Rare Earth Element Patterns .....	104
4.7 Multi-Element Patterns .....	104
4.8 Relation between clast petrography and geochemistry .....	107
4.9 Comparison with other volcanic rocks of the Aegean Sea .....	109
4.10 Geochemical constrains on the sources of the lithic clasts .....	113
<b>5. Directional analysis of pyroclastic rocks</b> .....	<b>114</b>
5.1 Introduction .....	114
5.2 Paleoflow indicators in Pyroclastic rocks .....	114
5.2.1 Orientation of elongate clasts on bedding planes .....	115
5.2.2 Imbrication of elongate clasts .....	115
5.2.3 Elutriation sheets and pipes .....	115

5.2.4 Erosional grooves .....	116
5.3. Paleoflow Indicators in Sedimentary Rocks .....	116
5.4 Ag. Stefanos .....	117
5.5 Ag. Fokas .....	123
5.6 Synthesis .....	125
<b>6. Discussion – Conclusions</b> .....	<b>127</b>
6.1 Stratigraphic position of the Upper Miocene pyroclastic rocks .....	127
6.2 Volcanology of the Upper Miocene volcanic rocks .....	129
6.3 The volcanic source of the thick pyroclastic successions .....	133
6.4 Conclusions .....	137
<b>Bibliography</b> .....	<b>141</b>

## LIST OF TABLES

<b>Table 3.1:</b> Types of lithic clasts in Upper Miocene pyroclastic and volcaniclastic rocks .....	79
<b>Table 3.2:</b> Distribution of clast types by unit .....	91
<b>Table 3.3:</b> Summary of abundance and sizes of lithic clasts .....	92
<b>Table 4.1:</b> Whole rock geochemical analyses of representative samples from the studied rocks .....	95

## LIST OF FIGURES

<b>Fig. 1.1:</b> Geotectonic map of Eastern Mediterranean and Aegean Sea. ....	2
<b>Fig. 1.2:</b> Simplified geological map of Kos. ....	4
<b>Fig. 1.3:</b> Spatial variation of the composition of the plutonic rocks in the Aegean Sea. ....	8
<b>Fig. 2.1:</b> Distribution of localities during the 2003, 2004, 2005, 2006 and 2007 field work on Kos. ....	15
<b>Fig. 2.2:</b> Geological map of the Tripa area. ....	17
<b>Fig. 2.3:</b> General view of the southern part of Tripa area looking south. The letters correspond to stratigraphic columns. ....	18
<b>Fig. 2.4:</b> Vertical slickenlines on NW dipping planar fault at locality 109. ....	18
<b>Fig. 2.5:</b> Dome of lava in Tripa overlain by marls. ....	19
<b>Fig. 2.6:</b> Schematic stratigraphic section of the Tripa area. ....	20
<b>Fig. 2.7:</b> Tectonic contact between the basement limestones and the stratigraphically overlying marls. ....	21
<b>Fig. 2.8:</b> Correlation of stratigraphic columns of Tripa area. ....	22
<b>Fig. 2.9:</b> Detailed map of Prof. Ilias area. ....	23
<b>Fig. 2.10:</b> Contact between lava and associated lava breccia in locality 276. ....	24
<b>Fig. 2.11:</b> Schematic section of a lava dome in Prof. Ilias (locality 178). ....	25
<b>Fig. 2.12:</b> Typical outcrop of coarse grained, polymictic lithic tuff. ....	26
<b>Fig. 2.13:</b> View of polymictic (cobble – pebble) conglomerate at Prof. Ilias. ....	27
<b>Fig. 2.14:</b> Correlation of stratigraphic columns of Prof. Ilias area. ....	28
<b>Fig. 2.15:</b> View of the continuous stratigraphic section in locality 276. ....	29
<b>Fig. 2.16:</b> View of the coarse conglomerate in locality 215. ....	32
<b>Fig. 2.17:</b> Geological map of “North of Club Mediterranee” area at Ag. Stefanos. ....	33
<b>Fig. 2.18:</b> Correlation of stratigraphic columns of “North of Club Mediterranee” area. ....	34

<b>Fig. 2.19:</b> Very coarse volcanoclastic conglomerate of unit A6 in locality 212.	35
<b>Fig. 2.20:</b> The white ignimbrite with the abundant limestone clasts. ....	36
<b>Fig. 2.21:</b> Geological map of the “North of Kastri” and “Cape Tigani” areas in Ag. Stefanos. ....	39
<b>Fig. 2.22:</b> Correlation of stratigraphic columns of “North of Kastri” area. ....	40
<b>Fig. 2.23:</b> General view of the upper parts of the Upper Sedimentary Unit with shales, marls, sandstones and conglomerates, overlain conformably by the basal beds of the Upper Pyroclastic Unit. ....	42
<b>Fig. 2.24:</b> Correlation of stratigraphic columns of the Upper Pyroclastic Unit of Kamila beach – Cape Tigani area. ....	43
<b>Fig. 2.25:</b> Panoramic view of the upper beds of the Upper Pyroclastic Succession.	47
<b>Fig. 2.26:</b> View of north end of the clast supported conglomerate (F25b) embedded in pyroclastic deposits at locality 137. ....	48
<b>Fig. 2.27:</b> a) Typical lithology of vitric-lithic tuff of Unit F25a at locality 206. b) Outcrop of vitric- lithic tuff of bed F28 (locality 149). ....	49
<b>Fig. 2.28:</b> Geological map of the “Ag. Fokas” and “North of Ag. Fokas” sub-areas. ....	51
<b>Fig. 2.29:</b> Correlation of stratigraphic columns of Ag. Fokas area. ....	52
<b>Fig. 2.30:</b> The basal part of the Lower Sedimentary Unit, viewed at locality 278/281. a) Detailed photograph of the sandstone and granule intercalations. b) General view of the stratigraphic and tectonic contacts of the sediments. c) Detailed photograph of the pebble conglomerate, partially covered by paleosoil. ....	54

<b>Fig. 2.31:</b> General view of the contact between the Lower Sedimentary Unit and the bottom beds of the pyroclastic succession at locality 130. ....	56
<b>Fig. 2.32:</b> a) Lenticular to spherical concretions into flow tuff on bed B12. b) Contact between the subjacent vitric tuff (B17) which is overlain by well stratified air-fall beds (B18). ....	57
<b>Fig. 2.33:</b> a) General view of the distinctive marl (E1, E2). b) Detailed photograph from the contact of the fine-grained tuff and the superjacent massive marl. ....	60
<b>Fig. 2.34:</b> The upper part of the clast supported conglomerate (K2) with abundant 5 cm lithic clasts. ....	63
<b>Fig. 2.35:</b> Correlation of stratigraphic columns of North of Ag. Fokas sub-area.	65
<b>Fig. 2.36:</b> Muddy lahar in North of Ag. Fokas sub-area, containing sparse lithic clasts within the grey matrix. ....	66
<b>Fig. 3.1:</b> Microphotographs which show a typical andesitic rock of A2 clast lithology. ....	71
<b>Fig. 3.2:</b> Microphotographs of a typical trachyandesite of type A3. ....	72
<b>Fig. 3.3:</b> Microphotographs of a vesicular trachyandesite of type A4. ....	73
<b>Fig. 3.4:</b> Microphotographs of relatively altered sample of clast type B2. ....	74
<b>Fig. 3.5:</b> Microphotographs of clast type C. ....	75
<b>Fig. 3.6:</b> Microphotographs of clast type D. ....	77
<b>Fig. 3.7:</b> Microphotographs of clast type E. ....	78
<b>Fig. 3.8:</b> Microphotographs of trachyandesitic flows from Tripa. ....	81
<b>Fig. 3.9:</b> Microphotographs of the basaltic trachyandesitic group from Prof. Ilias.	82
<b>Fig. 3.10:</b> Microphotographs of the rhyolitic group from Prof. Ilias. ....	83
<b>Fig. 3.11:</b> Microphotographs of the trachyte from Prof. Ilias. ....	84
<b>Fig. 3.12:</b> Synthetic stratigraphic column of Ag. Stefanos and distribution of samples of lithic clasts and their types. ....	86
<b>Fig. 3.13:</b> Synthetic stratigraphic column of Ag. Fokas and distribution of samples of lithic clasts and their types. ....	87
<b>Fig. 3.14:</b> Synthetic stratigraphic column of Ag. Fokas North and distribution of samples of lithic clasts and their types. ....	88

<b>Fig. 3.15:</b> Summary stratigraphic columns from Ag. Stefanos, Ag. Fokas and Ag. Fokas North and pie diagrams of the types of lithic clasts. ....	90
<b>Fig. 4.1:</b> Geochemical nomenclature of representative volcanic rocks and lithic clasts from the Miocene of Kos, by IUGS system for volcanic rocks. ....	100
<b>Fig. 4.2:</b> Harker diagrams showing variations in major elements versus SiO <sub>2</sub> for the Kos Upper Miocene volcanic rocks and the clasts from the pyroclastic rocks. ....	102
<b>Fig. 4.3:</b> Harker diagrams showing variations in selected trace elements versus SiO <sub>2</sub> for the Kos Upper Miocene volcanic rocks and the clasts from the pyroclastic rocks. ....	103
<b>Fig. 4.4:</b> Variations in REE for the Kos Upper Miocene volcanic rocks and the clasts from the pyroclastic rocks. ....	105
<b>Fig. 4.5:</b> Variations in selected trace elements, normalized to the primitive Mantle for the Kos Upper Miocene volcanic rocks and the clasts from the pyroclastic rocks. ....	106
<b>Fig. 4.6:</b> Geochemical nomenclature of the petrographical types of lithic clasts from the Miocene of Kos, by IUGS system for volcanic rocks. ....	107
<b>Fig. 4.7:</b> Variations in REE according to petrographical type classification. ....	108
<b>Fig. 4.8:</b> IUGS plots for volcanic rocks showing fields for principal rocks of Samos, Patmos, Limnos, Kefalos Peninsula and Nisyros, compared to this of the Miocene of Kos. ....	110
<b>Fig. 4.9:</b> REE plots for principal rocks of Limnos, Samos, Nisyros and Patmos. ....	111
<b>Fig. 5.1:</b> a) Typical dune x-bedding in sandstone at locality 156. b) Ripple x-lamination in medium-grained sandstone (locality 262). ....	118
<b>Fig. 5.2:</b> Paleocurrent data from Ag. Stefanos. ....	119
<b>Fig. 5.3:</b> Elongated clast orientations. The yellow line corresponds to the long axis of the elongated clast. On the upper left side, the rose diagram shows the preferred orientation of the measured clasts. ....	121
<b>Fig. 5.4:</b> Vitric-lithic ignimbrite from the Upper Pyroclastic Unit. Imbrication dips to SSE and flow direction from the right to the left. ....	121
<b>Fig. 5.5:</b> Erosional grooves at the bottom of a clast supported volcanoclastic	

conglomerate. ....	122
<b>Fig. 5.6:</b> a) Curved elutriation sheet shows flow direction towards NW. b) Concentration of lithic clasts in an elutriation sheet. ....	122
<b>Fig. 5.7:</b> Slump of marls and airfall tuff beds. Brittle deformation with synchronous reverse faults is also present (red lines and arrows). ....	123
<b>Fig. 5.8:</b> Paleocurrent data from Ag. Fokas. ....	124
<b>Fig. 5.9:</b> Suggested flow direction for the pyroclastic deposits of Ag. Stefanos and Ag. Fokas according to interpretations regarding the orientation of lithic clasts, their imbrication and the elutriation sheets. ....	126
<b>Fig. 6.1:</b> Schematic sections showing the three stages of the two proposed depositional environments for the channelised volcanoclastic conglomerates, before the arrival of the Lower Pyroclastic Succession. a) The case of sub-lacustrine deposition. b) The case of subaerial deposition. ....	131
<b>Fig. 6.2:</b> Map that shows the possible source volcano for the Miocene pyroclastic rocks of Ag. Stefanos and Ag. Fokas. The cross sections along A – B and C – D are shown in Fig. 6.3. ....	136
<b>Fig. 6.3:</b> A-B and C-D cross sections (Fig. 6.2) and three-dimensional cartoon (not to scale) of the idealized processes during the deposition of the Upper Pyroclastic Unit at Ag. Stefanos and the lavas at Prof. Ilias. ....	140

# CHAPTER 1

## *Introduction*

### **1.1. Introduction**

The island of Kos is one of the numerous islands of the Dodecanese complex (Greece). It lies at the eastern end of the geodynamically active Hellenic subduction zone, in the SE part of Aegean Archipelago (Fig. 1.1). The island covers an area of about 290 km<sup>2</sup>, and has bold relief. The highest peak (Dikeos Mt.) at 841m a.s.l., is in central-eastern Kos, whereas the northern regions are characterized by plains (Hellenic Military Geographical Service). Kos has a distinguished and significant history and many ancient monuments, and is well known as the island of Hippocrates, the father of medicine.

### **1.2 General Geology of Greece and adjacent areas**

Greece and its orogenic belt, known as the “Hellenides”, are part of the Alpine – Himalayan orogenic system. The Hellenides were constructed by the convergence and collision of microcontinental fragments between the southern Eurasian and the northern

African plates (van Hinsbergen et al., 2005). The geotectonic evolution of Hellenides is related to two main orogenic cycles: (1) the Paleo-Alpine orogeny of Late Jurassic – Early Cretaceous, and (2) the Alpine orogeny, between Late Eocene and Oligocene or even Miocene in some regions. Thus, the geotectonic units of the Hellenides are divided into two groups according to the influence of these two orogenies. Internal units are those that have been affected by both orogenies, whereas External units are those which show the effects only of the younger (Alpine) orogeny (Mariolakos et al., 2001). Both units are variably tectonized, deformed and metamorphosed. On the one hand, the Internal

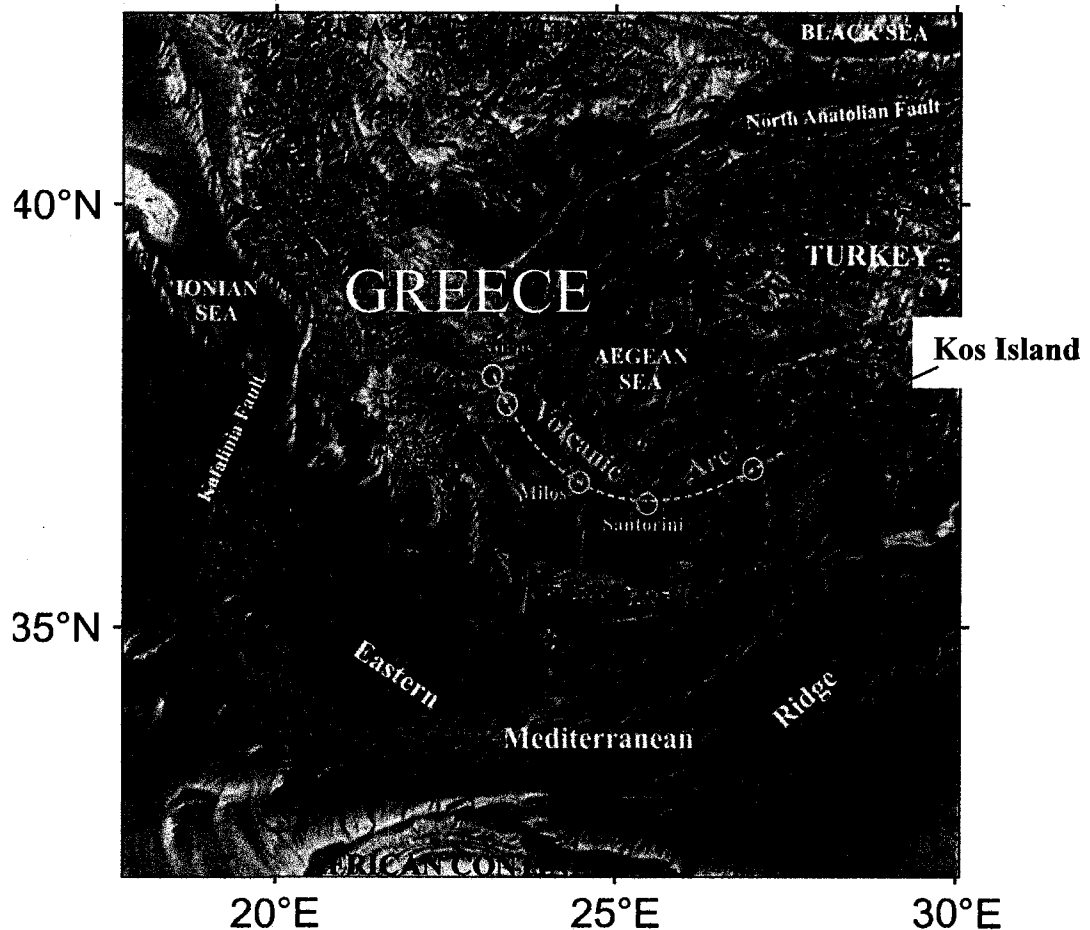


**Fig. 1.1:** *Geotectonic map of Eastern Mediterranean and Aegean Sea (modified from [www.oceanexplorer.noaa.gov](http://www.oceanexplorer.noaa.gov)).*

Hellenides are mostly exposed in the core of the Hellenic Arc, including also the pre-Alpine basement rocks. On the other hand, the External Hellenides extend to the periphery of the Hellenic Subduction zone (Fig. 1.1).

The tectonic plates after the most recent (Alpine) orogenic cycle remained active, causing movements and significant marine, lacustrine and terrestrial deposition in both large and small post-alpine basins. Brittle-ductile deformation occurred during and after sedimentation. In particular, during the Neogene, the westward – southwestward motion of the Aegean-Anatolian microplate (part of the Eurasian plate) over the African plate, led to subduction rollback and consequently to post-collisional extension in a back-arc setting. This led to extensional detachment faulting in those areas, causing widespread volcanic and plutonic activity (Pe-Piper & Piper, 2007). Modern magmatic activity is limited to the present Volcanic Arc (Fig. 1.1).

### **1.3 Geology of Kos**

Geotectonic units from both the Internal and External Hellenides are present in Kos. The pre-Alpine basement and the Alpine rocks are principally exposed on Dikeos Mountain (Fig. 1.2). Alpine rocks also crop out on the northern Kefalos peninsula. The most widespread rocks are the Neogene – Quaternary sedimentary and volcanic rocks, including the late Quaternary Kos Plateau Tuff.

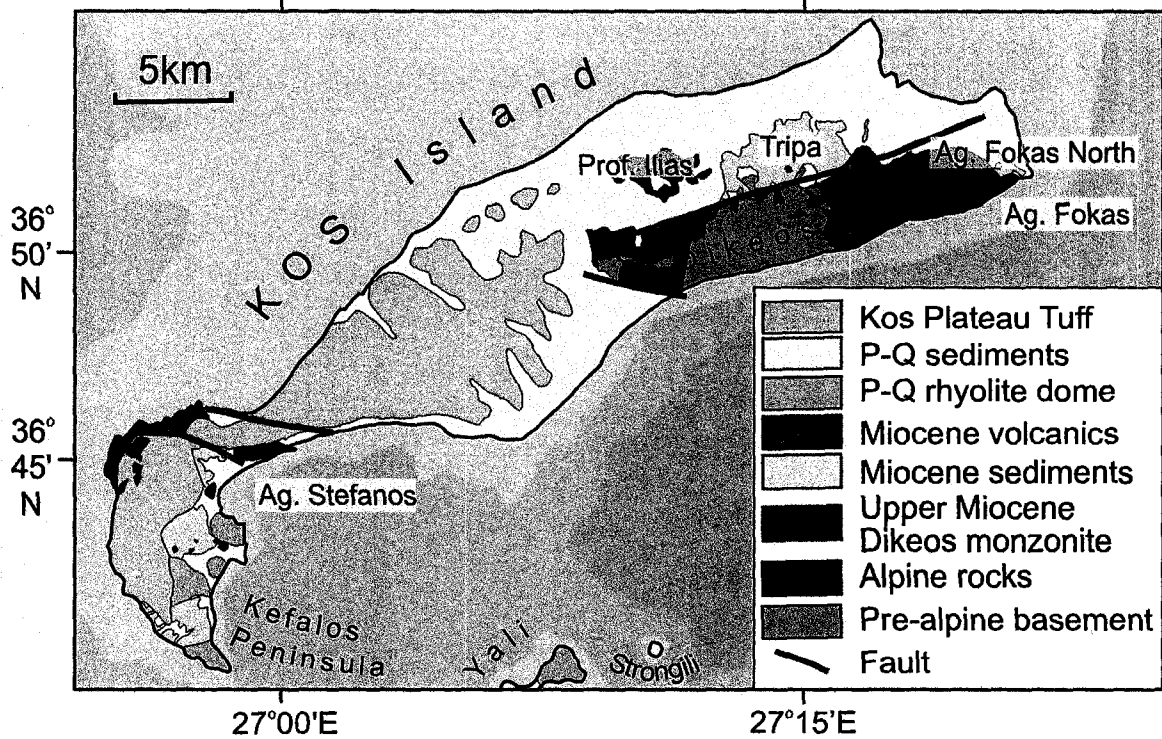


**Fig. 1.2:** Simplified geological map of Kos.

### 1.3.1 Individual lithological units:

#### • Pre-Alpine basement:

Pre-Alpine rocks in Kos are Paleozoic to Mesozoic in age and consist of low-grade metasedimentary rocks such as phyllites, pelites and marbles, with minor mafic intercalations (Altherr et al., 1976; Gralla, 1982).

#### • Alpine Rocks:

The Alpine rocks are divided into two geotectonic units. One is the Zia unit which is a neritic thick-bedded carbonate sequence with Upper Cretaceous to Upper Eocene age, overlain by middle Eocene flysch, equivalent to the upper part of the Tripolis unit, well-known in mainland Greece (Blondeau et al., 1975). The other unit consists of neritic

limestones overlain by early Cretaceous pelagic limestones and a flysch, probably similar to the Olonos – Pindos unit of mainland Greece. The Zia unit appears to have been thrust either on the pre-Alpine basement or on the Miocene plutonic rocks of Dikeos. The Olonos – Pindos - equivalent unit is thrust on the Zia unit.

• **Neogene Sedimentary Rocks:**

The oldest Neogene sedimentary rocks of western Kos are marine bioclastic limestones (Pesia Member) and siliciclastics that were probably deposited nearshore during the Middle Miocene (Böger, 1978, Besenecker & Otte, 1978). They are approximately 150 m thick (Triantaphyllis, 1994). These are deformed and unconformably overlain (Bignot & Guernet, 1976) by the Soccoro Member. The Soccoro Member has an age of Middle to Upper Miocene and consists of fluvial sediments. It is overlain by lacustrine marls and clays of the Protocaravo Member, that is interbedded with upper Miocene pyroclastic rocks (Besenecker and Otte, 1978). The Upper Pliocene(?) to Pleistocene lacustrine sediments of the Kefalos Member unconformably overlap the Miocene rocks.

In central Kos, Lower to Middle Miocene marine sediments were deformed and are overlain unconformably by Upper Miocene lacustrine sediments. A succession of Pliocene clastic sediments with marine intercalations unconformably overlies the upper Miocene rocks (Willmann, 1983).

In eastern Kos, tuffitic marine bioclastic limestone and siliciclastics (Asklupio beds) of Middle Miocene age constitute the oldest rocks in the Neogene sedimentary succession. Then the sequence continues with marls and sandstones of the Vasilios beds:

the upper parts contain tuff beds in northern Kos, and are interbedded with the thick Agios (Ag.) Fokas ignimbrites in SE Kos (Böger et al., 1974). In some areas cherty limestones (Palioskala beds) overlie the Vasilios beds. There is then an unconformity beneath the Pliocene to Quaternary succession of conglomerates, lacustrine marls and sandstones (Willmann, 1983).

• **Neogene Plutonic Rocks:**

The 1:50,000 geological map of eastern Kos (Triantaphyllis, 1998) shows a 10 km<sup>2</sup> pluton in the western part of Dikeos Mountain, which has intruded the pre-Alpine basement (Fig. 1.2). According to Altherr et al. (1982), the pluton is an I-type, medium to coarse grained biotite-hornblende monzonite.

The eastern margin of the pluton intrudes the Paleozoic basement. Thermal aureole minerals indicate a depth of emplacement exceeding 10 km (Altherr et al., 1972, 1976, 1982). The SSW boundary of the monzonite is a fault that juxtaposes the pluton and Pliocene marls (Triantaphyllis, 1998), whereas the northern edge of the monzonite is overthrust by Mesozoic-Eocene limestones, which appear undeformed and unaffected by the pluton (Altherr et al., 1976).

The Dikeos monzonite has been dated by the K-Ar method using biotite and hornblende. Hornblende is a better age indicator than biotite because it has a higher blocking temperature (550 °C compared to 340 °C for biotite). The hornblende yielded ages of 11.9±0.4 and 11.4±0.3 Ma and the biotite 10.8±0.45 Ma and younger ages (Altherr et al., 1976). Furthermore, fission track on titanites yielded an even younger age

for the monzonite (8.6 – 8.9 Ma), than the biotite. These dates were interpreted as cooling ages or as a result of a thermal overprint after the cooling ages (Altherr et al., 1982).

The Dikeos monzonite and its thermal aureole are cut by dykes (Wimmenauer, 1977). Wimmenauer examined the mineralogical and chemical composition of ten dyke rocks, and provided whole rock geochemical analyses, diagrams of chemical composition and brief descriptions of each type of dyke rock. The mineralogical and chemical composition of these dyke rocks show considerable variation ranging from mafic to felsic members. Moreover, the dykes have higher  $K_2O/Na_2O$  ratios and are more undersaturated than the monzonite, except for the micromonzonites and monzonite porphyry dykes, which are of similar composition to the monzonite. The chemistry of the dykes supports the presence of a volatile-rich mafic magma. Wimmenauer (1977) suggested the dyke rocks are the products of differentiation of a basaltic-parental magma or the products of mixing of more than one magmas. Altherr & Siebel, (2002) suggested that chemical and isotopic composition of lamprophyric dykes indicate an origin by partial melting of mantle including slab-derived materials. Lamprophyric dykes appear to be the youngest, cutting other dykes and sills with preferred orientation between N-S and NW-SE (Wimmenauer, 1977). Both the monzonite and dykes are cut by shear zones containing limonite and quartz veins.

I-type plutons in the Aegean Sea show a systematic variation in their composition from one side of the plutonic belt to the other. Thus, the western areas contain medium to high-K felsic rocks, whereas those of the middle of the belt are characterized by high-K and low-silica, and those of the eastern areas by high-K and high-silica (Fig. 1.3)

(Altherr et al., 1982; Altherr & Siebel, 2002). These authors have suggested that this regional variation in these plutons is related to the thicker crust in the west.

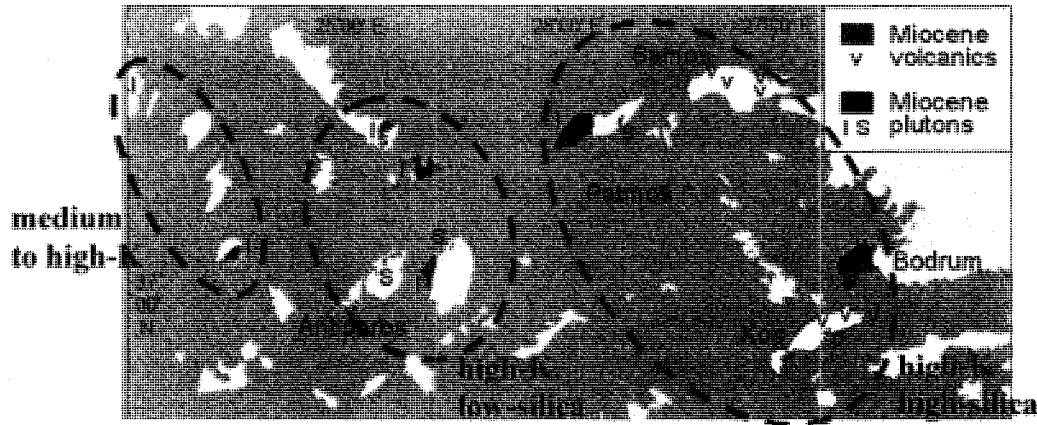


**Fig. 1.3:** *Spatial variation of the composition of the plutonic rocks in the Aegean Sea (Modified from Altherr & Siebel, 2002).*

Altherr & Siebel (2002) suggested that the Miocene I-type plutons of the Aegean Sea were produced as a result of the early stages of back-arc regional scale extension of the lithosphere. This extension is probably responsible for the creation of normal faults or shear zones exploited by magma during its ascent toward the surface. Flattened mafic enclaves with chilled margins, at the southern margins of the pluton, support this interpretation, as does the fact that there was no important mixing between the crust-derived felsic magma and the upper-mantle-derived mafic magma.

• **Neogene Volcanic Rocks:**

The Neogene volcanic rocks on Kos have been reported to have similar composition to the dykes that intrude the Dikeos monzonite (Triantaphyllis, 1998). K-Ar radiometric

dating by Bellon & Jarrige (1979) at Tripa indicated that the age of trachytes is about  $7.5 \pm 0.7$  Ma, whereas Besang et al. (1977) determined an age of 10.7 Ma for the same locality. These dates are upper Miocene; there are no geochronological data supporting a Pliocene age.

Apart from sporadic outcrops of lavas and domes in Tripa and Prof. Ilias, the upper Miocene volcanic activity is confined to two voluminous pyroclastic deposits, one in Ag. Fokas (eastern Kos) and the other in Ag. Stefanos – Cape Tigani (western Kos) (Triantaphyllis, 1994, 1998). The pyroclastic rocks at Ag. Fokas overlie the “Vasilios beds” which consist of 250 m fluvial sandstones and lacustrine marls of Upper Miocene age (Böger et al., 1974). The pyroclastic succession at Ag. Fokas yielded a K-Ar (biotite) age of  $10.7 \pm 0.1$  Ma (Altherr et al., 1982), whereas similar successions at Ag. Stefanos and Cape Tigani were dated at  $10.4 \pm 0.4$  Ma (Bellon & Jarrige, 1979), approximately the same age as the trachytes from Tripa.

The Upper Miocene caldera on the Bodrum peninsula (Fig. 1.3) is similar in age to the Kos pyroclastic rocks (Montigny & Robert, 1991). The Bodrum rocks consist of a monzonitic intrusion, and Upper Miocene volcanic rocks such as pyroclastic rocks, andesitic lava flows and dacitic lava domes (Robert et al., 1992; Ulusoy et al., 2004). It will be important to see if there is any correlation of these volcanic rocks with the pyroclastic rocks in Ag. Fokas and whether the Bodrum caldera was a source for these pyroclastic rocks.

The geological map of Kos shows the presence of “Pliocene Volcanics” in isolated outcrops in the Tripa, Profitis (Prof.) Ilias and Ag. Dimitrios areas, where Miocene and Pliocene marls are widespread (Fig. 1.2). The volcanic rocks include trachytes, andesites

and latites, that are mapped as cutting Late Miocene marls. However, as discussed above, the available geochronology indicates a Late Miocene age for the volcanic rocks.

The Pleistocene Kos Plateau Tuff eruption was probably one of the largest eruptions in the South Aegean during the Quaternary (Allen & Cas, 1998, 2001; Allen et al., 1999; Allen 2001). Allen & McPhie (2001) demonstrated that the interaction of a highly energetic pyroclastic flow and an unconsolidated sedimentary substrate, can lead to the deposition of a distinctive and characteristic chaotic breccia. In addition, Pe-Piper et al. (2004) demonstrated significant faulting after deposition of the Kos Plateau Tuff.

In the present study, these rocks will be compared with volcanic rocks from other localities such as the central Aegean, (Pe-Piper & Piper, 1989; Pe-Piper, 1994; Pe-Piper et al., 1995; Pe-Piper et al., 1997; Pe-Piper, 2000; Pe-Piper & Piper, 2002) in order to determine similarities and differences in petrology, provenance, geotectonic environment and geochemical variability.

### **1.3 Objectives**

- A rigorous study of the Miocene pyroclastic successions has been undertaken in order to better understand the volcanic stratigraphy and consequently the depositional environment, and the relationships with the underlying, overlying and the intercalated sediments.
- Geological mapping of each locality to document the spatial distribution of the volcanic rocks and related sediments, and consequently to define the tectonic setting and the structure.

- This study attempts to determine if there is any correlation between the ignimbrites of Ag. Stefanos and Ag. Fokas, and between these pyroclastic rocks and the lava flows and domes of Tripa and Prof. Ilias and beyond to the surrounding areas such as Bodrum, Nisyros and Samos.
- In addition, a directional analysis of the voluminous pyroclastic rocks of Ag. Stefanos and Ag. Fokas, by using paleoflow indicators, was carried out.
- This project also aims to determine whether an integrated study of pyroclastic rocks can be used for regional tectonic and volcanic reconstruction.
- The ultimate goal of this project was to test the hypothesis that the Tripa and Prof. Ilias localities were the sources for the thick pyroclastic accumulations and if not to determine where the source volcano(es) were.

## CHAPTER 2

# *Upper Miocene volcanology and pyroclastic stratigraphy*

### **2.1 Introduction**

As has been explained in the previous chapter, Upper Miocene volcanic rocks are widespread in Kos. The present chapter presents a description and interpretation of these volcanic rocks, and establishes a volcanic stratigraphy. The chapter is organized according to the spatial distribution of the rocks, and from oldest to youngest. Thus, the volcanic stratigraphy of Tripa, Prof. Ilias, Ag. Stefanos and Ag. Fokas are described in sequence.

### **2.2 Methods**

This is a field-based project. Protocols observed during mapping and sampling are described in the following section.

### **2.2.1 Field Equipment**

The required materials for doing field work properly included topographic or geological maps of scale 1:50,000 or less and of course a field note-book for detailed recording of measurements and observations and generally all of the actions in the field. For better organization, all these collected field data are categorized in each specific locality.

A geological compass is necessary for determination of bedding orientations in the stratified units. Moreover, the compass is used for the measurement of the orientation of elongate clasts on bedding planes. The compass and clinometer are also important for measurements that have to do with the dip direction and shear deformation of elutriation pipes, and the axes of erosional grooves at the base of coarse horizons. In addition, the paleocurrent directions are measured on single sets of planar cross bedding in clastic sediments that are interbedded with the voluminous ignimbrites. Last but not least, the compass is useful for measurements of fault planes and fold axes. In this thesis, dips are reported as dip amount and dip azimuth, corrected for magnetic declination.

Another instrument that is useful in the field is the GPS. A GPS receiver is important because, for each individual measurement or observation in the field, a locality is situated in a database, and the coordinates are recorded for their projection on a geological map, as well as for future visit of the locality if required. When the signal of the satellites is strong and the accuracy is better than 6 m, GPS can be used for measurements related with the distances between two localities in the field.

Furthermore, a variety of sizes of durable, clear, plastic bags for sampling is required, in order to ensure the incorruptibility of the sample between the collection in

the field until the arrival at the laboratory. Very often, there are samples that are not indurated and can easily be fragmented, so that special packing is essential. In addition, packing is very important because helps to avoid contamination and protects the identity of the item. For this reason, a permanent marker was used for labelling the sample, not only directly on the sample, but also on its plastic bag and even sometimes on a piece of paper inside the bag.

Last but not least, being in the field many hours during the day and especially in a Mediterranean island with high solar radiation and temperatures during the summer season, additional personal protection is compulsory. As a result, hat, long trousers, bottle of fresh water, a first aid kit and hiking boots are important for optimum productivity and safety in the field.

### **2.2.2 Field work**

Preliminary field investigation on the island of Kos took place in the spring of 2003 and 2004 by Drs Georgia Pe-Piper and David Piper. During that field work, the concern of the researchers was focused on the assessment of the potential study areas of the project according to the bibliographical reports. In these years, data were collected from 44 localities around the island of Kos (Fig. 2.1). Furthermore, 28 rock samples were collected from the Miocene monzonite, the pyroclastic rocks and the lavas.

During the summer of 2005, I carried out detailed field work under the supervision of Drs Georgia Pe-Piper and David Piper. 134 additional localities were visited, and 73 samples were collected from the monzonite, volcanic and pyroclastic rocks, and interbedded sediments (Fig. 2.1). Moreover, during the field work crucial information

concerning the architecture of the ignimbrites, the volcanic stratigraphy and generally the spatial distribution of the rock assemblages, was collected. The structure and the tectonic control of magmatism is something that can occupy your mind easily, because there is correlation with all the above. However, for someone who works in as tectonically active an area as Kos Island, it is important to have awareness that part of the tectonic deformation that appears in the studied rocks took place after the Miocene.

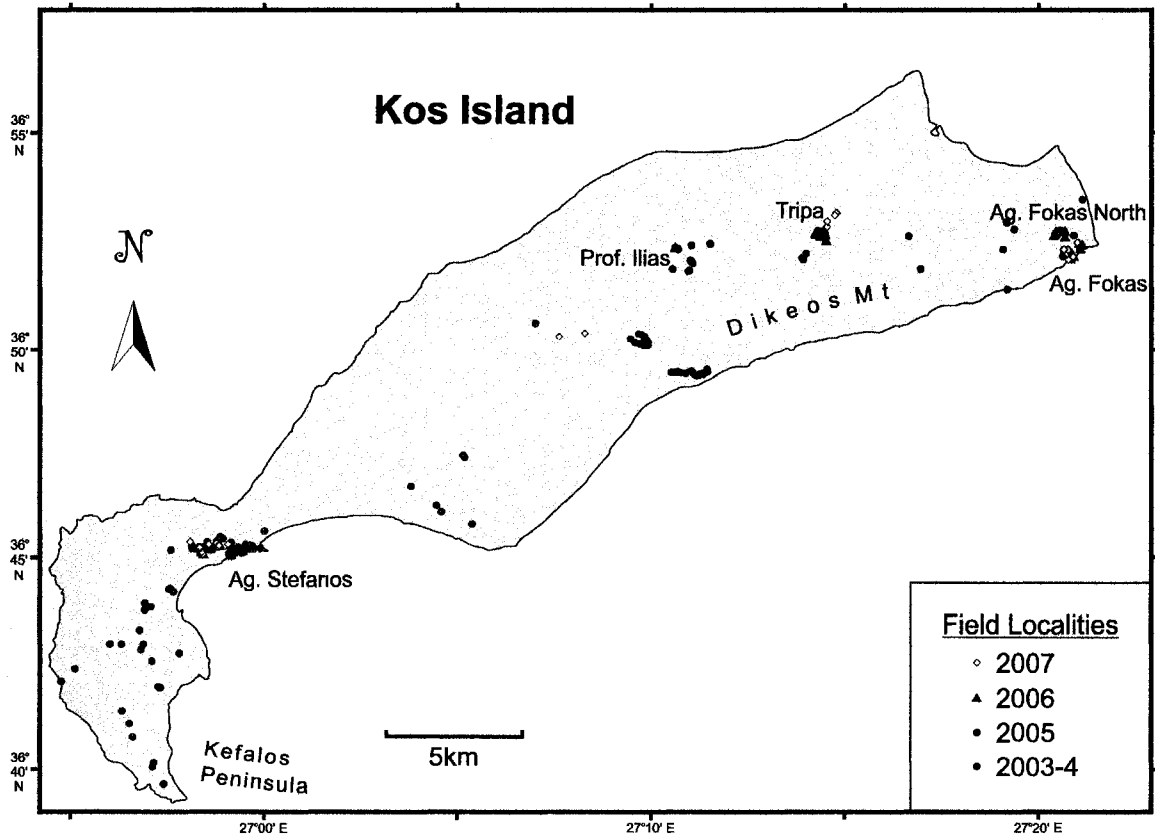


**Fig. 2.1:** *Distribution of localities during the 2003, 2004, 2005, 2006 and 2007 field work on Kos.*

I carried out more field work in the summer of 2006, giving priority and emphasis to the collection of paleocurrent indicators that contribute to the assessment of the source of the ignimbrites. Furthermore, three more samples were collected from interbedded

sediments and volcanic rocks from the 41 localities which were studied (Fig. 2.1). Also, detailed mapping on scale of 1:1000 or less took place in some of the localities.

Finally, in the spring of 2007, field work was conducted by Drs. Georgia Pe-Piper and David Piper, sixteen additional hand specimens were collected from 25 additional localities (Fig. 2.1). The researchers focused again on the collection of paleocurrent indicators (oriented clasts, imbrications and cross-bedding), and useful information about the structure and stratigraphy of the ignimbrites and the related sediments.

To unravel the architecture of the volcanic rocks and interbedded sediments, their stratigraphic sections were measured in the field. The stratigraphic columns were correlated locally either by direct tracing of beds, or on the basis of the size, abundance and type of lithic and vitric clasts.

In total, hundreds of photographs have been taken, displaying useful observations and characteristic examples of what had been found in the field. The 1 euro coin used as a scale in many photographs is 18 mm in diameter; the hammer is 33 cm long. Estimates of percentages of lithic clasts and pumice were made in the field by using comparison charts prepared for thin sections (Klein, 1989, Fig. 32.3) and many beds were photographed so that the consistency of the estimates could be checked in the laboratory. The precision of estimates of clast % was calculated to be ~40 %.

### **2.3 Volcanic stratigraphy of Tripa**

Tripa is one of the northern localities in Kos where the alpine basement is exposed along the northern part of Dikeos Mt. (Fig. 2.1). The Mesozoic basement consists of thick-bedded, creamy-coloured, micritic limestones containing stringers and nodules up

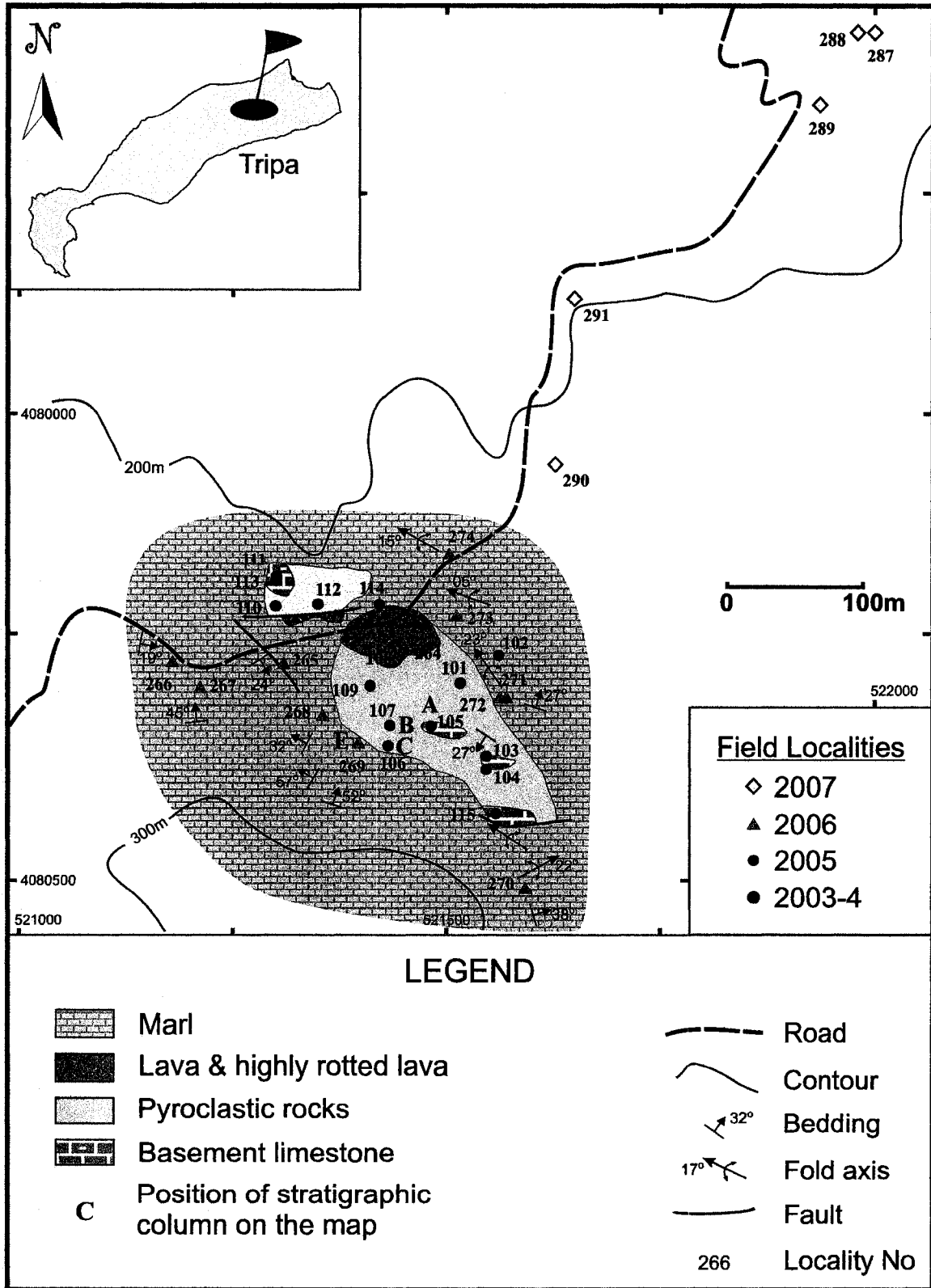


**Fig. 2.2:** Geological map of the Tripa area.

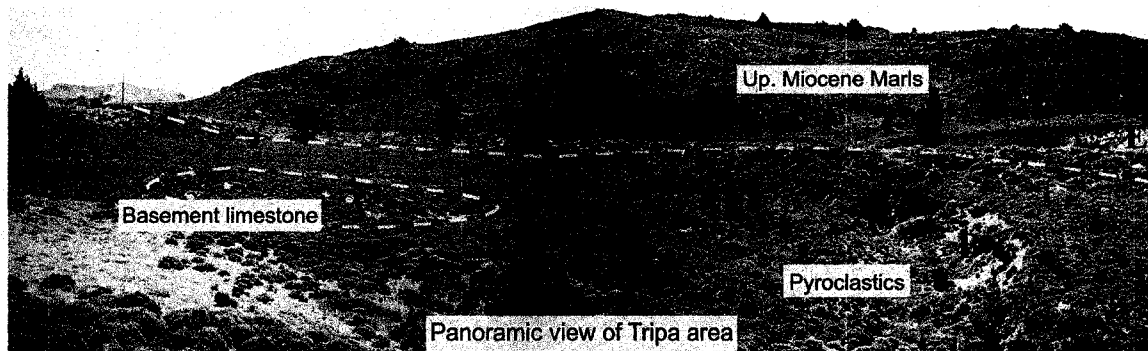


**Fig. 2.3:** *General view of the southern part of Tripa area looking south. The letters correspond to stratigraphic columns (see Figs. 2.2, 2.8)*

to 10 cm in size of black chert. During the field work, limestone basement was identified at localities 105, 111, 113 and 115 (Figs. 2.2, 2.3).

The micrites are unconformably overlain by **pyroclastic rocks** that cover a significant part of the study area (Figs. 2.2, 2.5, 2.6). In a 3-4 m cliff at locality 106 (see locality C in Fig. 2.3), fresh looking tuff is exposed and is fractured by numerous faults. A low angle fault dips to NE ( $33^{\circ}/030^{\circ}$ ) with slickenlines dipping N ( $005^{\circ}$ ) is cut by shear faults ( $89^{\circ}/337^{\circ}$ ) with vertical slickenlines. The brittle deformation is probably related to post-Miocene tectonic activity on a cataclastic west-trending fault. Faults with similar orientations dipping towards the NE were also identified at locality 101, where massive

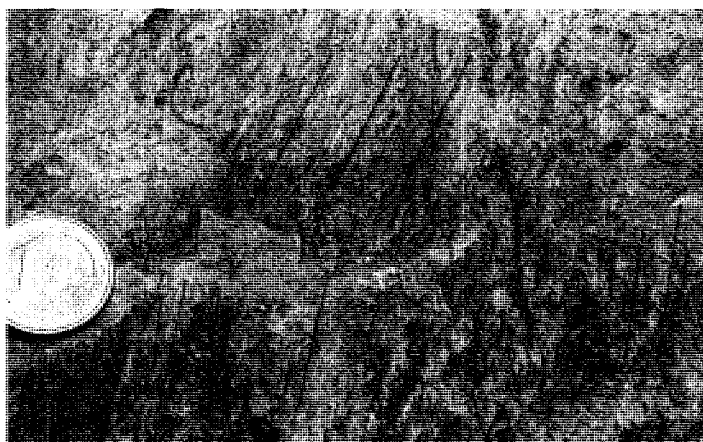


**Fig. 2.4:** *Vertical slickenlines on NW dipping planar fault at locality 109. Two sets of lines are visible, indicated by different colours.*

ignimbrite is exposed. Additionally, in locality 109, two different sets of slickenlines were observed in a planar fault, the older dipping SW ( $250^{\circ}$ ) (Fig. 2.4). Often, the slickenlines abut on oxidized surfaces.

The pyroclastic rocks present have a pinkish or greyish colour. These can be divided in vitric-lithic tuffs containing up to 10% of lithic clasts 1-3 cm in size (locality 106); fine vitric ignimbrites (109); and crystal-lithic ignimbrites (104). The outcrops range from massive to unconsolidated condition.

The dip of **lava flows** at locality 39/108/264 supports the idea that these lavas are stratigraphically above the pyroclastic rocks (Figs. 2.5, 2.8). The section along the road exposes at least 7 m of lava in total thickness, with almost 3 m being highly weathered. How much of any overlying volcanic succession might have been eroded prior to marl deposition is unknown. These lavas show distinctive flow banding dipping NNE ( $39^{\circ}/020^{\circ}$ ) in the east and NW ( $17^{\circ}/342^{\circ}$ ) in the west, implying a dome shaped structure,

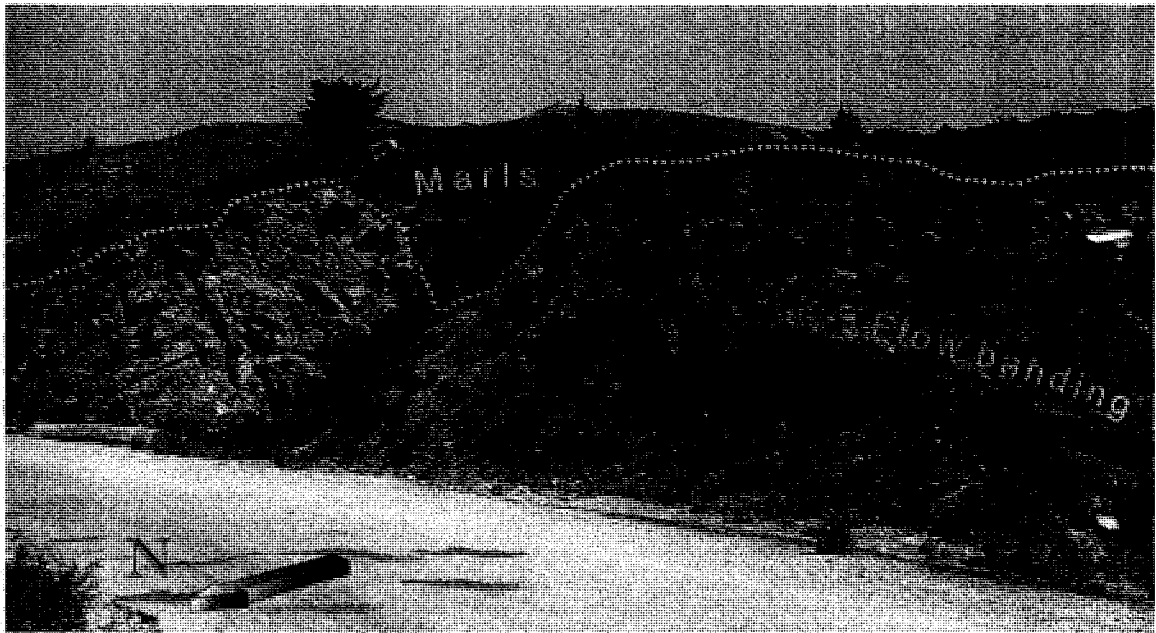


**Fig. 2.5:** *Dome of lava in Tripa overlain by marls.*

related probably to an effusive type of volcanic eruption (Fig. 2.5). Southwards, there is a limited outcrop of green volcanic rocks in locality 107 (see locality B at Figs. 2.3, 2.8). A few meters farther south, polymictic lava breccia is present, with clasts between 3 and 10 cm diameter.

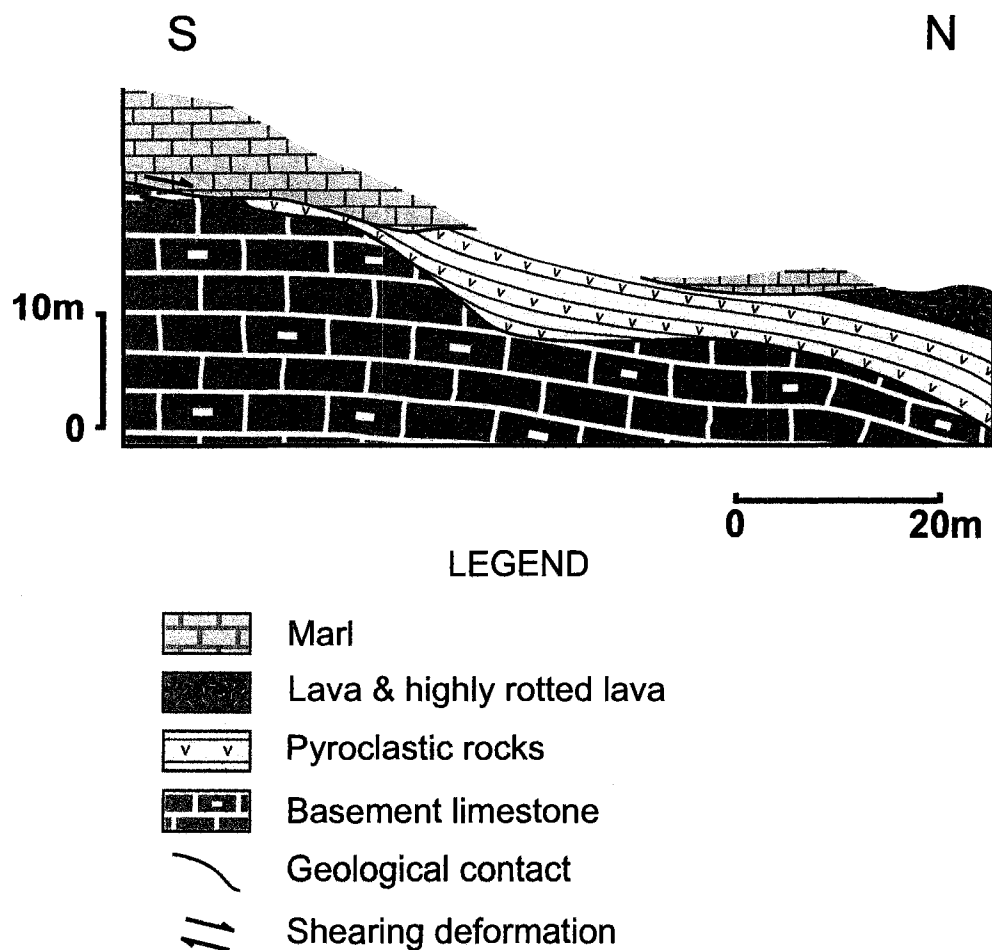


**Fig. 2.6:** *Schematic stratigraphic section of the Tripa area.*

The **marls** are the formation with the largest area extent (Fig. 2.2, 2.3). They unconformably overlie basement limestone, pyroclastic rocks and lava flows. Their thickness is estimated as a few tens of meters. The marls show variations in bed thickness from a few mm to a few cm. Muddy intercalations are also present. These marls are assigned to the Upper Miocene Vasilios beds of Böger et al. (1974).

The marls have variable dips (Fig. 2.2). Symmetrical, asymmetrical and overturned folds were observed in the field. Fold axis orientations were measured either directly in the field or by using the azimuth dip of the limbs, projected on a Schmidt net. All of the measurements, except one at locality 270, indicate that clear fold axes plunge to the NW (Fig. 2.2). A few faults were detected striking E – W and NW – SE (Fig. 2.2). At locality 115, the limestones occur juxtaposed against strongly folded marls probably along a faulted onlap contact (Fig. 2.7).

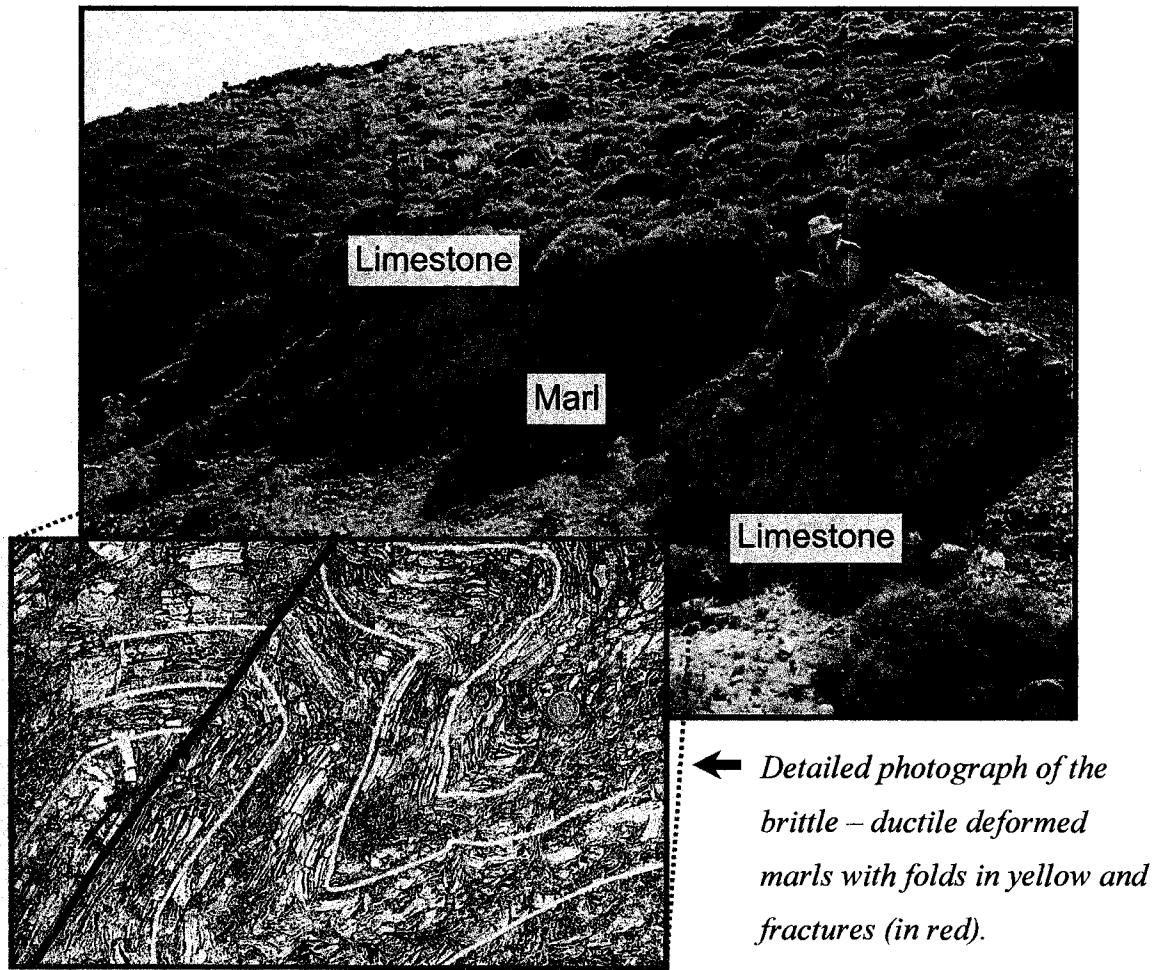


**Fig. 2.7:** Tectonic contact between the basement limestones and the stratigraphically overlying marls.

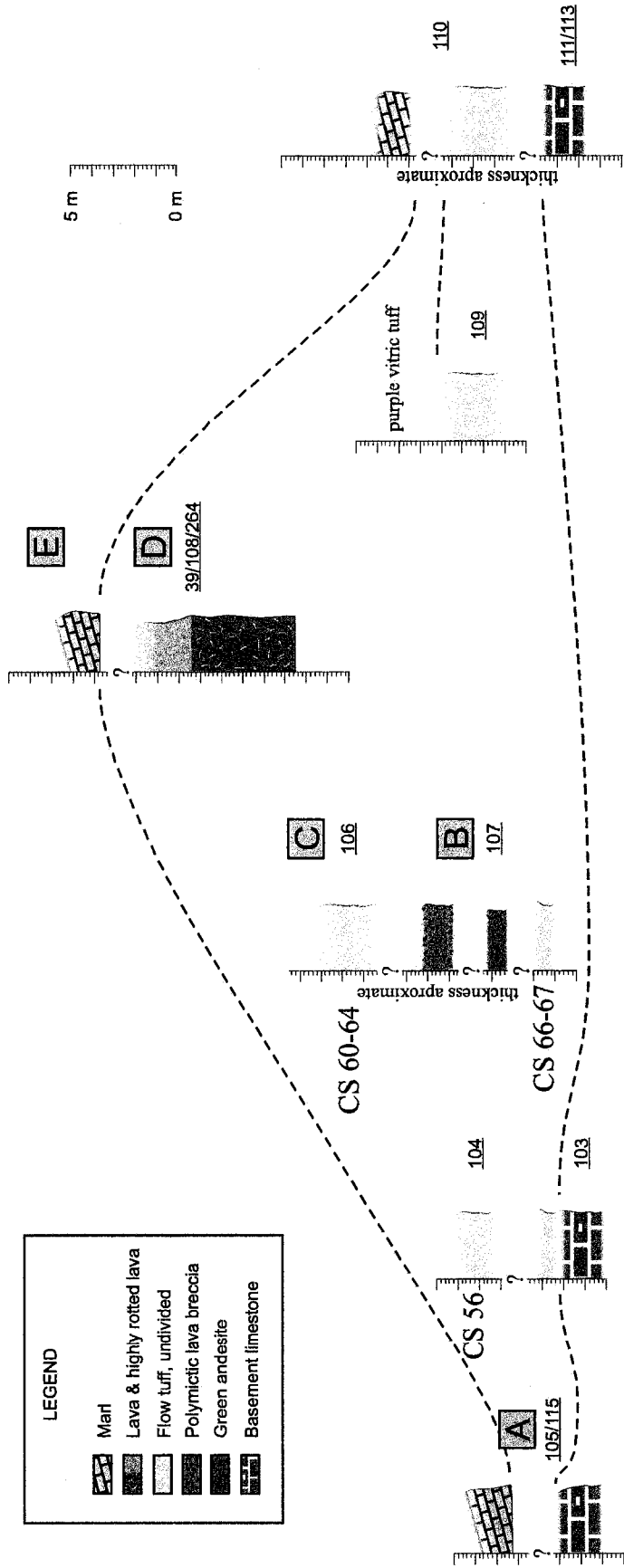


**Fig. 2.8:** Correlation of stratigraphic columns of Tripa area. The letters correspond to localities in Figs. 2.2, 2.3.

CS m: Sample number collected from this specific locality.

Underlined numbers refer to the localities.

## 2.4 Volcanic stratigraphy of Prof. Ilias

Upper Miocene volcanic rocks are also exposed near Prof. Ilias. In Tripa, the basement limestone has limited appearance, whereas here the basement is well exposed, building the Prof. Ilias Mt., north of localities 178/275, 176 and 43/175 (Fig. 2.9).

However, towards the south, the limestones are not exposed except at locality 119, where numerous limestone blocks are present. In addition, the basement in the area contains

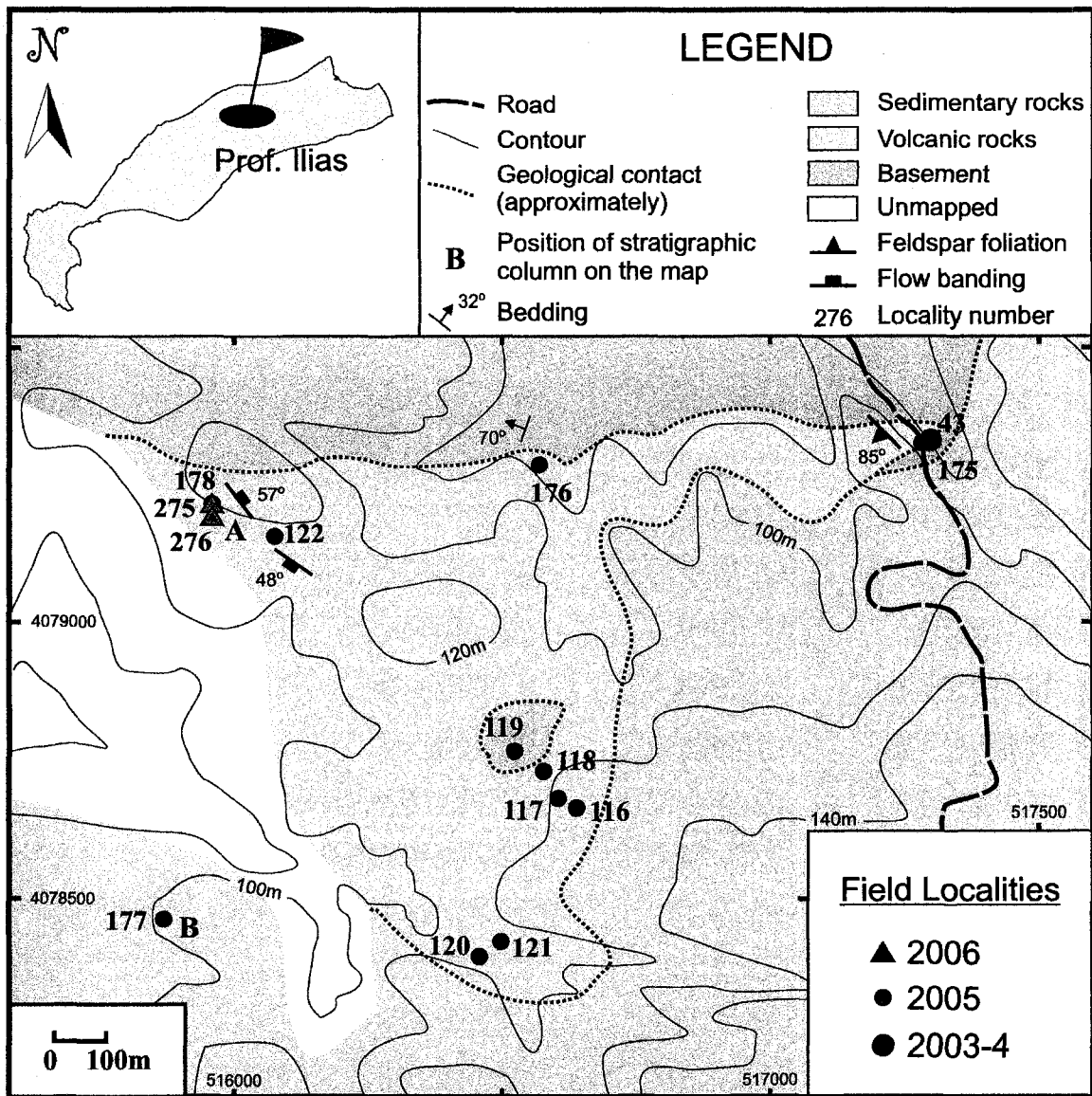


**Fig. 2.9:** Detailed map of Prof. Ilias area.

limited outcrops of Lias - middle Cenomanian **phyllites** of the Upper Tectonic Unit (locality 176) (Triantaphyllis, 1998).

South of Prof. Ilias, **lavas** overlie alpine basement at locality 276. The lavas appear to be massive, showing clear flow banding (Fig. 2.10), cut by small faults and joints. At locality 176, a 25 m wide dacite dyke or plug has a chilled margin on its south side towards country rock of phyllite, but the actual contact may be faulted. The dacite lava contains 2-8 cm mafic enclaves and locally shows pre-full-crystallization foliation picked out by feldspar megacrysts up to 1 cm with a dip of  $70^{\circ}/100^{\circ}$ , subparallel to the northern margin of the body. Moreover, the dacite is cut by conjugate normal faults that host 1 mm limonite veins. The degree of alteration of the flows varies from outcrop to outcrop. Those at locality 116 have onion-skin exfoliation, and are pervasively weathered. During the field work, lavas were mapped either as dacites (175, 176, 178/275) or as rhyolites (116, 120, 121). Detailed petrographical description of them follows in the next chapter.

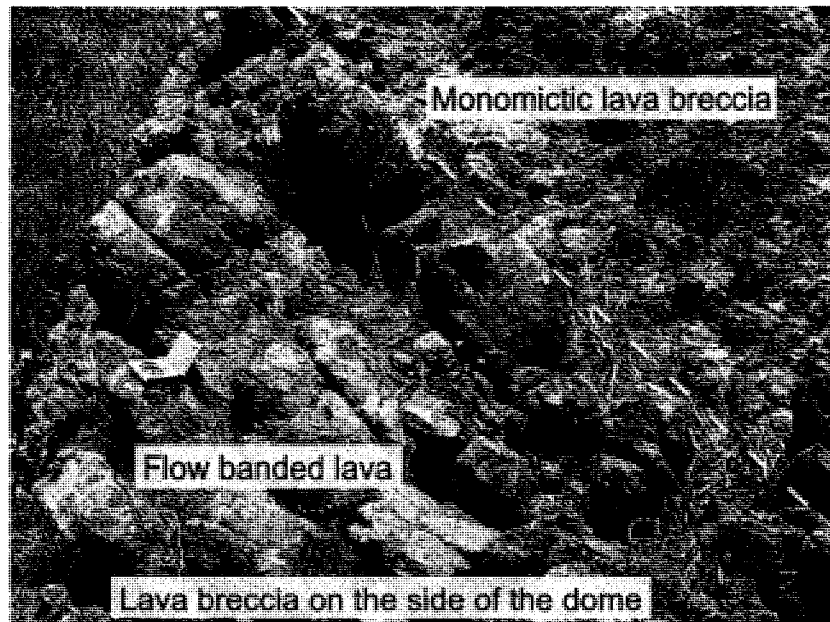


**Fig. 2.10:** *Contact between lava and associated lava breccia in locality 276.*



pyroclastic rocks is not uniform but changes from area to area. Thus, in the north-western outcrops (localities 122, 178/275 and 276) the pyroclastic rocks are characterized by white pumice lapilli. At locality 116, the pyroclastic deposits are silicified, with some brown staining. The maximum thickness of this lithology could be measured only in locality 276, where a complete 35 m cross section is exposed.

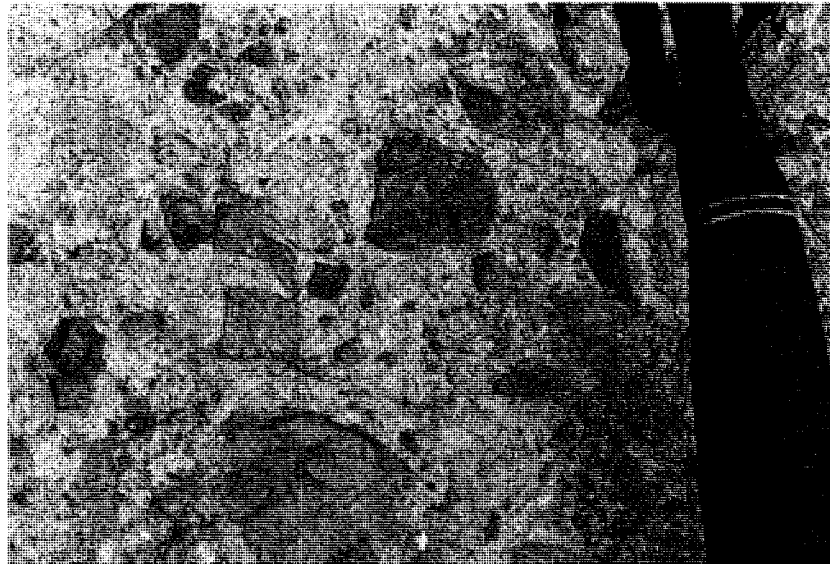


**Fig. 2.12:** *Typical outcrop of coarse grained, polymictic lithic tuff.*

The field work indicated that there is a unit of **clastic sedimentary rocks** that comprises different types of **conglomerates** and **sandstones**. This unit is underlain by the subjacent lavas (43/175) and pyroclastic rocks at outcrops 177 and 276, suggesting that the contact is unconformable. The conglomerates can be divided into cobble – pebble and granule conglomerates. The cobble – pebble conglomerates contain elongated (inequant), rounded to well-rounded clasts mostly of limestone, with some metamorphic rocks and some pinkish felsic volcanic rocks (Fig. 2.13). This conglomerate is as at least 1.2 m

thick (43/175), and up to 4.5 m thick in locality 276. With regard to the granule conglomerate, this was found to be resting directly on the coarser conglomerate, at locality 177 and overlain by sandstone, showing a gradual diminution in clast size. The total thickness of both granule conglomerate and sandstone measured 1.2 m.



**Fig. 2.13:** *View of polymictic (cobble – pebble) conglomerate at Prof. Ilias.*

At locality 276, the sedimentary succession is overlain by an **upper pyroclastic unit** which was measured as 15 m thick (Figs. 2.14 & 2.15). This is the only outcrop that demonstrates the division between the two pyroclastic units. How much of any overlying pyroclastic succession might have been eroded prior to marl deposition is unknown.

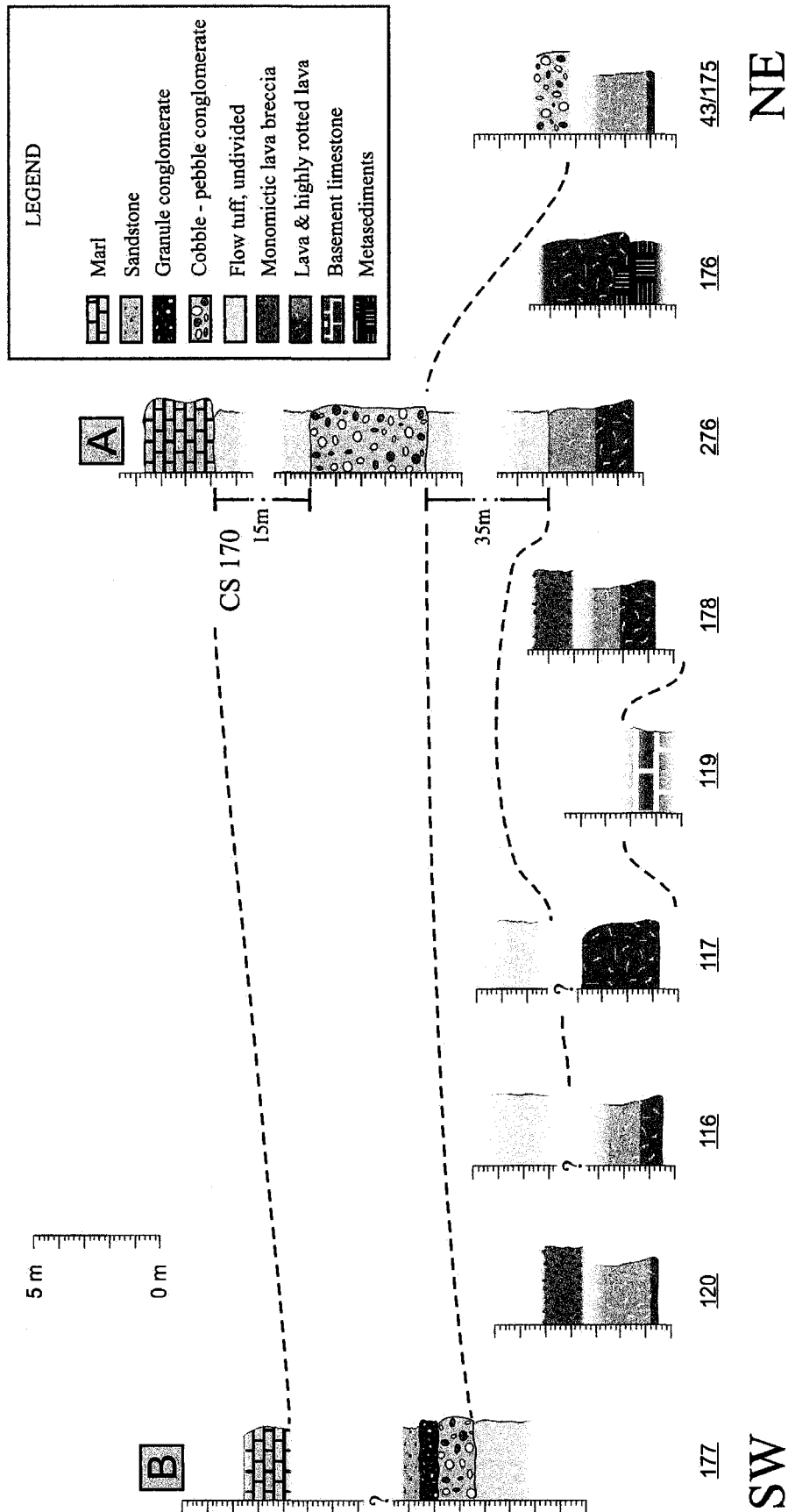


**Fig. 2.14:** Correlation of stratigraphic columns of Prof. Ilias area. The letters correspond to localities in Fig. 2.9.

CS m: Sample number collected from this specific locality.

Underlined numbers refer to the localities.

The uppermost stratigraphic unit at Prof. Ilias area is the lithological unit of **marls**. Large outcrops such as those at Tripa are lacking. In addition, the relationship to the previously referred lithologies is unclear everywhere except section 276 in which marls sit on the upper pyroclastic succession, either conformably or unconformably (Figs. 2.14 & 2.15). The marl sequence is at least 2.5 m thick. The marls in this area appear to be more massive than those at Tripa.

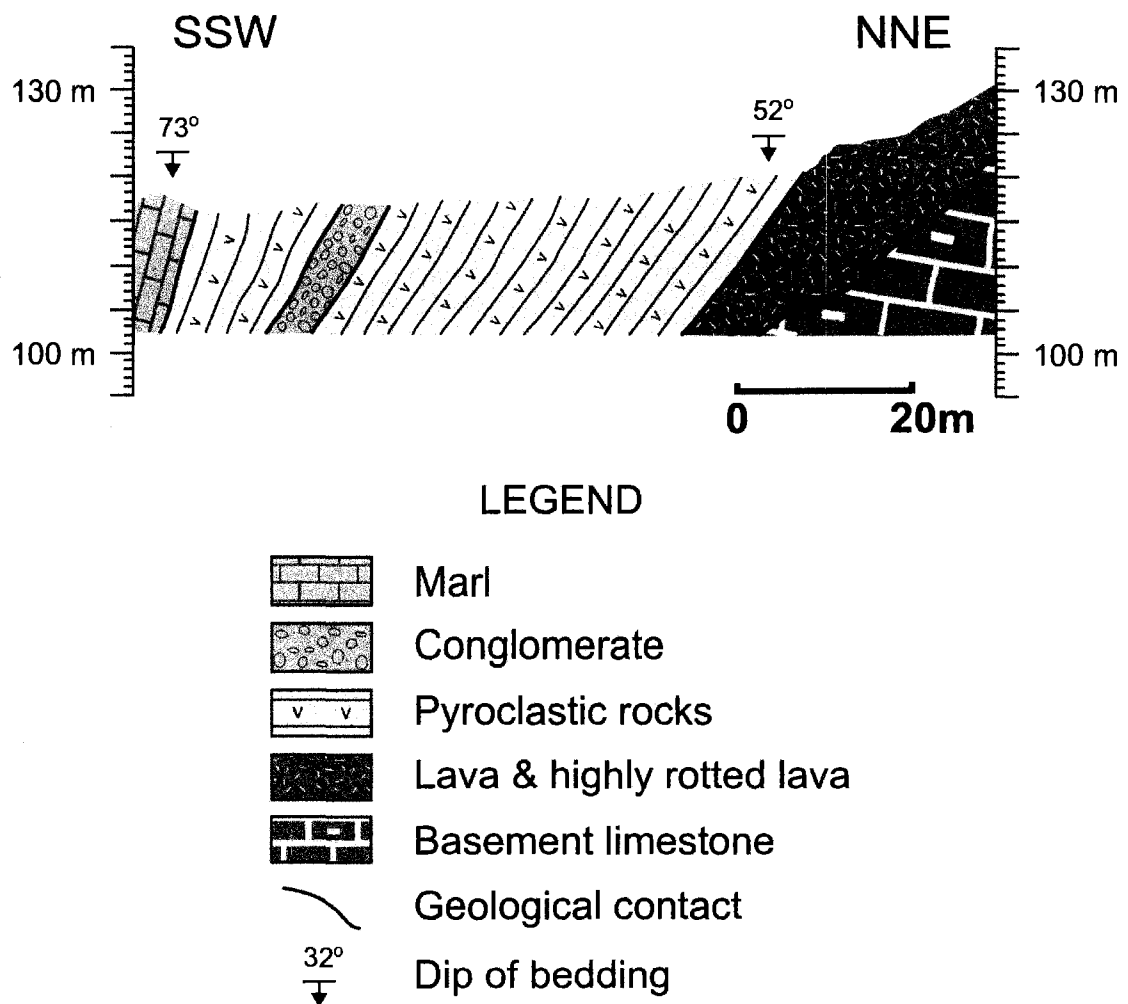


**Fig. 2.15:** *View of the continuous stratigraphic section in locality 276.*

Due to poor exposures of the rocks and their relatively shallow dips and thin units, it is difficult to precisely map lithologic boundaries. In general, the limestone – phyllite basement is overlain by lavas and pyroclastic rocks and finally by clastic sediments and marls that comprise the Konstantinos Formation of middle Pliocene age (Willman, 1983).

## **2.5 Volcanic stratigraphy of Ag. Stefanos**

Ag. Stefanos in south-western Kos is undoubtedly the most important locality for the study of the Upper Miocene volcanic rocks of Kos. In this area, the voluminous pyroclastic deposits are divided into 3 main units (lower, middle, upper), as are the sediments interbedded with the pyroclastic rocks. For better organization of the data, the area is divided into two sub-areas: (1) “North of Club Mediterranee” in the eastern part, corresponding to the lower lithostratigraphic units, and (2) “North of Kastri – Cape Tigani”, corresponding to the middle and upper stratigraphic units of the succession (Figs. 2.17, 2.21). The stratigraphic columns in Figs. 2.18, 2.22 and 2.24 illustrate the correlation between lithologies and units of the deposits.

### **2.5.1 “North of Club Mediterranee”**

#### **Lower Sedimentary Unit:**

The following units were recognized from base to top of the Lower Sedimentary Unit:

A1 is an undivided sedimentary group at the base of the succession. It consists of the Protocaravo Member of Besenecker and Otte (1978) and is of middle Miocene age.

These sediments have a significant areal extent in the western and central parts of Ag. Stefanos (Fig. 2.17). The limited outcrops and the weathered faces led to only an estimate of thickness of the unit at a few tens of meters. At localities 211/213, nodular marls are overlain by medium sandstone with rare volcanic pink dacite granules. Close to those localities, green and red shales and rather deformed marls are exposed. Moreover, at locality 152, the basal unit is a 1 m thick, blocky and friable marl. Toward north, the basal sediments are unconformably overlain by the “Kos Plateau Tuff”, a voluminous pyroclastic succession of Pleistocene age (Chapter 1).

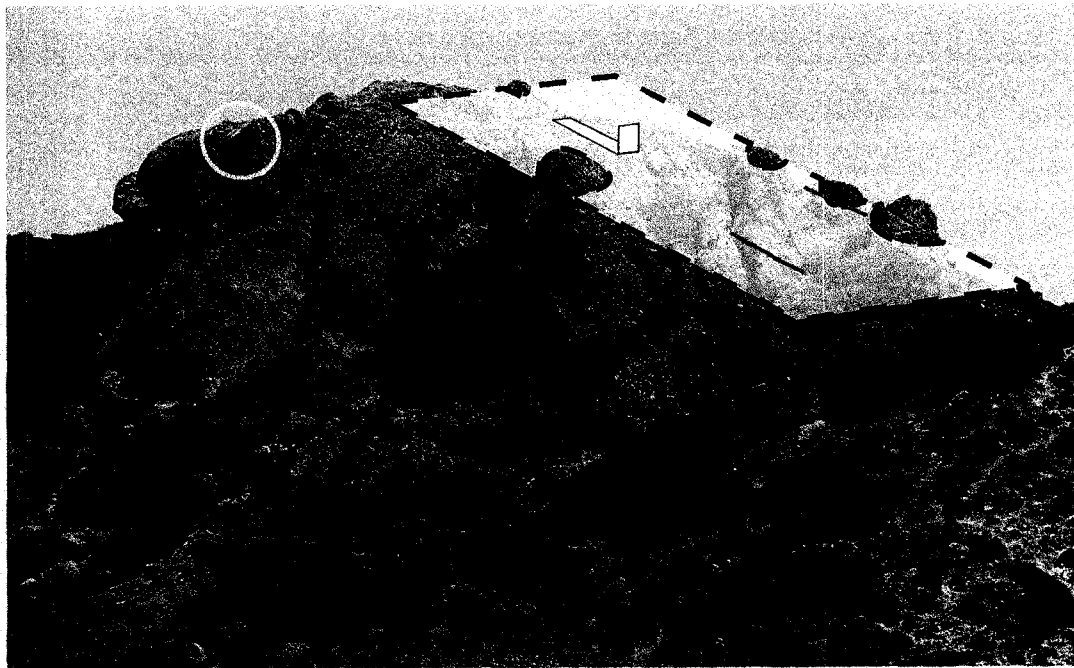
Generally, units A2 to A6 comprise very coarse conglomerates which appear to be laterally discontinuous to the previously mentioned sediments (A1) and therefore probably represent channelised deposits. The outcrops (Fig. 2.17) show dark brown cliffy slopes and topographic bulges (Fig. 2.16), that stand out in contrast to the smooth topography and the whitish – creamy outcrops of the surrounding sediments. At localities 259 and 260, a large NW – SE elongated tongue of these conglomerates has a disconformable relationship to the superjacent units to the east and west, and possibly it represents a landslide (Fig. 2.17).

A2 is a coarse grained conglomerate resting on poorly exposed marls of unit A1, comprising 1.8 m of weakly stratified conglomerate with 5 % of vitric clasts of less than 5 cm in size and 35 % of lithic clasts of 1-5 cm in size. The matrix seems to be crystal – lithic supported.

A3 is a 1.5 m bed of 12 % vitric clasts less than 10 cm and 20 % of lithic clasts less than 2 cm in size.

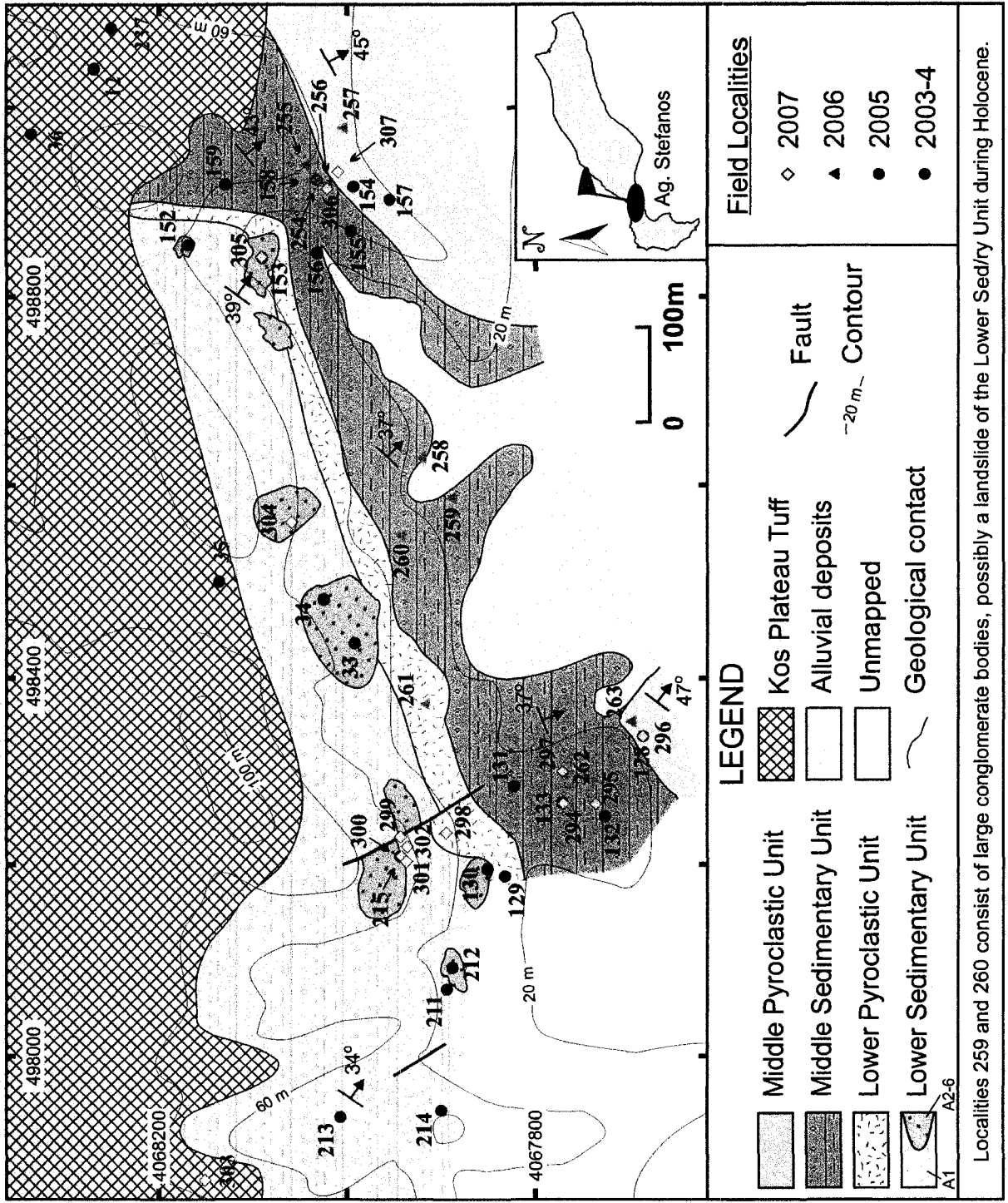
A4 is a pebbly volcaniclastic sandstone similar to the previous unit (A2), containing 5 % vitric clasts less than 2 cm in size and 35 % lithic clasts up to 10 cm. The thickness of this bed is 1 m.

A5 comprises a 2-meter bed of pebbly volcaniclastic sandstone which includes 5 % vitric fragments smaller than 2 cm, whereas the lithic pebble component is 20 % with the size ranging up to 10 cm.



**Fig. 2.16:** *View of the coarse conglomerate in locality 215. Yellow circle marks a 1.5 m lithic clast. Blue lines and translucent white plane shows regional bedding plane.*

**Fig. 2.17:**  
*Geological map  
of "North of  
Club  
Mediterranee"  
area at Ag.  
Stefanos.*



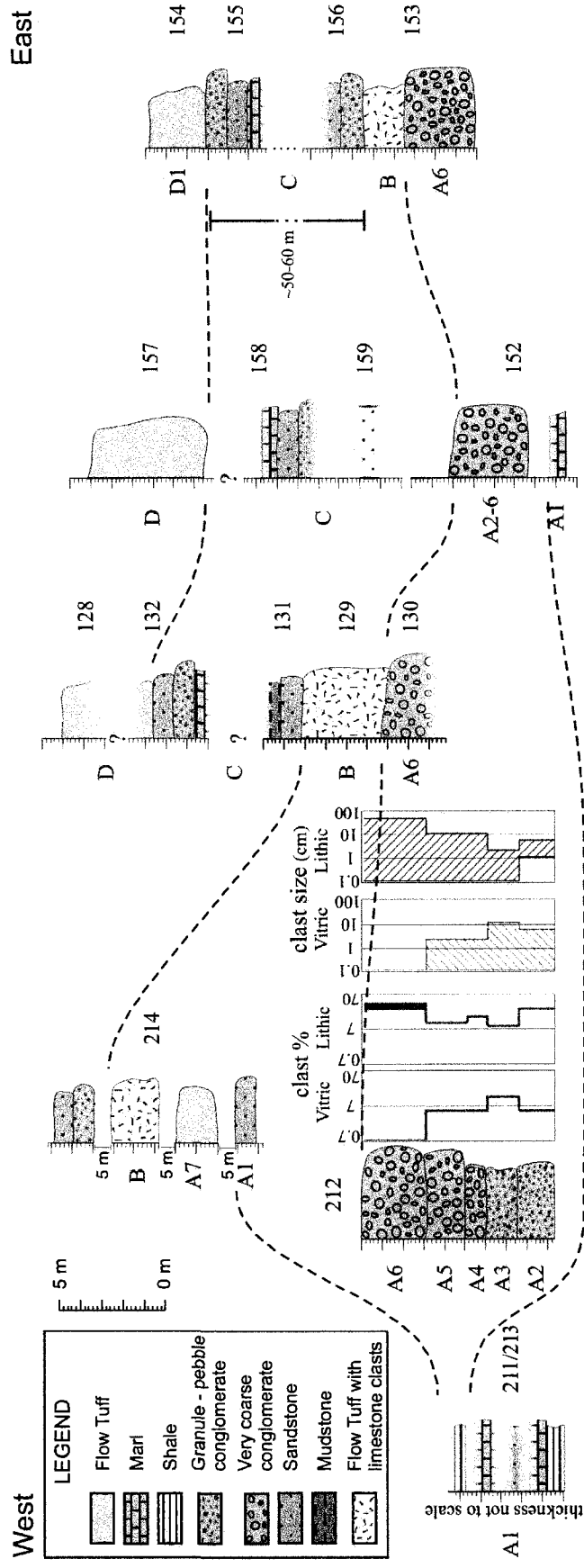


**Fig. 2.18:** Correlation of stratigraphic columns of "North of Club Mediterranee" area. The letters (A3) correspond to units and the numbers (159) correspond to localities. At locality 212, the 2<sup>nd</sup> and 3<sup>rd</sup> columns show the percentage of vitric and lithic clasts in the rock whereas the 4<sup>th</sup> and 5<sup>th</sup> columns show their size on a logarithmic scale.



**Fig. 2.19:** *Very coarse volcaniclastic conglomerate of unit A6 in locality 212. Inset shows details of the matrix.*

**A6** is a poorly sorted conglomerate characterized by upward coarsening and a lack of pumice lapilli (Figs. 2.16, 2.18). The conglomerate bed is at least 3 m thick, and consists of lithified massive lithofacies with abundant volcanic clasts 20 – 40 cm, forming a clast-supported conglomerate with volcaniclastic sandstone matrix. There are a few larger than 50 cm clasts with the largest being 1.5 m in diameter (Fig. 2.16). A similar conglomerate unit is present at localities 130, 153 and 215 (Fig. 2.19).

A7 is a pyroclastic layer which has been identified in two relatively proximal localities 300 m apart (214 and 301). It consists of a crystal lithic tuff with 2 % lithic clasts up to 20 cm. This horizon has maximum thickness 2 m and appears to pass laterally within 5 to 8 m into the sediments of A1. The superjacent lithology is unit B.

#### **Lower Pyroclastic Unit:**

B is a very distinctive bed of massive ignimbrite, representing the total Lower Pyroclastic Unit. Often the limited outcrops are related with morphological anomalies and small cliffs with absence of vegetation. The thickness varies around 3 m. The characteristic that makes this unit a marker is the fact that this ignimbrite contains abundant limestone clasts, generally up to 10 cm in size, but a 0.5 m grey limestone clast was found at locality 298. A typical outcrop contains approximately 10 % lithic clasts and a similar percentage of small lapilli size, whitish to pale greenish pumice clasts (Fig. 2.20).

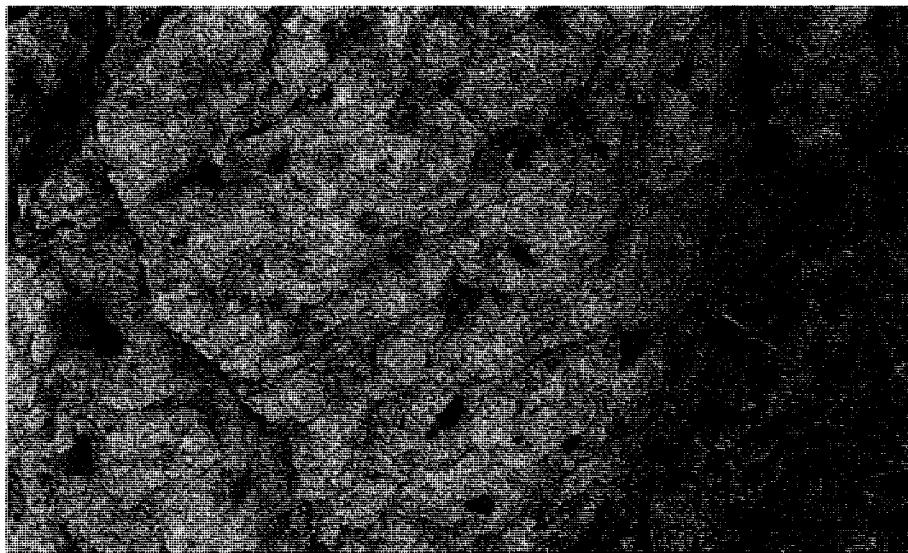


**Fig. 2.20:** *The white ignimbrite with the abundant limestone clasts.*

### **Middle Sedimentary Unit:**

**C** unit comprises a sedimentary sequence which is rather similar to unit A1, containing clastic sediments such as sandstones, conglomerates, mudstones, shales and marls.

Although unit C has great thickness, which was estimated to be between 50 and 60 m, and comprises a variety of sediments, limited outcrop and alluvial cover preclude its subdivision. These sediments occur in topographic depressions and the lower parts of the slopes, and they are oriented parallel to the strike of the beds which dip  $40^{\circ}$  –  $50^{\circ}$  toward the SE. Fine to coarse-grained **sandstones** are common in this succession.

They are often cross-bedded and generally well stratified. Usually they occur in yellowish – beige beds 5 cm to 1 m thick. Often, pebble and granule **conglomerates** are intercalated with the sandstones. They are massive to stratified and weakly lithified rocks. In places, beds are not sharply defined, but there are intervals of inclined layering, comprising rippled, cross-bedded sands. The petrography of the clasts varies. Pebbles consist of volcanic rocks, limestones, and red chert. Generally, sandstones or granule conglomerates lie immediately above unit B, but they also appear at higher stratigraphic levels. **Mudstones** and **shales** are also present in beds usually less than 1 m at various stratigraphic levels of unit C. The shales are of grey, green and reddish colours. The **marls** form relatively thin beds, 2 m or less, with nodular beds a few mm up to 10 cm thick with colour ranging from whitish to creamy and beige.

### 2.5.2 “North of Kastri – Cape Tigani”

#### **Middle Pyroclastic Unit:**

The Middle Pyroclastic Unit is visible in both sub-areas (Figs. 2.17, 2.21), but in the “North of Club Mediterranee” sub-area the basal parts are visible, whereas in the “North of Kastri” sub-area the central and topmost beds are visible. The outstanding characteristic of this unit is the white – beige color of the pyroclastic rocks.

**D1** is a tuff that rests directly on the sediments of the Middle Sedimentary Unit at locality 154 (Fig. 2.18) and consists of 20 % pumice and 5 -10 % lithic clasts mostly less than 2 cm in size. The thickness of this unit is no more than 2 m.

**D2** is not exposed. The thickness of this unit is estimated at only a few meters.

**D3** has a minimum thickness of 3 m. It is a weakly lithified, fine-grained lithic tuff, as observed in locality 134. Most of the lithic clasts are less than 1 mm, but increase near the base of the unit to up to 1 cm.

**D4** is a 2 m thick tuff including 10 % lithic clasts that range in size from 1 to 2 cm. As in bed D2, clasts coarsen (to 7 cm) toward the base. Pumice clasts comprise ~ 2 % of the rock. They are up to 15 cm long. In the upper 50 cm of the unit, the percentage of pumice reaches 5 %. Moreover, this bed shows distinctive limonitic weathering of yellowish – beige colour, especially along a complex of thin veins. Quartz crystals a few mm in size are distributed in the matrix of the tuff.

**D5** is a 3 m interval not visible due to the roadway.

**D6** is a 2 m thick crystal – lithic tuff with common quartz crystals as in Unit D4. It is composed generally of 2 % lithic clasts of less than 1 cm, but is characterized by the

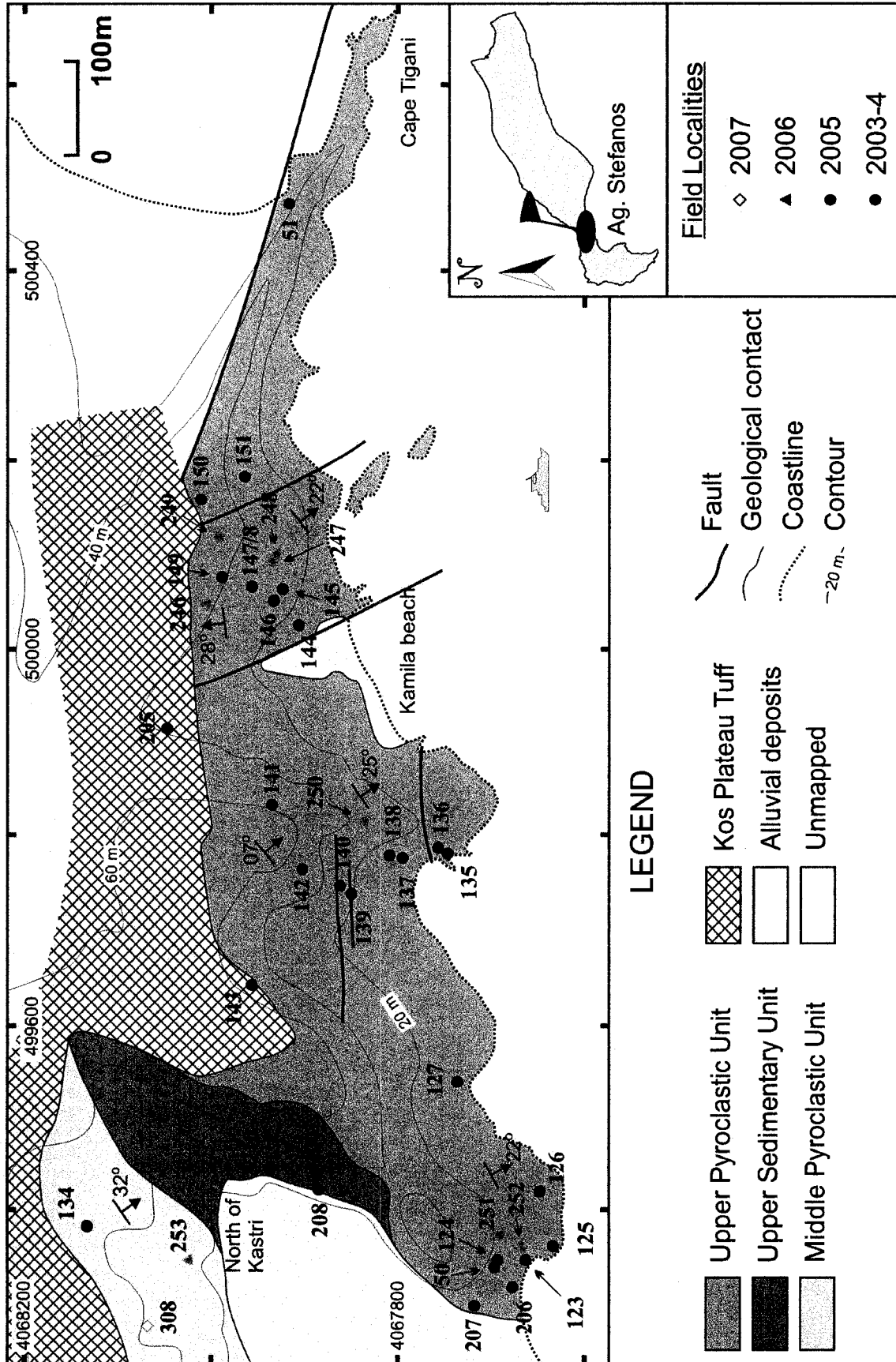


**Fig. 2.21:** Geological map of the "North of Kastri" and "Cape Tigani" areas in Ag. Stefanos.

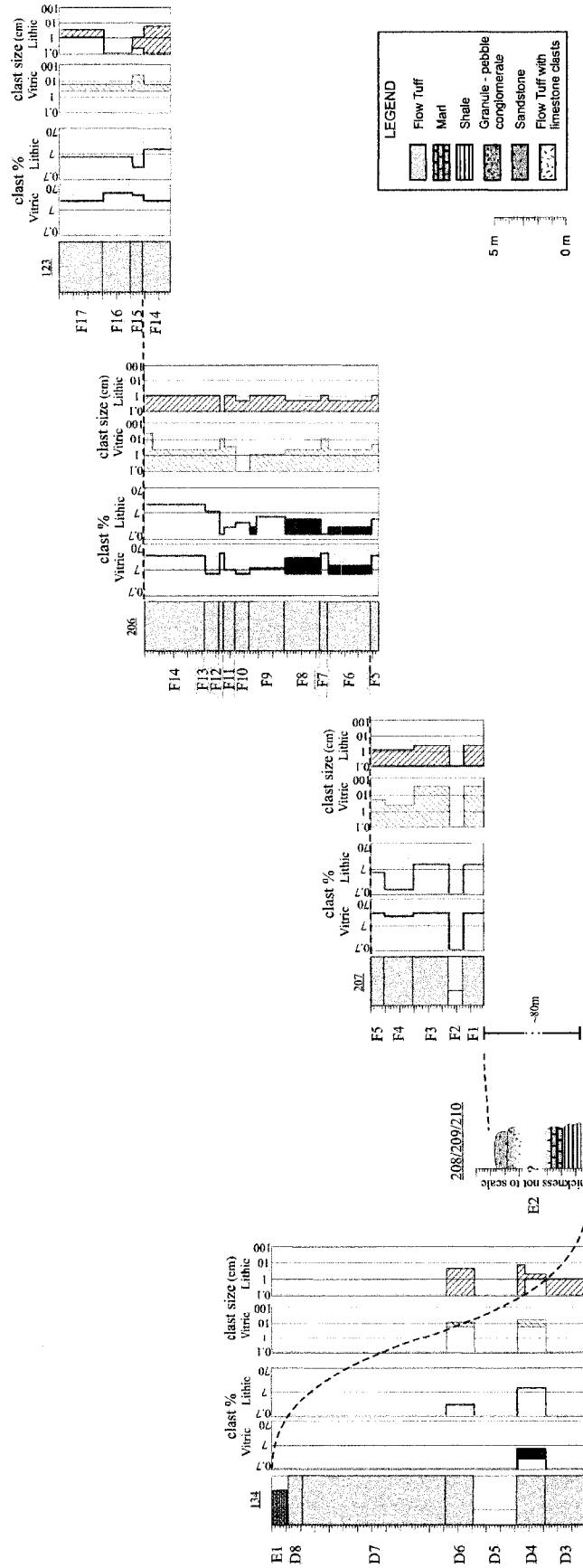


**Fig. 2.22:** Correlation of stratigraphic columns of "North of Kastri" area. The letters (F5) correspond to Units and the numbers (134) correspond to localities. The 2<sup>nd</sup> and 3<sup>rd</sup> columns show the percentage of vitric and lithic clasts in the rock whereas the 4<sup>th</sup> and 5<sup>th</sup> columns show their size on a logarithmic scale.

occurrence of 30 cm wide elongated elutriation pipes and sheets in which a high concentration of larger clasts (2-4 cm) is present.

**D7** is a very thick (~10 m) tuff unit, similar to D6, but has finer pumice. Both quartz and biotite crystals are present. In addition, the bed is cut by limonite veins, quite similar to those of D4. In the upper part of the unit, a 40 cm thick bed of black chert is present.

**D8** is a 1 m thick bed of very altered fine-grained tuff.

#### **Upper Sedimentary Unit:**

**E1** marks the top of the Middle Pyroclastic Unit and contemporaneously the base of the Upper Sedimentary Unit. It consists of very light white marl which directly and conformably overlies the pyroclastic layer of D8. Moreover, black - brown chert is also interbedded within the marl. Its largest exposure appears east of the localities 134 and 253, forming the slope of a hill. The maximum thickness is approximately 1.1 m at the top of the hill.

**E2** is the rest of the sedimentary unit. Undivided, it has similar features as the underlying sedimentary units (A1, C). Upwards, part of the succession is not exposed until a prominent outcrop of **nodular marl** in a stream. Then, there is probably 10 m or more of **green – grey shales**, and a few more marls. Above this, medium grained **sandstones** and granule - pebble **conglomerates** make resistant prominent horizons, capped by a weathered face of possibly marls and shales extending to the top of the succession (Fig. 2.23).

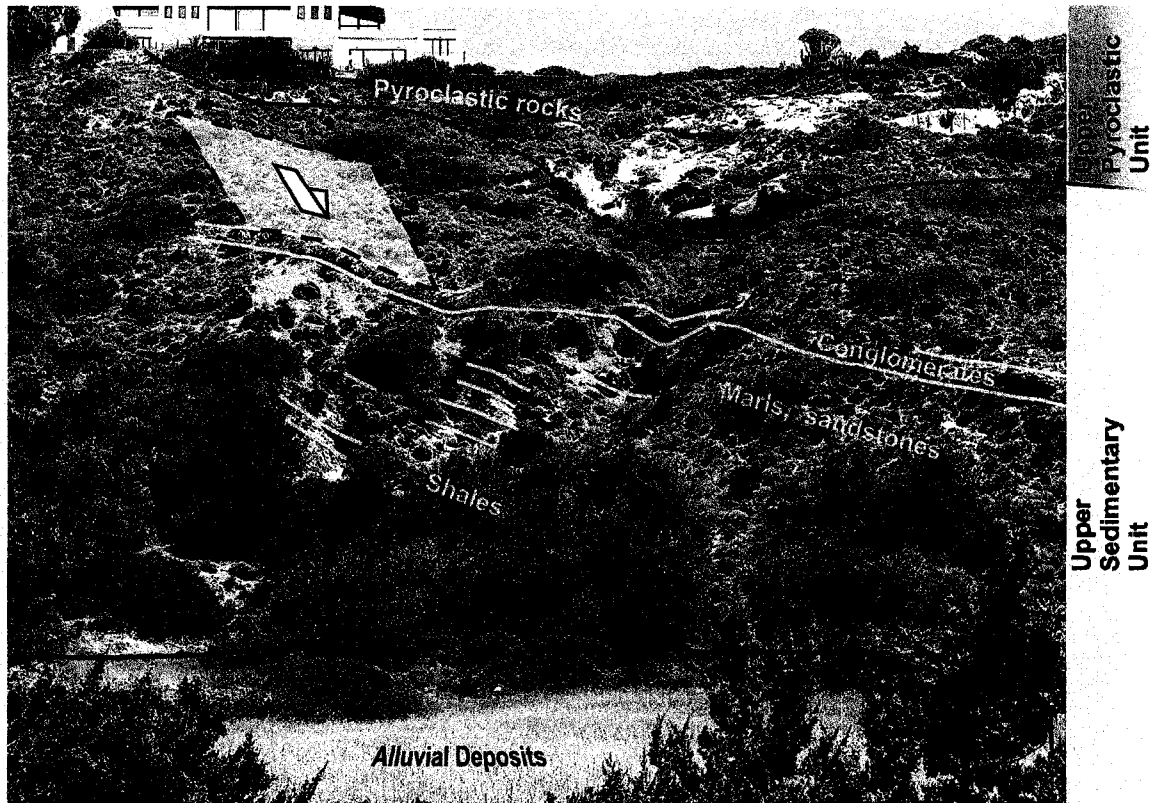


**Fig. 2.23:** *General view of the upper parts of the Upper Sedimentary Unit with shales, marls, sandstones and conglomerates, overlain conformably (upper red line) by the basal beds of the Upper Pyroclastic Unit. Translucent white plane shows regional bedding plane.*

### **Upper Pyroclastic Unit:**

The Upper Pyroclastic Unit is the most voluminous pyroclastic succession in Ag. Stefanos and generally of the Miocene on Kos. The deposits are limited between the coast line in the south and the Kos Plateau Tuff northwards, outcropping over an elongated area of 1.5 km x 0.4 km (Fig. 2.21). How much of any overlying volcanic succession might have been eroded prior to the KPT deposition is unknown. The pyroclastic succession contains also few very thin (up to few meters) laterally discontinuous intercalations of conglomerates (Fig. 2.24). The bedding dip follows the

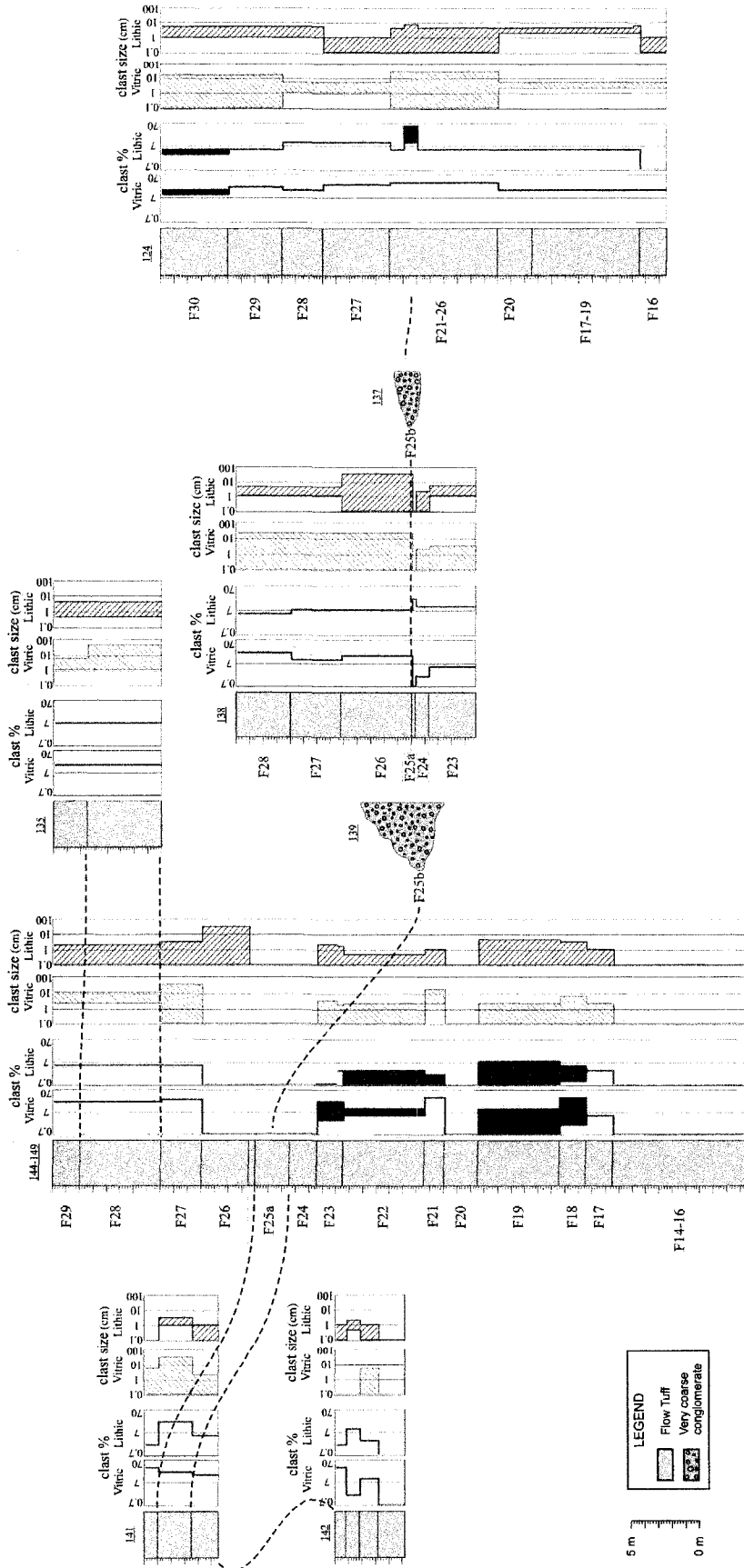


**Fig. 2.24:** Correlation of stratigraphic columns of the Upper Pyroclastic Unit of Kamila beach – Cape Tigani area.

The letters (F13) correspond to Units and the numbers (138) correspond to localities. The 2<sup>nd</sup> and 3<sup>rd</sup> columns show the percentage of vitric and lithic clasts in the rock whereas the 4<sup>th</sup> and 5<sup>th</sup> columns show their size on a logarithmic scale.

general trend of the whole area towards SE, but at locality 246 there is an opposite inclination, probably due to folding or faulting. The total thickness of this unit, measured and estimated, is about 60 to 65 m. It is a distinguishable unit that usually has beige/reddish to whitish appearance, reflecting the large amount of pumice lapilli and ash. The whole unit is formed by alternating thinner or thicker lithic rich and vitric rich beds in different proportions.

**F1** represents the base of the voluminous Upper Pyroclastic Unit of Ag. Stefanos (Fig. 2.22). It is a 1.5 m soft lithic – vitric ignimbrite with 20 % pumice lapilli mostly less than 2 cm in size and rare larger clasts. The lithic component is 10 %, mostly 1 -5 mm and a few 1- 2 cm in size.

**F2** is an approximately 1 m not exposed unit.

**F3** is very similar to F1, with its thickness around 2.5 m.

**F4** is a soft 2 m thick tuff unit that has 15 % vitric clasts less than 2 cm, containing also a few larger clasts up to 20 cm. Lithic clasts are absent.

**F5** is a 0.9 m thick tuff characterized by high resistance to erosion. It comprises 20 % vitric fragments less than 4 cm and 5 % lithic clasts less than 1 cm.

**F6** is a soft tuff unit approximately 3 m thick which includes 5 to 10 % pumice mostly up to 2 cm and 1-2 % lithic clasts mostly less than 0.5 cm.

**F7** is a thin 0.5 m resistant tuff with a high proportion (30 %) of mostly equidimensional pumice up to 10 cm and a small lithic component (less than 1 %) up to 0.5 cm in size.

**F8** is a 2.5 m thick tuff unit characterized by alternating lithic-rich and pumice rich layers. The vitric component varies from 5 to 20 %, mostly less than 2 cm, whereas the lithic material ranges from 1 to 4 %, mostly up to 0.5 cm in size.

**F9** is a 2.5 m thick cliff forming bed of tuff containing 8 % vitric clasts, mostly less than 1 cm. Lithic clasts less than 1 cm make up 5 % of the rock, decreasing to less than 2 % in the top 50 cm.

**F10** is a 1 m weakly welded tuff, including 5 % small vitric clasts and 2-3 % lithic clasts, mostly less than 0.5 cm in size.

**F11** is a 0.8 m tuff bed with 7 % mostly less than 3 cm pumice clasts and 2 % less than 1 cm lithic clasts.

**F12** is a 0.3 m thick tuff bed, very rich in large fragments of pumice of up to 10 cm in size (30 %) and rare 1 % lithic clasts. Beds F11 and F12 are cliff-forming.

**F13** is a soft almost 1 m thick tuff which contains 5 % smaller than 2 cm vitric and 8 %, mostly less than 1 cm lithic clasts respectively.

**F14** is another pumice-rich unit, 4.2 m thick, with 25 % pumice mostly no larger than 2 cm which increases up to 20 cm in the topmost 0.5 m. The lithic lapilli constitute 15 % mostly less than 1 cm in size.

**F15** was studied in locality 123 where it is a 0.8 m thick bed of pumicious tuff with 25 % pumice clasts generally up to 2 cm, but only at the base with a few 20 x 10 cm clasts in size. The lithic component includes up to 2 % black to red volcanic fragments between 0.2 – 1 cm.

**F16** is an at least 2 m thick tuff that has less pumice than unit F15, typically 15 %, as larger than 2 cm clasts. The lithic component is absent.

**F17** is a 2 -3 m thick tuff that has the same vitric clast abundance and size as in unit F16, but there is also present 5 % of black lithic clasts larger than 1 cm.

**F18** is a 2 m thick tuff bed that was studied in locality 144. It is characterized by variations in vitric and lithic clasts which constitute 2 to 30 % and 1 to 5 % of the rock, respectively. Pumice clasts can reach up to 10 cm in size, whereas lithic clasts usually do not exceed 5 cm.

**F19** is a 6 m tuff bed that also displays variations in the percentages of ejecta. Thus, vitric clasts up to 2 cm in size make up between 0 and 15 % and lithic clasts up to 5 cm in size between 0 and 10 % of the rock.

**F20** is a 2 – 3 m of soft purplish vitric tuff.

**F21** is another pumicious bed 1.5 m thick, with 30 % of pumice clasts generally 10 to 15 cm in size. It also contains 2 % lithic clasts 1 cm or less, but only in the lower part of the unit.

**F22** is an approximately 6 m thick tuff bed including 5 to 10 % vitric clasts up to 2 cm, and 0 to 5 % lithic clasts less than 0.5 cm in size.

**F23** can be divided into two subunits. The lower 0.5 m thick subunit includes 3 % fine vitric and 3 % lithic clasts, both less than 2 cm in size. The 1.5 m thick upper subunit shows an increase in pumice clasts to 20 %, mostly up to 3 cm in size. On the contrary, the lithic clast component decreases and does not exceed 1 %.

**F24** is a soft vitric tuff that is poorly exposed and about 2 m thick.

**F25a** is a unit rich in lithic lapilli. This distinctive bed contains 20 % pumice clasts mostly 1 to 3 cm in size with few of 30 cm, and 20 % lithic clasts of the same size (at locality 141). Laterally, there are important variations not only in thickness but also in the

composition of this unit, with variable abundances of vitric and lithic components. This unit passes laterally into F25b, which is a coarse conglomerate. The coarse lithic bed was used as stratigraphic marker, correlating very similar beds between different sections (124, 138, 141 and 147) (Figs. 2.25, 2.27a)

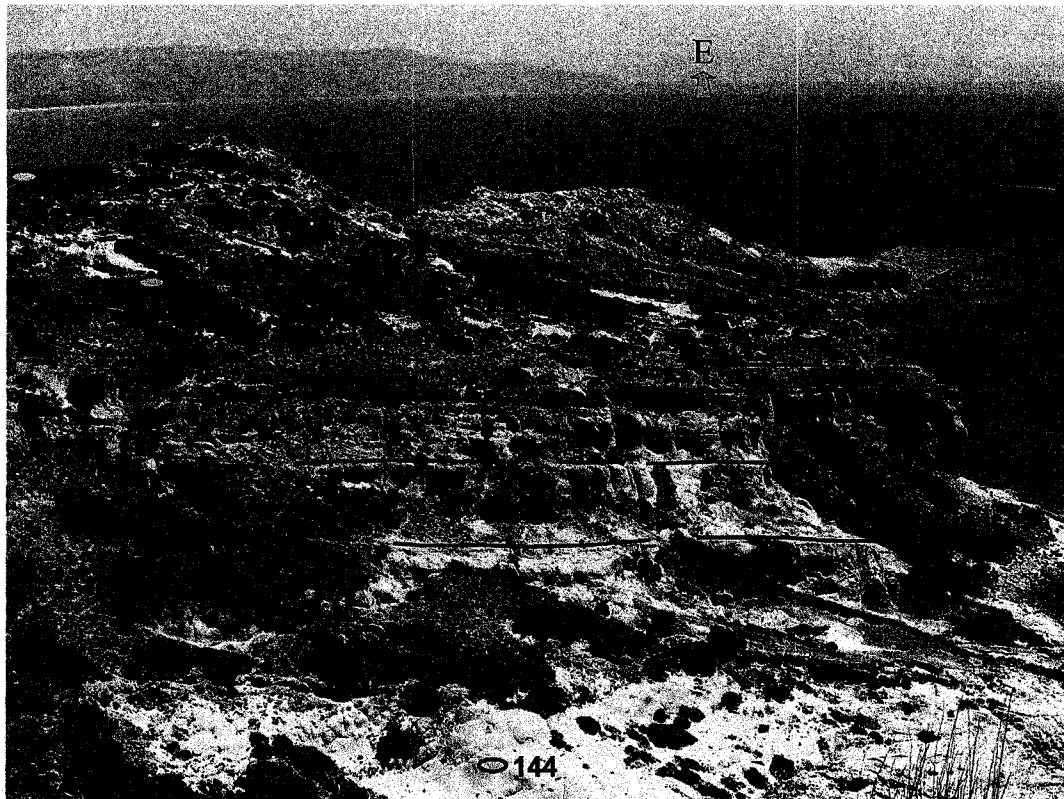


**Fig. 2.25:** *Panoramic view of the upper beds of the Upper Pyroclastic Succession. The position of bed F25a is marked as well as studied localities. The repetition of bed F25a is related to a fault (invisible in the photograph) in-between the two hillcrests.*

**F25b** is a coarse volcanoclastic conglomerate with variable thickness from 0 to 6.2 m.

This conglomerate is present at localities 137 and 139 and directly rests on erosional surfaces with ridges and grooves of the subjacent pyroclastic deposits. The conglomerate consists of rounded greenish, reddish, purplish and grey volcanic clasts of a variety of sizes, from a few millimetres up to 15 cm and rarely up to 40 cm at the

base of the bed. The proportion of lithic material is very high, approaching 85 %, producing a dark brown, cliff-forming layer. The lithofacies is massive and unstratified and the contact with the surroundings is sharp (Fig. 2.26). However, close to the areas where the unit fades out laterally, the lithic material shows progressive degradation to smaller clasts and higher proportion of fine grained matrix. This fine



**Fig. 2.26:** *View of north end of the clast supported conglomerate (F25b) embedded in pyroclastic deposits at locality 137. A normal fault (red line) with vertical slickenlines offsets the lithologies for about 50 cm. Translucent white plane shows plane of fault.*

**cgl:** *Conglomerate.*

matrix appears either as a coarse lithic sandstone or as yellowish fine tuffitic material. The fact that this unit is a distinguishable horizon led to the recognition of tectonic discontinuities such as normal faults with offsets from a few centimetres to several meters. For example, the fault shown in Fig. 2.26 dips to the NNE ( $55^{\circ}/018^{\circ}$ ) with

vertical slickenlines, whereas at locality 139, a major fault dips in the opposite direction (to S - 66°/175°) with oblique slickenlines to 200°.

**F26** is an approximately 3 – 5.2 m thick vitric-lithic tuff. The vitric clast component is 15 % with clasts typically 20 cm and the lithic clasts can reach up to 30 cm in size.

**F27** is another vitric-lithic tuff, 3 to 5 m thick, with higher proportion of pumice (25 %) of larger sizes (up to 30 cm), and a lower concentration of lithic clasts (5 %), but with much smaller clasts up to 3 cm.

**F28** is a 6 m thick tuff bed similar to unit F27 (Fig. 2.27b). It contains 20 % vitric clasts 2 to 10 cm in size and the same percentage (5 %) of lithic clasts, mostly less than 2 cm in size.

**F29** is a tuff with 2 to 4 m variable thickness and is lithologically comparable to F28.

**F30** is the upper most preserved bed of the whole pyroclastic succession and is a vitric – lithic lapilli tuff at least 5 m thick. The vitric clast component is 25 %. These clasts are mostly between 1 to 5 cm in diameter, whereas the lithic fragments are almost all less than 1 cm, and make up ~10 % of the bed.

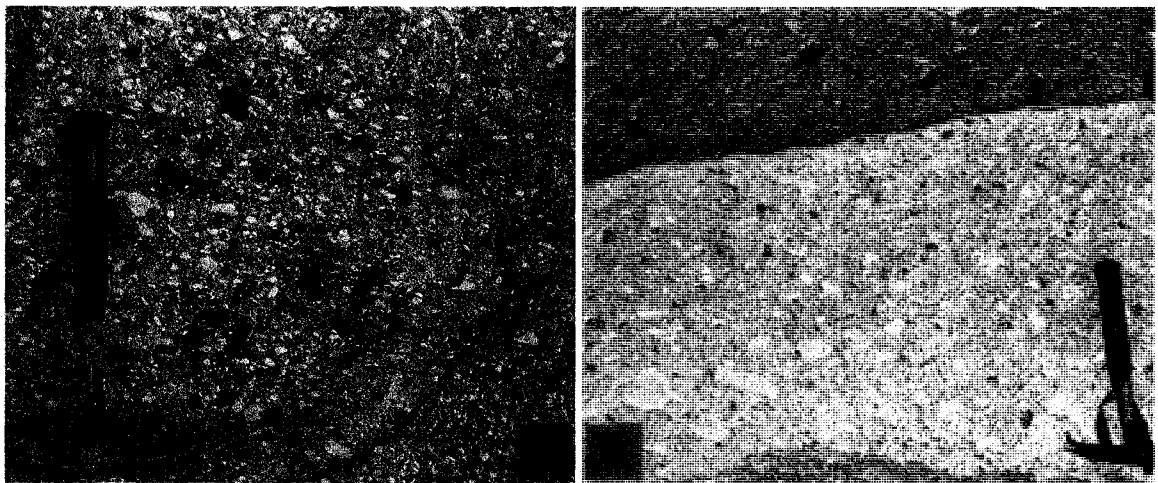


**Fig. 2.27:** a) Typical lithology of vitric-lithic tuff of Unit F25a at locality 206.  
b) Outcrop of vitric- lithic tuff of bed F28 (locality 149).

## **2.6 Volcanic stratigraphy of Ag. Fokas**

The Ag. Fokas area, in south-eastern Kos (Fig. 2.1), hosts significant outcrops of Upper Miocene pyroclastic deposits. These pyroclastic deposits are particularly well exposed near “**Ag. Fokas**” where the outcrops extend from the coastline towards the north until the hillcrest of the very first mountain chains, as well as in a limited outcrop located inland, approximately 500 m to the north labelled as “**North of Ag. Fokas**”, where the pyroclastic rocks are interbedded with sediments.

The **alpine basement** in the area consists of limestones and dolomitic limestones of Lias to Middle Cenomanian age. These limestones are overlain by a metasedimentary succession of phyllites and sandstones. Together, they represent the Upper Tectonic Unit (Triantaphyllis, 1998). The basement outcrops, and especially the carbonate rocks, form steep hills at the western and north-western part of the study area (Fig. 2.28).

### **2.6.1 “Ag. Fokas”**

#### **Lower Sedimentary Unit:**

The Lower Sedimentary Unit forms a significant part of the cliffy coastline. This succession is many tens of meters thick. It contains sandstones, marls and pebble conglomerates (Units A1-A3), that have variable dips toward north to the eastern exposures (localities 278/281), and towards southwest to the western outcrops (localities 228, 230/277/280). The following units are presented from base to the top of the succession.

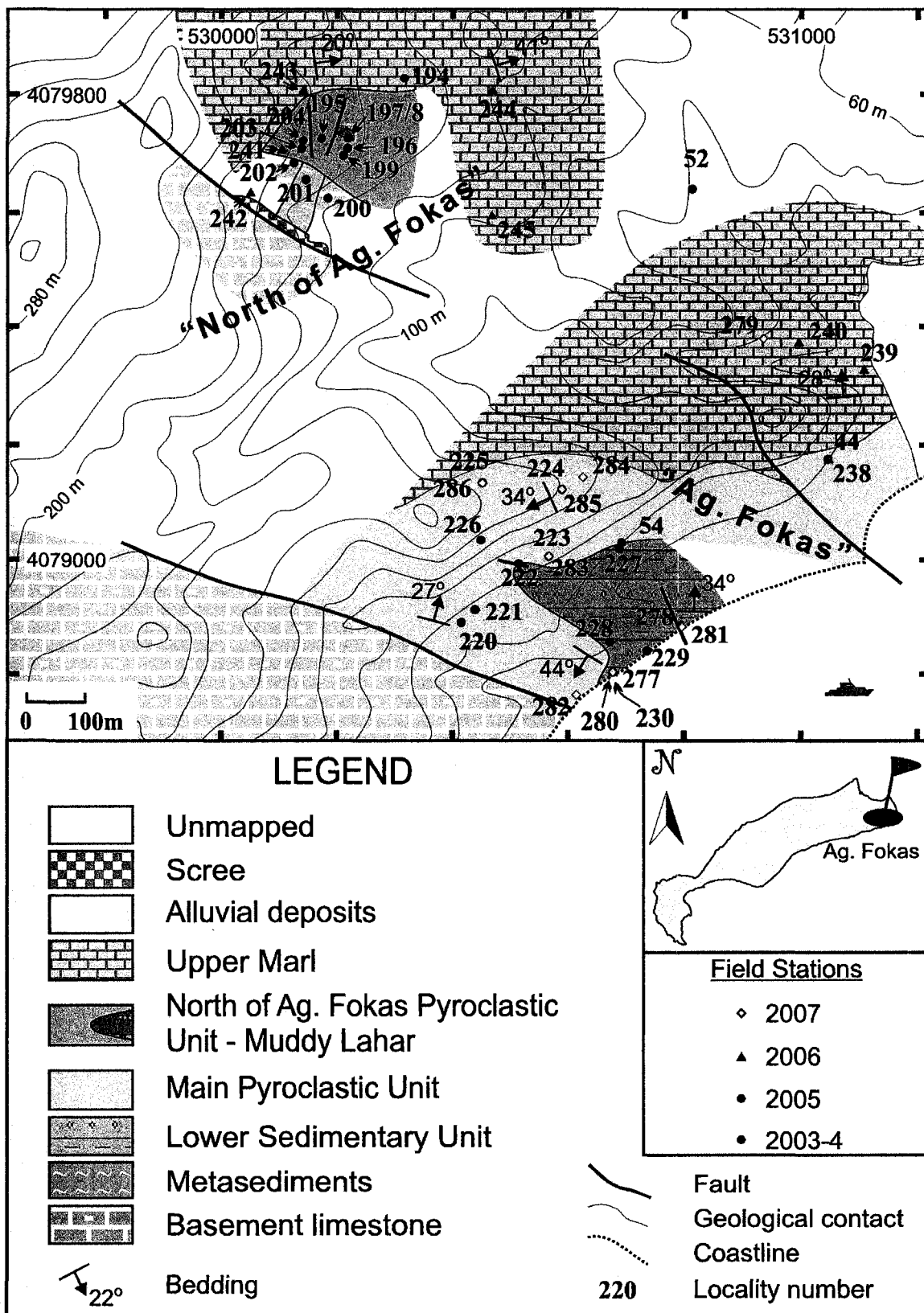


**Fig. 2.28:** Geological map of the “Ag. Fokas” and “North of Ag. Fokas” sub-areas.



A1 is at the base of the unit. It consists of massive indurated whitish marl at locality 281, right on the coastline (Fig. 2.30). The visible thickness is less than 2 m and its exposure is limited, because the western edge is faulted with a several meters offset, and to the east it dips below sea level.

A2 is a unit of clastic sediments about 10 m thick (Fig. 2.29). At the base there is a 40 cm thick polymictic pebble conglomerate with up to 5 cm clasts (Fig. 2.30b, c). This conglomerate and the lower part of the directly overlying lithology are mostly covered by a 1 m red mudstone paleosoil. Right above this pebble conglomerate, there is at least 3 m of medium grey – green sandstone and granule conglomerate that has a matrix similar to the sandstone (Fig. 2.30a, b). Both lithologies alternate in beds ranging from 5 to 20 cm in thickness, with the sandstone predominant. This is overlain by no more than 5 m of poorly exposed grey mudstone.

A3 is a thick creamy marl, many tens of meters thick. Beds appear to be up to 10 cm thick, showing significant ductile deformation with radius of curvature from few millimetres to many meters. Some of this deformation is syn-sedimentary and some is post-sedimentary or tectonic. Both types of structures were identified in the upper horizons and the syn-sedimentary structures are discussed in chapter 5. This unit is well exposed along the coastline. The upper 7 m also outcrop near locality 230, and the lower 5 m near locality 278. On the contrary, the middle part of the unit is nowhere visible due to lack of proper rock exposures; however, the total thickness

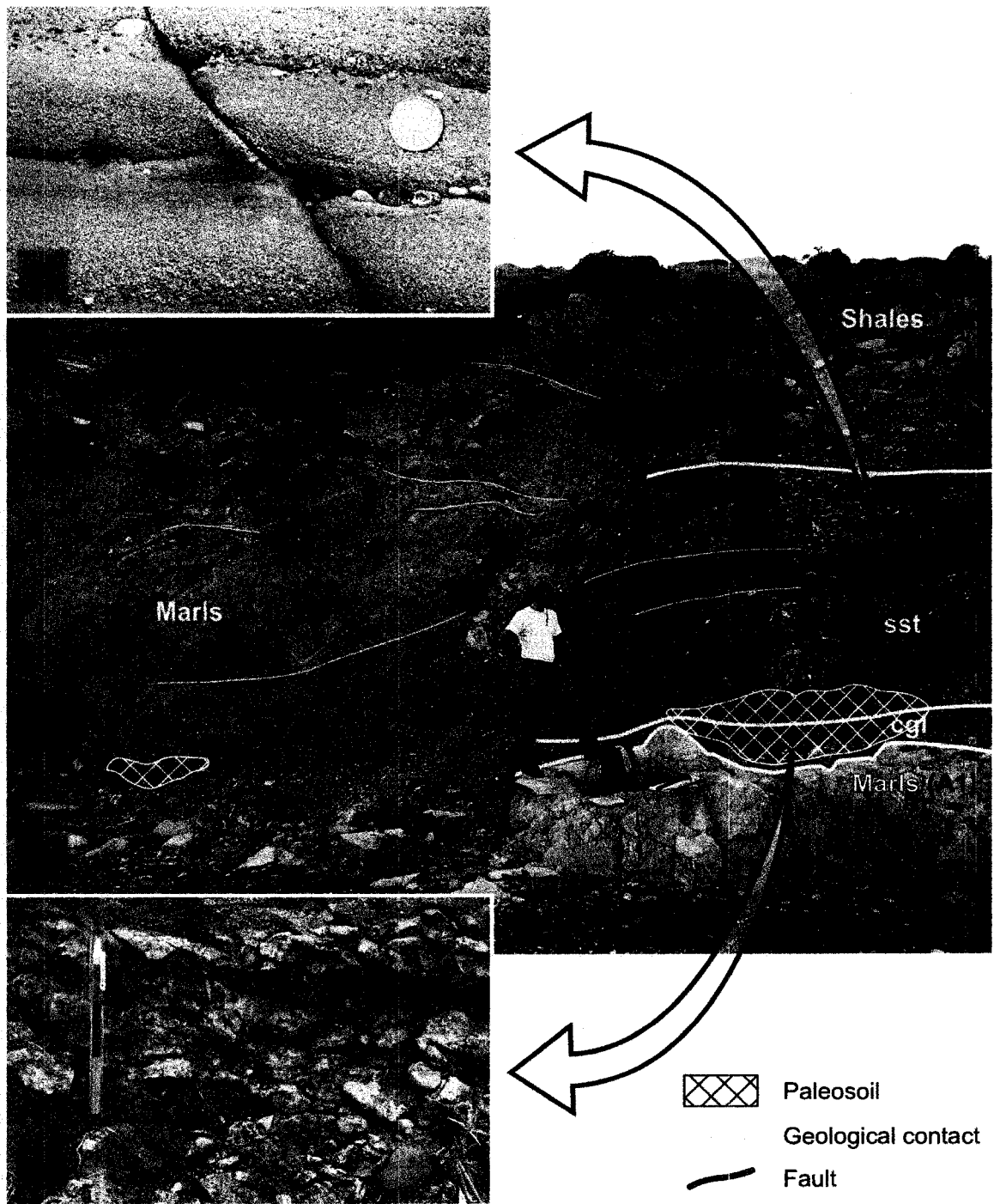


**Fig. 2.30:** *The basal part of the Lower Sedimentary Unit, viewed at locality 278/281.*

- a) *Detailed photograph of the sandstone and granule intercalations.*
- b) *General view of the stratigraphic and tectonic contacts of the sediments.*
- c) *Detailed photograph of the pebble conglomerate, partially covered by paleosil.    sst: Sandstone, cgl: Conglomerate.*

was estimated according to bed dip and outcrop extent to be a few tens of meters. The upper part was studied for fossiliferous horizons but with no success. In addition, the upper part of the succession close to locality 229 contains  $\leq 1$  cm beds of gypsum as well as intercalations of grey or reddish shales. Approximately 5 m below the contact with the pyroclastic unit, two  $\sim 1$ -2 cm thick lithic-vitric tuffs are interbedded, having brown weathering.

### **Pyroclastic Unit:**

**B1** is the basal unit of the Pyroclastic Unit. It is a bedded air-fall tuff that conformably overlies the marls (A3) of the Lower Sedimentary Unit at locality 230 (Fig. 2.31). It is up to 1.3 m thick, and is thinly layered (1 mm to 1 cm). The layers of the air-fall tuff that are close to the base and the subjacent marls are apparently slump-folded. In addition, remobilized parts of this air-fall tuff with a few decimetres thick beds are structureless.

**B2** is a 2.3 m thick bed of vitric-lithic tuff, mainly whitish – yellowish in colour. It contains  $\sim 10$  % vitric clasts and 3 % lithic clasts, each up to  $\sim 1$  cm in diameter. This layer is not massive, but there are lateral variations to rafts of marl, 4 m long and up to 40 cm thick.

**B3** is a 5 m thick tuff bed that shows an increase in lithic clast component compared with unit B2. Pumice in this bed is of similar abundance to unit B2 ( $\sim 10$  %), mostly flattened and up to 2 cm long, but lithic clasts make up less than 20 % of the rock, with individual clasts up to 3 cm. 10 cm below the top of the bed, there is a large raft of marl approximately 4 m long and 40 cm thick.

**B4** is a 4.7 m tuff bed with variable concentrations of vitric and lithic clasts. Pumice makes up 5 to 20 % of the rock, occurring up to 2 cm long flattened sherds. On the other hand, lithic clasts are of the same size throughout the bed and make up 3 % of the rock.

**B5** is a 0.4 m thick light purple fine vitric-crystal tuff. Pumice clasts occupy ~ 4 % of the rock. Lithic fragments are small (< 4 mm). A few centimetres of bedded marl occurs at the base of the bed.

**B6** is weathered or sheared vitric tuff that is about 0.8 m thick.

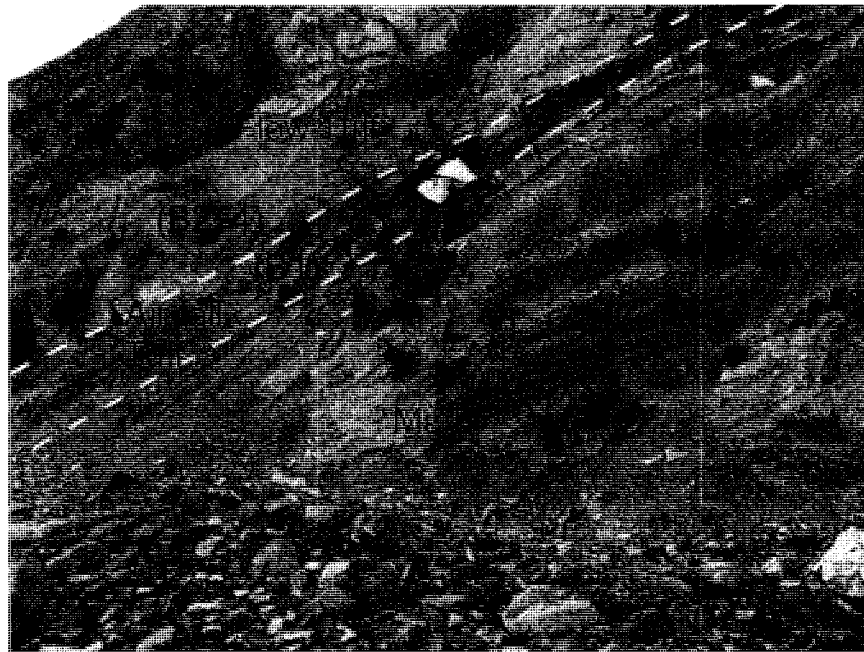


**Fig. 2.31:** *General view of the contact between the Lower Sedimentary Unit and the bottom beds of the pyroclastic succession at locality 130.*

**B7** is a 2 m thick, massive vitric tuff with the same percentage (4 %) of vitric clasts as unit B5, that are up to 3 cm in size in this bed. Small lithic clasts up to 4 mm in size make up 2 % of the bed. Some isolated quartz crystals are present.

**B8** is again a massive lithic-vitric tuff, 2 m thick. Flattened pumice clasts up to 2 cm long comprise ~ 6 % of the volume of the rock. Lithic clasts, mostly ranging between 1 and 4 cm, make up 5 % of the rock.

**B9** is a 0.3 m thick lithic-vitric tuff, with a slight increase in pumice to 8 % compared with unit B8 and a trivial decrease to 4 % of lithic clasts (less than 2 cm in size).

**B10** is a distinctive 3.2 m pink pyroclastic horizon, also identified in nearby sections (locations 223, 230). The basal part of the unit is pumice rich, close to 15 % of 1 to 5 cm pumice clasts, which decreases upwards to 4 – 5 % of vitric material.

**B11** is a light purple approximately 1.8 m thick tuff bed. Pumice clasts make up 7 % of the rock with clasts less than 1 cm. The lithic clasts are up to 4 mm and make up 2 %.

**B12** is again a soft purple tuff, 4.2 m thick. This tuff has the characteristic that in the upper one meter, large lenticular concretions with brownish – beige weathering, are present (Fig. 2.32a). In the rest of the unit, 5 % pumice clasts less than 3 cm and 2 %

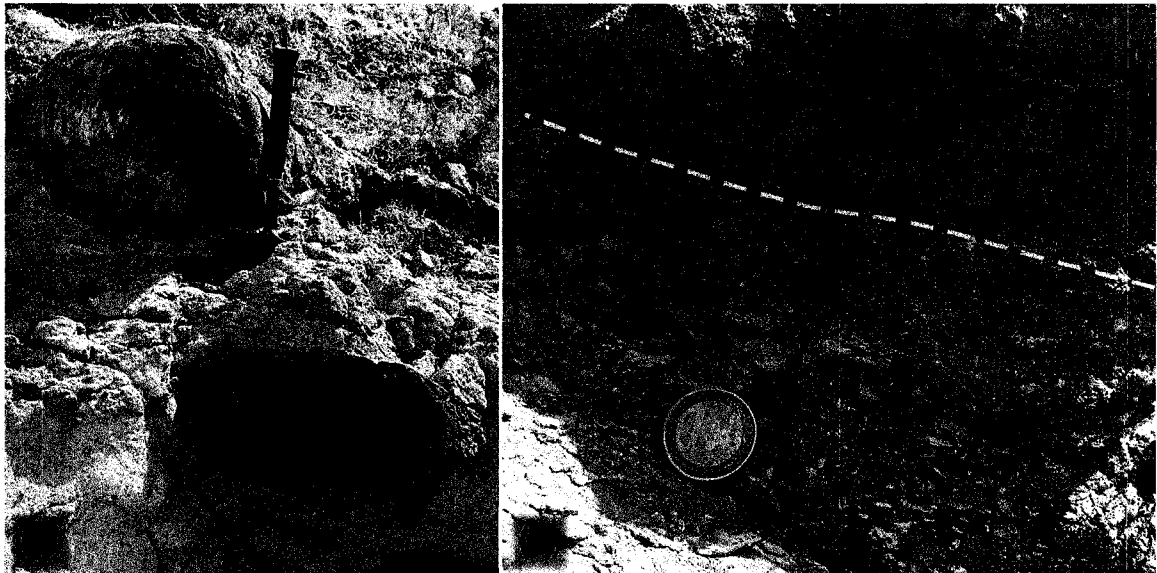


**Fig. 2.32:** a) *Lenticular to spherical concretions into flow tuff on bed B12.*  
b) *Contact between the subjacent vitric tuff (B17) which is overlain by well stratified air-fall beds (B18).*

lithic clasts, mostly less than 2 mm but some 5 mm, are present.

**B13** is a 3.4 m unit that is not exposed.

**B14** is a 0.6 m welded pumice lapilli tuff with 8 % flattened vitric clasts mostly less than 1 cm long and rarely attaining 3 cm. This concentration of pumice in combination to the presence of ash results in a light pink colour of unit B14. Moreover, rare isolated crystals including biotite are visible.

**B15** is a 1.1 m thick fine-grained tuff. The lowermost 10 cm of the bed is stratified with successive alternations of layers with ~50 % pumice and layers lacking pumice. The rest of the bed is massive, with 3 % of subequal pumice mostly up to 0.5 cm and 5 % lithic clasts up to 0.5 cm.

**B16** is a 4.2 m thick grey lithic-vitric tuff with variable proportion of vitric and lithic lapilli. At its base, 10 % or more subequal flattened pumice clasts up to 8 cm are present. The lithic component (10 %) is represented by clasts less than 1 cm in diameter. At superjacent parts of this bed, pumice clasts (7 %) have the same dimensions as below, and lithic lapilli remain approximately the same percentages but the size of the clasts increases up to 3 cm.

**B17** is a 0.9 m thick vitric tuff, with 20 % of vitric clasts usually up to 5 cm in size (Fig. 2.32b). On the other hand, lithic clasts are generally absent, composing  $\leq 1$  % of the rock, and are small (2 mm). Some crystal fragments of less than 4 mm were also observed.

**B18** is only 7 cm thick but is a well stratified, medium to very fine grained tuff. It appears to comprise several air-fall beds (Fig. 2.32b).

**B19** is a pumice-rich deposit 2.2 m thick. The lower 0.8 m contain 20 % pumice clasts, whereas the superjacent part has 60 % vitric material, mostly between 1 and 3 cm. Lithic clasts make up only 1 % of the rock, mostly up to 2 mm, with a few clasts up to 0.7 cm in size.

**B20** is well lithified brown-weathered fine-grained crystal tuff 0.2 m thick.

**B21** is another pumiceous bed with 40 % vitric clasts mostly less than 1 cm. Lithic clasts are rare (up to 1 %) and average 4 mm in diameter.

**C1** is characterized by change in facies from pyroclastic deposition to terrigenous sedimentation. It is a 0.55 m unit of medium sandstone with some marl intercalations.

**C2** is a 0.6 m thick, very hard bedded marl.

**D1** is the basal unit of renewed pyroclastic sedimentation. It is a 0.6 m thick very vitric tuff. Pumice clasts make up 60 % of the rock with subequal clasts of no more than 2 cm in diameter. Very rare lithic clasts and crystal fragments were recognized.

**D2** is a 0.35 m fines- rich tuff with sparse vitric or lithic clasts.

**D3** is an extremely pumiceous 0.15 m bed that has up to 70 % pumice clasts less than 5 mm in diameter.

**D4** is a 0.15 m fissile tuff bed with flattened pumice, resulting in "streakiness" parallel to bedding.

**D5** is a very thin 0.05 to 0.15 m bed of either volcanoclastic granule conglomerate with vitric and lithic clasts, or a tuff. The rock type identification was uncertain.

**E1** marks the base of a marl unit. It is a 0.07 m thick fissile marl.

**E2** is a 2.2 m thick hard marl, in places silicified, that contains abundant gastropods and other identified macro-fossils. This horizon, together with E1, forms a very

characteristic stratigraphic marker that was very useful during field work for lateral correlations with individual sections (Fig. 2.33).

**F1** is a 6 m thick bed of weakly lithified light green vitric tuff. Pumice clasts make up 10 % of the rock with clasts less than 1 cm. Lithic clasts show little increase in both size and concentration from the base to the top where clasts reach 4 % and are smaller than 2 cm.

**F2** is a vitric-rich and lithic-poor 1.6 m pyroclastic deposit. Large pumice clasts, with some of them flattened, up to 10 cm, make up 15 % of the rock, whereas the lithic clasts make up only 2 % and are up to 1 cm in diameter.

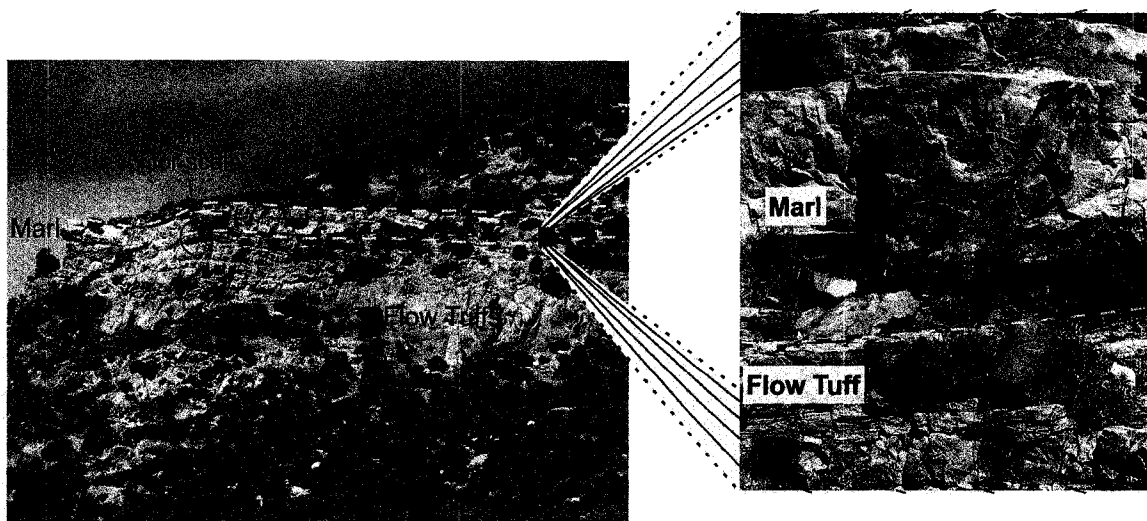


**Fig. 2.33:** a) *General view of the distinctive marl (E1, E2).*

b) *Detailed photograph from the contact of the fine-grained tuff and the superjacent massive marl.*

**F3** is a 1.6 m thick cliff-forming rubbly tuff. The pumice component continues to increase upwards from F1, reaching 15 %, with clasts up to 2 cm. A similar trend

appears also for the lithic component, with clast concentration of 3 % and size less than 8 mm.

**F4** is at least 2 m thick and similar to unit F3, but less well lithified.

**G1** is a 0.9 m thick bed of medium sandstone.

**G2** is a 1.43 m thick interval that is not exposed.

**H1** marks the return to pyroclastic deposition. It is a less than 0.35 m thick tuff bed containing 30 % pumice clasts mostly up to 1 cm, but some larger up to 3 cm. The lithic clasts represent 2 % of the rock and are <2 cm in diameter.

**H2** is a tuff bed, 0.22 m thick, in which pumice clasts make up only 3 % of the rock, mostly up to 0.5 cm and the lithic clast component is 1 %, with clasts less than 3 mm.

**H3** is a weakly stratified 1.35 m thick cliff-forming tuff. The vitric fragments represent the 10 % of the bed with a flattened shape and up to 3 cm in size. The lithic fragments constitute 4 % and are <4 cm in diameter.

**H4** is a poorly exposed and soft vitric-lithic tuff, approximately 1.5 m thick. It is very similar with the stratigraphically underlying H3 unit, but is softer.

**I1** is a poorly sorted volcanoclastic coarse sandstone bed about 2 m thick.

**I2** is an unexposed stratigraphic interval estimated to be 1.5 m thick.

**J1** continues the pyroclastic deposition with a 0.2 m bed of soft, light purplish, vitric tuff.

**J2** is a 1.7 m well lithified vitric tuff bed that consists of 35 % pumice clasts, with most of them flattened and 1 to 4 cm in size. The lithic clasts make up 3 % and they are not more than 1 cm in diameter.

**J3** is a white vitric tuff, 2 m in thickness. Generally, the vitric clast concentration varies between 5 and 8 % with the largest clasts up to 10 cm. The lithic clasts are up to 1 cm

in diameter and occupy 1 to 3 % of the rock. In the lowermost 50 – 70 cm, there are brown-weathering, irregular concretions. Furthermore, there are subvertical sheets with dimensions 40 cm high by 50 cm long, by 10 cm wide of high concentrations of large lithic clasts up to 10 cm in diameter.

**J4** is a white vitric tuff 0.6 m thick, with 5 % large pumice up to 20 cm in diameter.

There are no lithic clasts.

**J5** is a 5 m thick bed of light purple vitric-lithic tuff. The vitric clasts are 8 % of the rock, with rarely flattened pumice up to 6 cm and the lithic clasts also constitute 8 % of the rock, with clasts mostly from 1 to 4 cm in diameter.

**J6** is a tuff bed at least 6 m thick with 3 to 4 % vitric clasts, generally less than 2 cm, and 7 % of lithic clasts, mostly up to 1 cm, but some approaching 3 cm.

**J7** is an unexposed stratigraphic interval estimated to be 4 m thick.

**J8** is a 0.5 m bed of white tuff. It contains 2 % of small pumice clasts up to 1 cm in diameter and 1 % of lithic lapilli, also up to 1 cm.

**K1** is a nodular and massive to laminated marl 1.7 m thick.

**K2** is a 1 m thick bed of bedded, clast supported conglomerate, with a few 1 to 3 cm thick intercalations of sorted medium to very coarse sandstone. The lowest part is pumiceous, containing 1 cm vitric clasts, whereas the upper parts have similar pumice too, but also abundant 5 mm lithic clasts (Fig. 2.34).

**K3** is a 1.5 m poorly exposed succession which seems to be similar to K2.

**L1** is the stratigraphically uppermost pyroclastic bed of the main succession in Ag.

Fokas. It is 1.4 m thick, containing quite variable proportions of pumice clasts, from 5 to 60 %, with clasts less than 3 cm in size. Lithic clasts are rare (1 %) and of less than

2 mm size. The pumice in this tuff contains biotite phenocrysts. The field interpretation indicated that it is a sandy lahar.

**M1** is a 0.15 m thick sorted granule conglomerate, which contains 60 % vitric and 40 % lithic clasts.



**Fig. 2.34:** *The upper part of the clast supported conglomerate (K2) with abundant 5 cm lithic clasts.*

#### **Upper Sedimentary Unit:**

The Upper Sedimentary unit directly overlies both the thick Pyroclastic Unit of Ag. Fokas and the pyroclastic rocks at North Ag. Fokas. It consists mostly of whitish to beige marls. These beds are thicker and more lithified close to the base with some 50 cm or more thick beds, and thinner towards the upper stratigraphic horizons with beds typically only 10 cm thick. The upper and thinner beds, especially close to “North of Ag. Fokas” appear to be relatively deformed (folded). The Upper Sedimentary Unit extends over a

large part of the study area, forming either topographical depressions or highs. Its thickness is estimated at a few tens of meters.

### 2.6.2 “North of Ag. Fokas”

The “North of Ag. Fokas” sub-area is located north-northwest inland from the “Ag. Fokas” sub-area, at between 120 and 220 m elevation above sea level (Fig. 2.28). The field study indicated that there is a limited outcrop of pyroclastic rocks, approximately 250 m long by 200 m wide which overlies the alpine basement (limestones, metasediments) in the SW and is covered by the Upper Sedimentary Unit. The thickness of the pyroclastic rocks does not exceed 20 m. The lithologies appear rather tectonized by several faults trending N – S to NE – SW. Furthermore, abundant limonitic and calcite veins cut the pyroclastic rocks, and the calcite veins appear to be the younger of the two.

N1 is the unit at the base of the pyroclastic succession (Fig. 2.35). It is a 1.5 m thick lithic tuff with 3 % lithic clasts up to 1 cm in diameter.

N2 is also a 1.5 m lithic tuff with 15 % of the same size lithic clasts as in N1.

N3a is a crystal vitric tuff, probably 2 m thick.

N3b is a characteristic unit of grey muddy lahar (Fig. 2.36). Sparse lithic clasts, mostly between 1 and 5 cm, are present within a greyish muddy matrix. The maximum thickness is more than 4 m, but it thins out laterally into the tuff of unit N3a.

Numerous calcite-filled veins are present, possibly related to shearing.

N4 is an almost 4 m thick poorly exposed white vitric tuff.

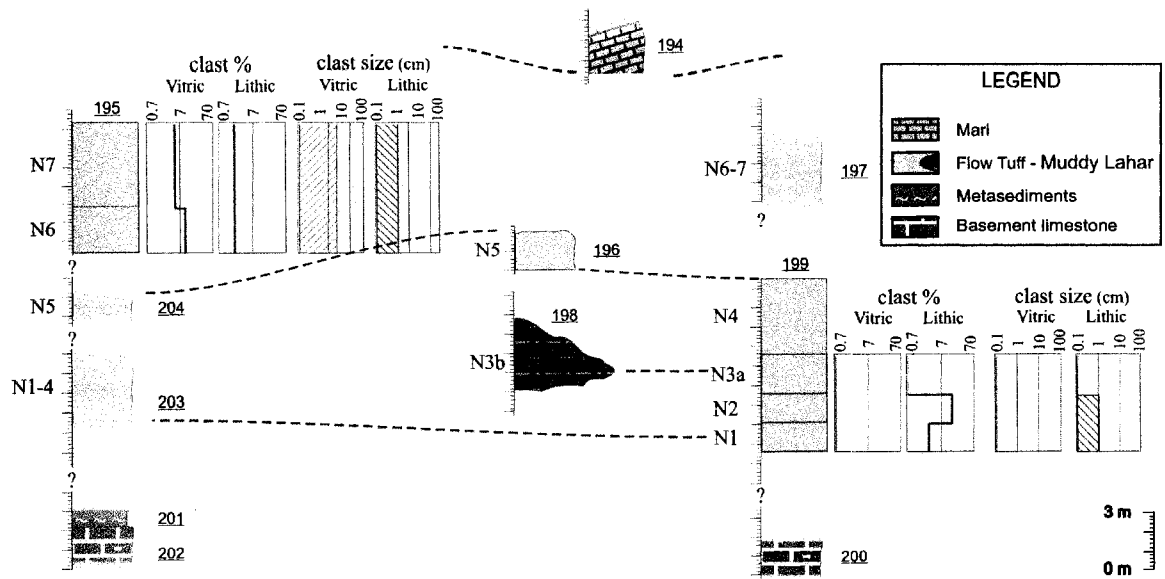


**Fig. 2.35:** Correlation of stratigraphic columns of North of Ag. Fokas sub-area. The letters (N1) correspond to Units and the numbers (203) to localities. The 2<sup>nd</sup> and 3<sup>rd</sup> columns show the percentage of vitric and lithic clasts in the rock whereas the 4<sup>th</sup> and 5<sup>th</sup> columns show their size on a logarithmic scale.

**N5** is a 1.5 m thick, purplish to pinkish densely welded crystal tuff. The vitric fraction occupies 5 % of the rock, occurring in clasts up to 1 cm in diameter, whereas lithic lapilli (1 %) are up to 5 mm. Additionally, the crystal component is very high, including both quartz and biotite.

**N6** is a bed at least 2.5 m thick, of vitric-lithic tuff that does not directly overlie layer N5. Probably, few meters of unexposed tuff are intercalated. It contains roughly 10 % of vitric clasts less than 5 cm and 2 % of mostly up to 4 mm in diameter.

**N7** The topmost bed is a 4.5 m thick vitric-lithic tuff. The abundances of vitric and lithic clasts are 5 % and 2 %, respectively, and they are similar in size to those in unit N6.

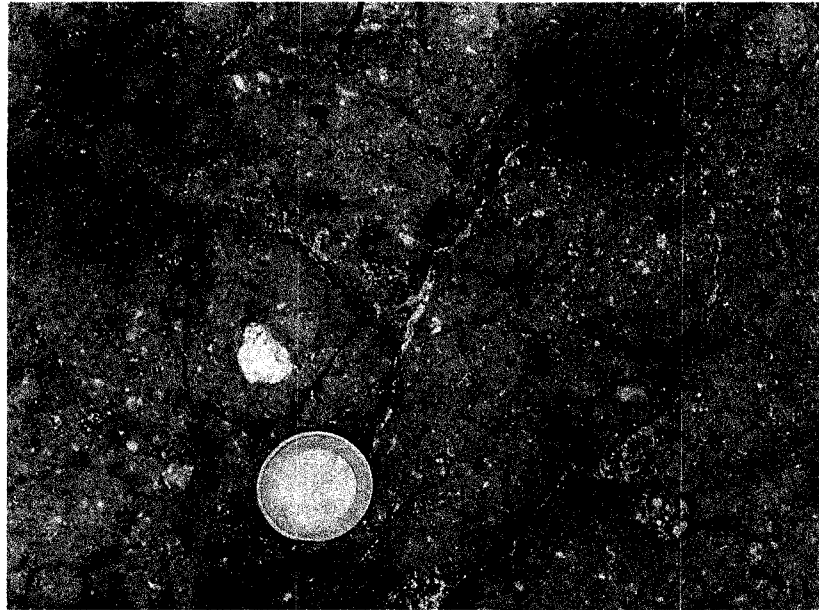


**Fig. 2.36:** *Muddy lahar in North of Ag. Fokas sub-area, containing sparse lithic clasts within the grey matrix.*

## CHAPTER 3

# *Petrography*

### **3.1. Introduction**

In this chapter, the petrography of the Miocene volcanic rocks of Kos is described. These include the lava flows and domes from Tripa and Prof. Ilias and the lithic clasts from the pyroclastic rocks from Ag. Stefanos and Ag. Fokas (Figs. 1.2, 2.1). The main purpose of this chapter is to study and consequently to compare lithic clasts from different localities spatially and stratigraphically, in order to examine possible correlations between the Ag. Stefanos and Ag. Fokas pyroclastic successions. Furthermore, the clast petrography will help constrain the source of the ignimbrites from the domes and lava flows of Tripa and Prof. Ilias, or from more distal localities. In Patmos (Fig. 1.3), Late Miocene volcanic rocks of the “Old volcanic series” have been dated at 7.4 Ma (Fitikas et al., 1976), and thus are younger than the pyroclastic rocks of Kos. However, these dated rocks may not necessarily be the oldest volcanic rocks on Patmos. The volcanic centre of Bodrum peninsula was active between 8.6 to 12 Ma (Piper & Piper, 2002). Bodrum is a possible source for the ignimbrites of Kos as well. Lithic clasts were studied macroscopically and microscopically, and categorized into

groups according to their mineral assemblages and textures. They were compared with samples from the lava flows and domes.

## **3.2 Methods**

### **3.2.1 Macroscopic division of lithic clasts**

During field work, tens of lithic clasts were collected from individual beds of the pyroclastic successions both at Ag. Stefanos and Ag. Fokas. These clasts were washed in water and grouped according to their macroscopic appearance and texture. For example, sample CS 111 is a collection of 22 lithic clasts from a specific bed of the North of Ag. Fokas succession, that was divided into seven groups, labelled as CS 111(1), CS 111(2) and so on. Further study relied on thin sections.

### **3.2.2 Thin section preparation**

A total of 93 thin sections of both volcanic and pyroclastic rocks were prepared. Rock samples were cut into slabs, using a larger and a smaller trim saw. A face of the slab is smoothed more and is glued to the glass slide. Afterwards, the part of the slab rock from the opposite side of the glass has to be removed with a fine trim saw. Finally, the outside was polished, reducing the topographic anomalies and thickness. Unfortunately, the polished thin sections that are used for electron microprobe analyses are often thicker than the optimum which is 30  $\mu\text{m}$  for normal covered thin sections, causing less transparency and higher order birefringence colours.

### **3.3 Petrographical description of lithic clasts**

The examination of the thin sections and comparison with the groups into which the handspecimens of lithic clasts were initially divided, allowed a classification into types based on petrographical characters that are independent of geography or stratigraphic setting (Tb. 3.1). For instance, type A contains porphyritic rocks with microcrystalline groundmass whereas, type C has a glassy supported groundmass. In addition, a rare mineral contained only in few samples, such as olivine, characterizes an individual type (type D). Consequently, types such as A1 and A2 indicate minor differences in major minerals and/or differences on the proportion of phenocrysts, microphenocrysts, and groundmass.

#### **3.3.1 Type A1**

Type A1 clast lithology is a trachyte which macroscopically is porphyritic to aphanitic with grey to reddish colour. Microscopically it has fine to medium-grained interlocking crystals, represented by the samples CS 137(3) and 160(5). It contains phenocrysts of sodic and potassic feldspar as well as rare brown biotite and green clinopyroxene that is mostly subhedral. The microcrystalline groundmass consists of columnar laths of feldspars without any preferred direction of feldspar alignment. Zoning in feldspar phenocrysts is present but not common. In addition, there is significant amount of microphenocrysts of opaque minerals dispersed in the rock. Orthopyroxene and apatite were recognized as accessory minerals. The main characteristic of group A1 is that groundmass occupies large amount of the rock, even more than 50 %.

### 3.3.2 Type A2

Type A2 is the most common petrographical type of clast in the studied rocks. With the naked eye it appears to have a porphyritic texture and a groundmass colour ranging from light red–grey [CS 61, 64, 75, 138(2), 160(1)], light grey [111(2), 111(5), 111(6)], and dark grey [68, 76, 111(1), 137(1), 137(2), 142(3), 143(1), 143(4)], to brown [137(4), 138(5), 141(2)]. A whole rock geochemical analysis of sample CS 68, classifies it to trachyandesite field (Fig. 4.1). Although it is petrographically similar to the previous group (A1) containing the same phenocrysts and microphenocrysts minerals, the proportion and the size of the ferromagnesian minerals, and to a lesser extent the feldspar, is higher (Fig. 3.1). The feldspar phenocrysts and microphenocrysts mainly consist of plagioclase, but alkali feldspar is also present. The phenocrysts of plagioclase are commonly embayed and often dusty due to alteration to dusty opaque oxides. The samples 137(1) and 143(1) show plagioclase with spongy and boxy cellular textures. Some resorbed plagioclase crystals are also present. Clinopyroxene and biotite typically occur as euhedral to subhedral crystals. Clinopyroxene is a pale green pyroxene rarely zoned. Biotite appears brown to green in colour, but often it shows alteration which varies from moderately opaque rims to entire replacement of the original crystal. Locally, biotite crystals appear bent.

The microcrystalline groundmass has trachytic texture and consists of opaques and feldspars, but it is too fine-grained to determine the nature of the feldspar. In some samples it appears flow banded, with feltic–pilotaxitic texture (e.g. thin sections 142(3), 143(1)) with randomly oriented feldspar laths. In addition, several veinlets of reddish–

brownish oxides penetrate the rock. Orthopyroxene, muscovite, calcite and zircon are present as accessory minerals.

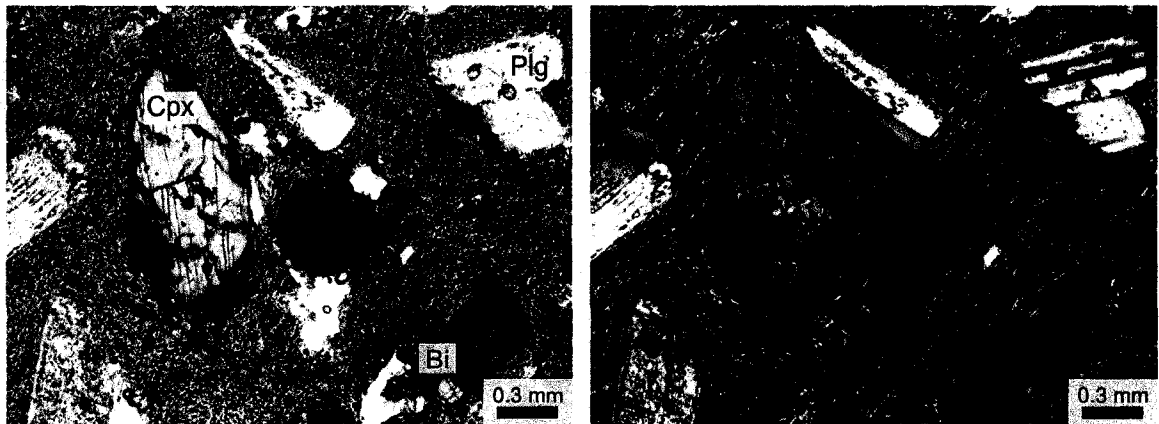


**Fig. 3.1:** *Microphotographs which show a typical andesitic rock of A2 clast lithology with plagioclase (Plg), clinopyroxene (Cpx) and biotite (Bi) phenocrysts in a pilotaxitic groundmass, in plane polarized light (left) and cross polarized light (right) (sample CS 76, 50x).*

### 3.3.3 Type A3

Type A3 clast lithology is a trachyandesite with pale brownish groundmass [CS 66, 115]. The only major mineral is plagioclase feldspar. Alkali feldspar is possibly present in a pilotaxitic groundmass, but cannot be identified with certainty due to their small grain size (Fig. 3.2). Accessory phases include subhedral phenocrysts of biotite and clinopyroxene as well as microphenocrysts of orthopyroxene and apatite. Feldspars and clinopyroxene are unaltered; however, biotite crystals have opaque rims. Sample CS 115 is very altered with ubiquitous chlorite, mainly in the form of spherulites.

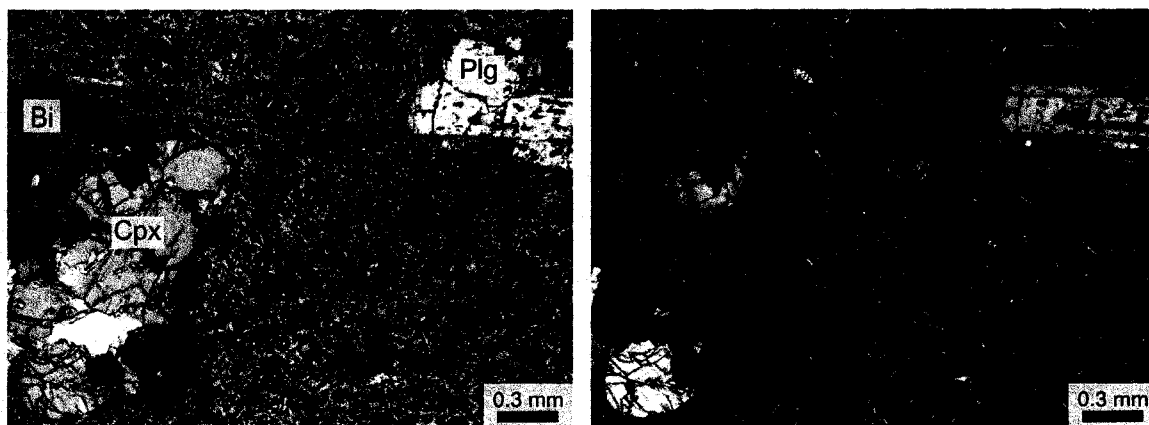


**Fig. 3.2:** *Microphotographs of a typical trachyandesite of type A3 with plagioclase (Plg), greenish clinopyroxene (Cpx) and brown biotite (Bi) phenocrysts in a microcrystalline groundmass of mostly feldspar. The left photograph is under plane polarized light and the right under cross polarized light (sample CS 66, 50x).*

### 3.3.4 Type A4

This type of clast consists of a vesicular trachyandesite of dark brown colour [CS 42, 43, 83, 138(1)]. The majority of the phenocrysts are subhedral twinned plagioclase, commonly zoned. Alkali feldspars are lacking. Euhedral to subhedral phenocrysts and microphenocrysts of greenish clinopyroxene are also present, rarely zoned. Brown biotite, as euhedral to subhedral phenocrysts and microphenocrysts, is an accessory mineral.

The groundmass consists of fine-grained macroprismatic subhedral microlites of feldspar, too small to identify precisely. This groundmass has trachytic texture, with its crystals aligned subparallel to the outline of the phenocrysts. Furthermore, irregularly shaped vesicles are abundant in this trachyandesite (Fig. 3.3).

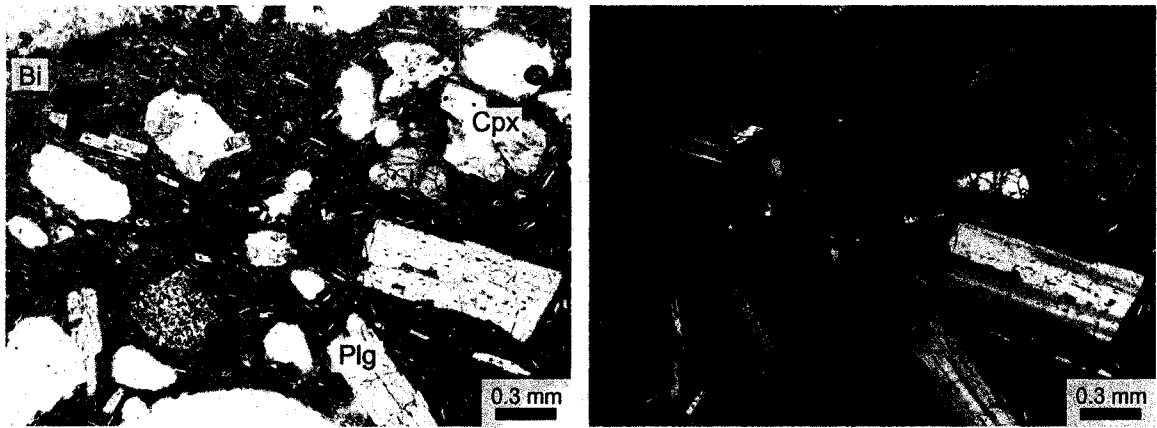


**Fig. 3.3:** *Microphotographs of a vesicular trachyandesite of type A4. Plagioclase (Plg), clinopyroxene (Cpx) and brown biotite (Bi) phenocrysts are present in a very fine crystalline groundmass of feldspar microlites. The left photograph is under plane polarized light and the right under cross polarized light (sample CS 83, 50x).*

### 3.3.5 Type B1

Type B1 clast lithology is a probably brown rhyolite [CS 142(1), 142(2), 148(1), 148(2)], characterized by abundant microcrystalline groundmass containing alkali feldspars (sanidine) phenocrysts and possibly quartz. There are also few microphenocrysts of clinopyroxene and biotite.

### 3.3.6 Type B2

Type B2 clast lithology also seems to be a rhyolite [CS 141(3), 141(4), 143(6)]. The colour is grey, but whitish – yellowish in the altered samples. Plagioclase phenocrysts appear euhedral to anhedral with albite twinning and occasionally zoned with a thin rim and showing sieve texture mostly in the cores. A few zoned subhedral alkali feldspars are

also present. Feldspars are embayed and extremely fractured. Biotite crystals are widespread with opaque rims of variable thickness (Fig. 3.4).

This type comprises porphyritic rocks with a microcrystalline groundmass made up of feldspar and possibly quartz, but identification is difficult because the samples are heavily altered and the thin sections are thick. Extensive zones of yellowish oxides penetrate both groundmass and crystals. Accessory phases include microphenocrysts of zircon and muscovite.

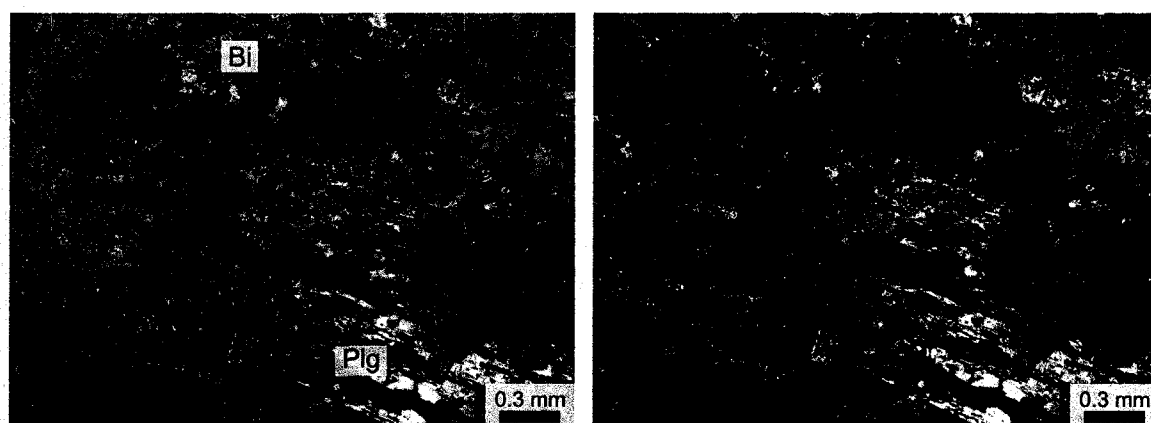


**Fig. 3.4:** *Microphotographs of relatively altered sample of clast type B2. Plagioclase (Plg) forms phenocrysts to microcrystalline groundmass and biotite (Bi) rims are altered to fine dusty opaque minerals, in plane polarized light (left) and cross polarized light (right) (sample CS 143(6), 50x).*

### 3.3.7 Type C

The samples CS 91, 93, 111(7), 138(6) and 160(4) represent type C clast lithology, which is probably a rhyodacite. Although it shares similar mineralogy with type B, it is a hypocrySTALLINE and highly porphyritic rock (Fig. 3.5). The phenocrysts and

microphenocrysts are plagioclase and in many cases also alkali feldspar (?sanidine), commonly showing an interlocking texture. Both feldspar types are euhedral to anhedral with common thick bands of zoning. Many zoned feldspar crystals show sieve texture in their intermediate zone. Greenish clinopyroxene occurs as euhedral to subhedral phenocrysts and microphenocrysts, rarely zoned. Biotite is also a major mineral of these rocks. It occurs mostly as unaltered with euhedral and subhedral phenocrysts and microphenocrysts that are often bent. Apatite, zircon and orthopyroxene are the accessory minerals.

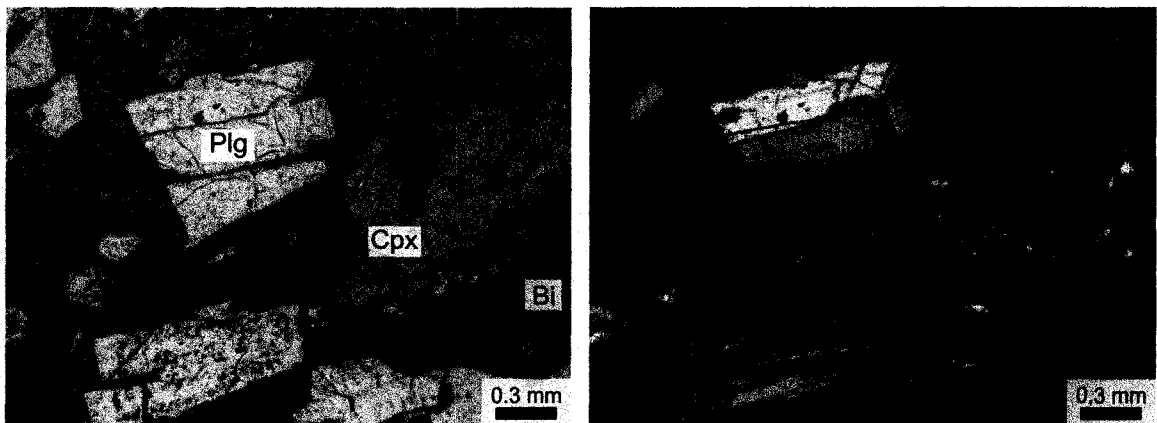


**Fig. 3.5:** *Microphotographs of clast type C which show phenocrysts of plagioclase (Plg) and clinopyroxene (Cpx), and microphenocrysts of biotite (Bi) in flow banded glassy brownish groundmass. On the left plane polarized light and on the right cross polarized light (sample CS 93, 50x).*

The glassy groundmass has a brown colour, containing microlites of feldspar and mostly biotite, forming hyalopilitic texture. Biotite microlites show a preferred elongation direction and follow the flow banding of the glass. The flow commonly parallels the outline of large phenocrysts.

In sample CS 93, there are medium-grained crystals which are clustered in glomeroporphyries with rounded shape. Most of these glomeroporphyries comprise clinopyroxene with lesser amount of feldspars, opaque minerals and brown glass.

### **3.3.8 Type D**

This type is comprised of lithic clasts containing olivine as either a major or an accessory mineral [CS 62, 77, 78, 80, 81, 84, 148(3)]. Macroscopically the samples are porphyritic microgranular rocks with reddish to greyish groundmass and phenocrysts of feldspars and clinopyroxene, with variable degree of alteration.

Under the microscope, abundant laths of plagioclase phenocrysts commonly have spongy cores and clear rims or the opposite. Euhedral to anhedral alkali feldspar is also present at least in small quantities. Zoning in both types of feldspars is very rare.

Clinopyroxene is also abundant with euhedral to subhedral phenocrysts and microphenocrysts, showing wide zoning. Biotite is ubiquitous except for sample CS 84.

Olivine is the determinant mineral of this type. It appears both as an accessory [CS 62, 80, 81] and as a major mineral in samples CS 77, 78 and 84 (Fig. 3.6). Olivine phenocrysts are olive-green to brown in PPL and appear mostly subhedral. The crystal habit was used to identify olivine entirely altered to dusty brown minerals [CS 77, 78].

Common accessory phases are apatite, orthopyroxene and zircon.

The microcrystalline groundmass consists principally of laths of feldspars, showing pilotaxitic texture, but in CS 84 trachytic texture. There are also small patches of altered dark brown and dusty glass.

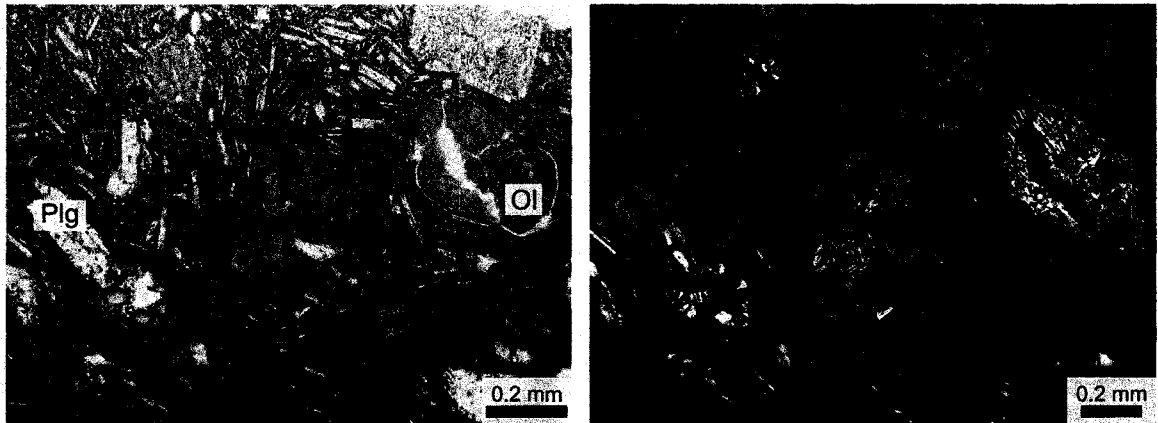


**Fig. 3.6:** *Microphotographs of clast type D. Subhedral to unihedral crystals of olivine (Ol) are present together with plagioclase (Plg) phenocrysts and microlites under plane polarized light (left) and cross polarized light (right) (sample CS 84, 100x).*

### 3.3.9 Type E

The presence of hornblende in both highly porphyritic and trachytic samples (CS 41, 44, 90, 92, 143(5), 160(2), 160(3)) is characteristic of type E clasts. Hornblende is typically brown or olive green occurring as euhedral to subhedral microphenocrysts.

Plagioclase and alkali feldspars phenocrysts and microphenocrysts show interlocking texture and extensive zoning, often throughout the whole crystal. Sieve texture with wide bands of dark rims is widespread in feldspars. In addition to the prominent marginal zoning, feldspars show lines of small inclusions. Green clinopyroxene lacks zoning, but many crystals show poikilitic texture and numerous inclusions of very small crystals of apatite, devitrified glass and other undetermined minerals. The elongated inclusions are arranged in trails parallel to the outline of the phenocrysts. Brown and green subhedral phenocrysts and microphenocrysts of biotite are relatively abundant.

These samples accommodate medium-grained glomeroporphyritic aggregates of clinopyroxene. In addition, feldspars, biotite and opaque minerals are also present. Brown oxides are ubiquitous in the rock, but appear to be more abundant in these glomeroporphyritic aggregates.

Apatite and orthopyroxene are present as accessory minerals. The groundmass is hyalopilitic with minute crystals of feldspars and biotite and brown glass. Flow banding is visible locally.

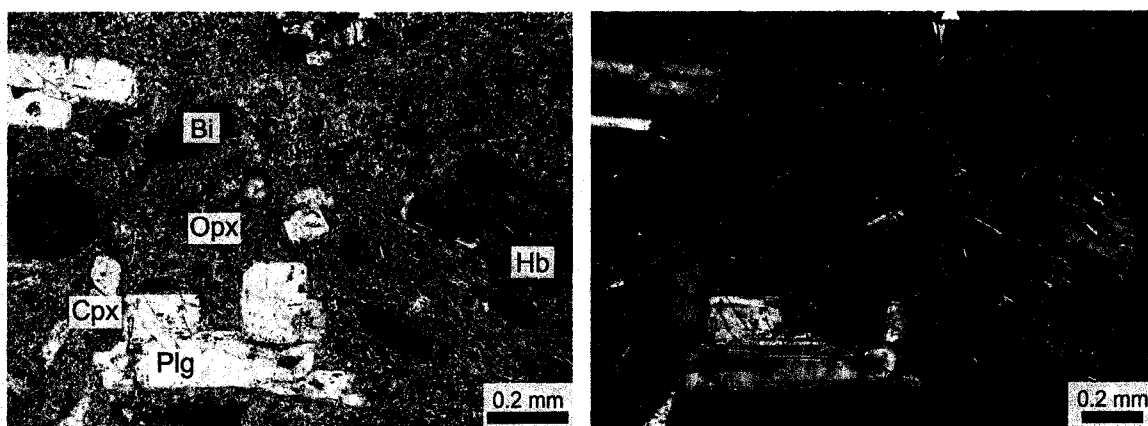


**Fig. 3.7:** *Microphotographs of an example of clast type E. Phenocrysts of hornblende (Hb), plagioclase (Plg), biotite (Bi), clinopyroxene (Cpx) and orthopyroxene (Opx) in a trachytic microcrystalline groundmass, in plane polarized light (left) and cross polarized light (right) (sample CS 143(5), 100x).*

### 3.3.10 Type F

Type F is represented by only one sample (CS 67), which seems to be a basaltic trachyandesite, but unfortunately it is very altered to dusty opaque minerals. It has porphyritic texture with phenocrysts and microphenocrysts of plagioclase and clinopyroxene, the latter is often zoned. Primary quartz crystals are present but

Type	Phenocrysts & microphenocrysts	Texture	Samples
A1	Plg + K-feld ± Cpx ± Bi	Porphyritic rock with microcrystalline groundmass and pilotaxitic texture.	137(3), 160(5)
A2	Plg ± K-feld + Cpx ± Bi	Porphyritic rock with microcrystalline groundmass and pilotaxitic texture, very high proportion of groundmass.	CS 61, 64, 68*, 75, 76, 111(1), 111(2), 111(5), 111(6), 137(1), 137(2), 137(4), 138(2), 138(5), 141(2), 142(3), 143(1), 143(4), 160(1)
A3	Plg ± Cpx ± Bi	Porphyritic rock with microcrystalline groundmass and pilotaxitic or trachytic texture.	CS 66*, 115*
A4	Plg + Cpx ± Bi	Porphyritic rock with microcrystalline groundmass and trachytic texture.	CS 42*, 43*, 83, 138(1)
B1	Plg + K-feld + Cpx ± Bi + ?Qz	Porphyritic rock with microcrystalline groundmass with trachytic texture of groundmass.	CS 142(1), 142(2), 148(1), 148(2)
B2	Plg + K-feld + Bi + ?Qz	Porphyritic rock with microcrystalline groundmass of feldspar and possibly Qz.	CS 141(3), 141(4), 143(6)
C	Plg + K-feld + Cpx + Bi	Porphyritic and highly porphyritic rock with hyalopilitic texture.	CS 91*, 93*, 111(7) and 138(6), 160(4)
D	Ol + Plag + Cpx ± Bi	Pilotaxitic rock with microcrystalline groundmass.	CS 62, 63, 77*, 78*, 80*, 81, 84, 148(3)
E	Hb + Cpx + Bi ± K-feld	Porphyritic rocks with hyalopilitic to trachytic texture.	CS 41*, 44*, 90*, 92, 143(5), 160(2), 160(3)
F	Plag + Cpx + ?Qz	Porphyritic texture. Very altered.	CS 67*
G	Plag + K-feld + Cpx + ?Bi	Pilotaxitic rock with microcrystalline groundmass.	CS 45*

\*: Analysed sample

Plg: Plagioclase, K-feld: K-feldspar, Cpx: Clinopyroxene, Bi: Biotite, Qz: Quartz, Ol: Olivine, Hb: Hornblende

**Table 3.1:** Types of lithic clasts in Upper Miocene pyroclastic and volcanoclastic rocks.

only in small quantities. Irregularly shaped vesicles are common. They are either empty or filled with secondary quartz, calcite and chlorite.

### **3.3.11 Type G**

Type G contains the philitaxitic rock CS 45 which according to the geochemical data is the unique andesite (Fig. 4.1). Both plagioclase and K-feldspars form the largest phenocrysts of the rock. Plagioclase phenocrysts have complex zoning with dusty cores, and narrow zones of small inclusions close to the rim. Sieve texture is also present in feldspars. This clast type is characterized by the abundance of small uniformly-sized and subhedral microphenocrysts of clinopyroxene. On the contrary, phenocrysts of clinopyroxene are very rare. In addition, few dusty phenocrysts are likely altered biotite and they are probably xenocrysts. The groundmass of the rock has microcrystalline character, consisting of feldspar microlaths and clinopyroxene, as well as opaque minerals with haphazard orientation.

## **3.4 Petrographical description of lava flows**

### **3.4.1 Tripa volcanic rocks**

In Tripa, sampling (CS 46, 47 & 70) took place on a small outcrop of lava flows (Fig. 2.2). Whole rock geochemical data show that these lava flows are trachyandesites (Fig. 4.1). Plagioclase is the only major mineral, forming laths of phenocrysts and microphenocrysts, as well as groundmass microlites (Fig. 3.8). Biotite and clinopyroxene are accessory phases, occurring as phenocrysts and microphenocrysts. Generally there are only a few isolated phenocrysts and microphenocrysts, whereas the groundmass occupies

the greater part of the rock. The groundmass consists of feldspar microlites that display a trachytic texture. Furthermore, feldspar microlites appear aligned around some phenocrysts.

Sample CS 70 is characterized by the presence of round, ovoid and irregular vesicles, up to 1 cm or more in diameter and apparently randomly distributed. These vesicles are either completely or partly filled by an aggregate of medium-grained quartz. Accessory phases are altered biotite, clinopyroxene, and orthopyroxene.

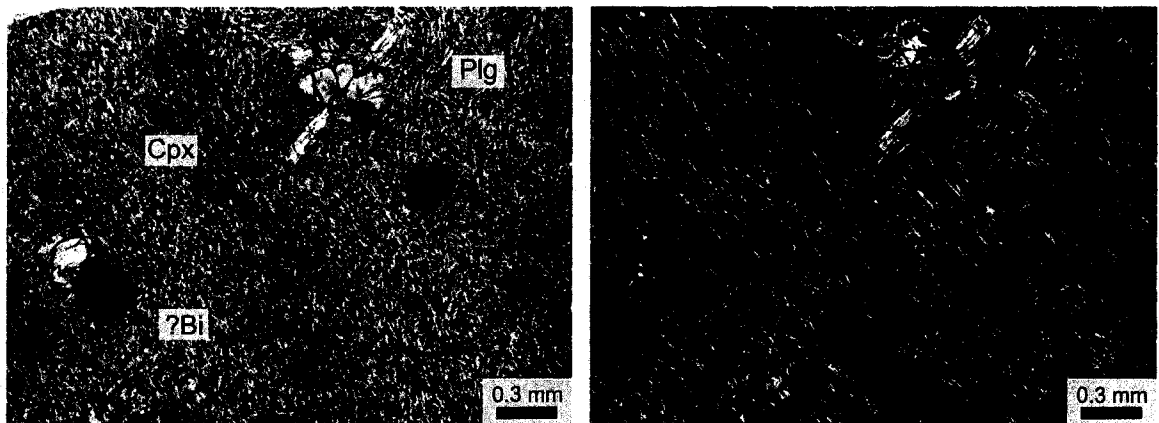


**Fig. 3.8:** *Microphotographs of trachyandesitic flows from Tripa. Phenocrysts of plagioclase (Plg), clinopyroxene (Cpx) and possibly biotite (Bi) which now have been completely altered to dusty opaque minerals, set in trachytic microcrystalline groundmass of feldspars. Plane polarized light on the left and cross polarized light on the right (sample CS 46, 50x).*

### 3.4.2 Prof. Ilias volcanic rocks

The volcanic rocks sampled from Prof. Ilias can be divided into three groups on the basis of geochemistry (Fig. 4.1), mineralogy and texture: basaltic trachyandesite (CS 73, 74); rhyolite (CS 71, 72); and trachyte (CS 101).

The basaltic trachyandesites (CS 73, 74) are porphyritic rocks with abundant phenocrysts of clinopyroxene and subordinate plagioclase (Fig. 3.9). The euhedral to anhedral clinopyroxene phenocrysts are usually pale green with oscillatory zoning and poikilitic texture and they are often embayed. The hyalopilitic groundmass consists mostly of plagioclase laths and clinopyroxene microphenocrysts. The difference between the two samples is related to the percentage of phenocrysts to groundmass (sample CS 73 has more phenocrysts). In addition, sample CS 74 shows many irregularly shaped vesicles, either empty or filled with unidentified crystallites. There are numerous glomeroporphyritic rocks with coarse-grained crystals either only of clinopyroxene or with feldspars. Orthopyroxene is also present as an accessory phase.

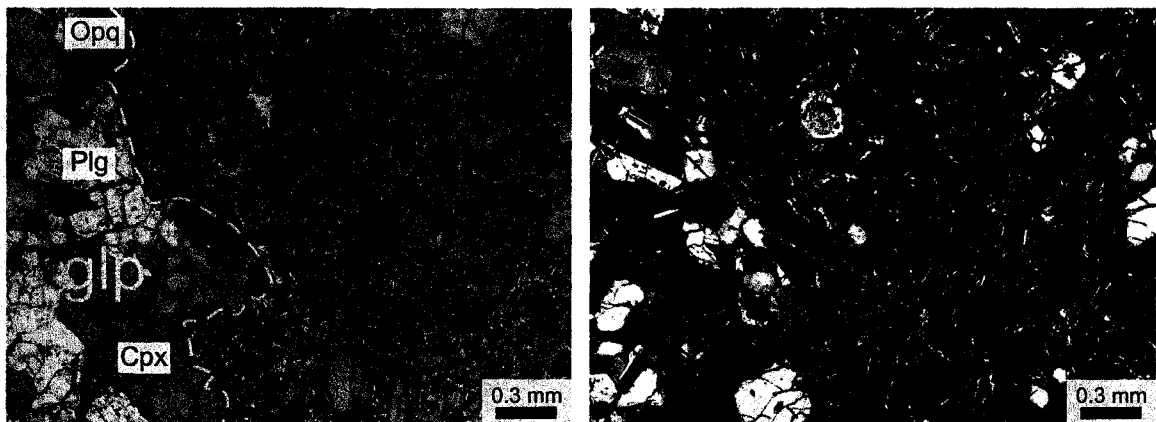


**Fig. 3.9:** *Microphotographs of the basaltic trachyandesitic group from Prof. Ilias. The part of the photo at the left of the dash yellow line illustrates a glomeroporphyry (glp) with coarse phenocrysts of plagioclase (Plg), clinopyroxene (Cpx) and opaque minerals (opq). The rest of the rock contains abundant phenocrysts and microphenocrysts of clinopyroxene and plagioclase in a pilotaxitic microcrystalline and glassy groundmass. Plane polarized light on the left and cross polarized light on the right (sample CS 73, 100x).*

The rhyolites (samples CS 71 and 72) differ from the basaltic trachyandesites in several ways. Feldspars are ubiquitous as microphenocrysts (Fig.3.10). Pseudomorphs of calcite after pyroxene are present. Brown biotite is also present, with typical altered rims to opaque minerals. The hyalopilitic groundmass is similar to that of the basaltic trachyandesites, containing microlites of feldspars in glass.

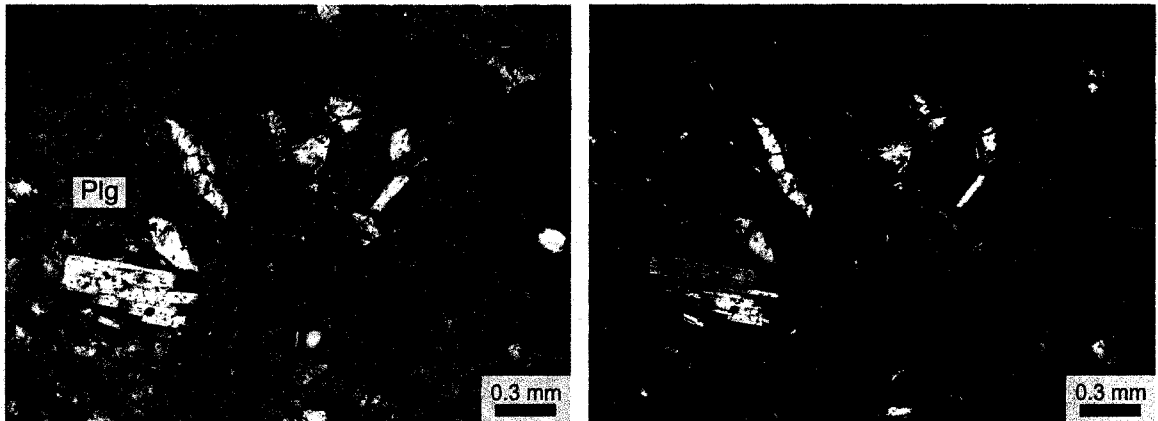


**Fig. 3.10:** *Microphotographs of the rhyolitic group from Prof. Ilias. Plagioclase (Plg) is ubiquitous as phenocrysts, microphenocrysts and groundmass microlites. Plane polarized light on the left and cross polarized light on the right (sample CS 71a, 50x).*

Sample CS 101 is the only sample of the trachyte group from the Prof. Ilias area. This rock consists of very large euhedral and subhedral phenocrysts more, than 0.5 cm in size, of alkali feldspars and plagioclase (Fig. 3.11). Most of the plagioclase crystals show varying degrees of oscillatory zoning. Plagioclase phenocrysts contain dusty, inclusion-charged cores, and thin clear rims. A few biotite phenocrysts and microphenocrysts are also present. The fine-grained groundmass has hyalopilitic texture, with glass and feldspar microlites in random orientations.

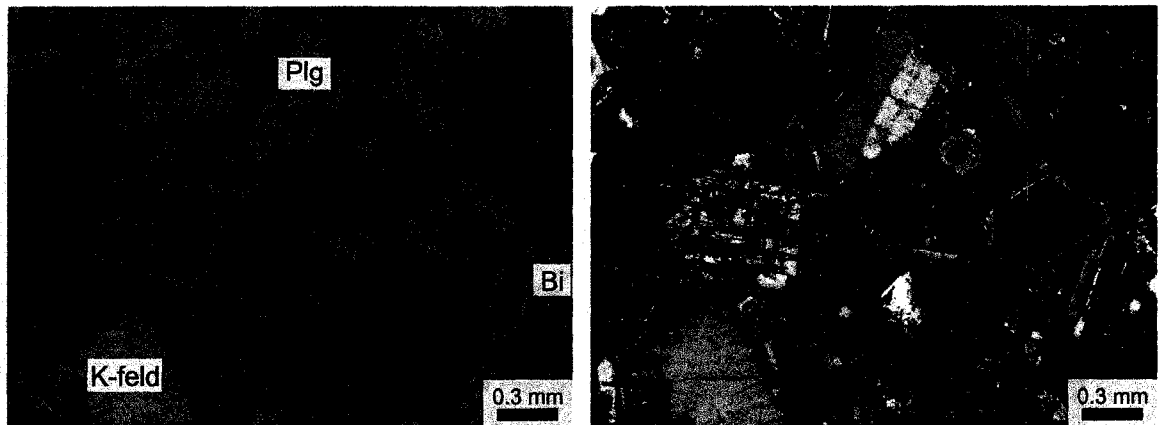


**Fig. 3.11:** *Microphotographs of the trachyte from Prof. Ilias. This rock consists of large phenocrysts, microphenocrysts and microcrystalline groundmass of plagioclase (Plg) and alkali feldspar (K-feld) often zoned, in plane polarized light (left) and cross polarized light (right) (sample CS 101c, 50x).*

### 3.4.3 Comparisons between lavas and lithic clasts

Comparing the trachyandesite from Tripa with the lithic clast types, it seems that is petrographically similar to type A3, based on the high proportion of groundmass, the predominance of feldspar phenocrysts and the presence of rare clinopyroxene and biotite phenocrysts.

The basaltic trachyandesites from Prof. Ilias lavas, are very similar to clast CS 45 and consequently to type G clast lithology. The rhyolite from Prof. Ilias does not closely resemble any clasts, but has few similarities with clast CS 66. Moreover, the trachyte from Prof. Ilias is similar to altered clast CS 143(6), and consequently to type B2.

### **3.5 Comparative results from petrographical study**

The stratigraphic distribution of different types of lithic clasts at Ag. Stefanos and Ag. Fokas (Figs. 3.12, 3.13, 3.14, 3.15 & Tb. 3.2) is used to assess whether there are stratigraphic changes in the sources of lithic clasts and whether successions at Ag. Stefanos and Ag. Fokas can be correlated on the basis of lithic clast petrography.

In Ag. Stefanos, lithic clasts from four different horizons have been studied petrographically (Fig. 3.12). At the bottom of the succession in beds A4 to A6, the collection of the lithic clasts includes the types A1, A2, A4, C and E. Moving upwards, in bed D6 the clasts have different composition, of types A1 and A2. Higher up in the sequence, at bed F17, types A1 and A2 are also present, together with type C, which was present at the base of the succession. Finally, the uppermost horizon, where clasts have been collected and studied (F23), contains type A2, as in most of the stratigraphic succession, but new types A4 and D are also identified.

In Ag. Fokas, the lithic clasts were collected from three different stratigraphical levels (Fig. 3.13). The lower, in beds B3 to B6, contains types A2 and B2. Bed J2 has type A2 again and type B1, and the upper layer J3 includes types B1 and D.

In Ag. Fokas North, collections of lithic clasts have been taken place from two beds (Fig. 3.14). In bed N1, type A3 was identified, whereas in the superjacent bed N3, types A2, B2 and C were recognized.

Some specific types are unique to one of the four locations of Ag. Stefanos, Ag. Fokas and Ag. Fokas North. Type A1 is present only in Ag. Stefanos and particularly in the lower three studied horizons. A2 is the most abundant type of clast and is present

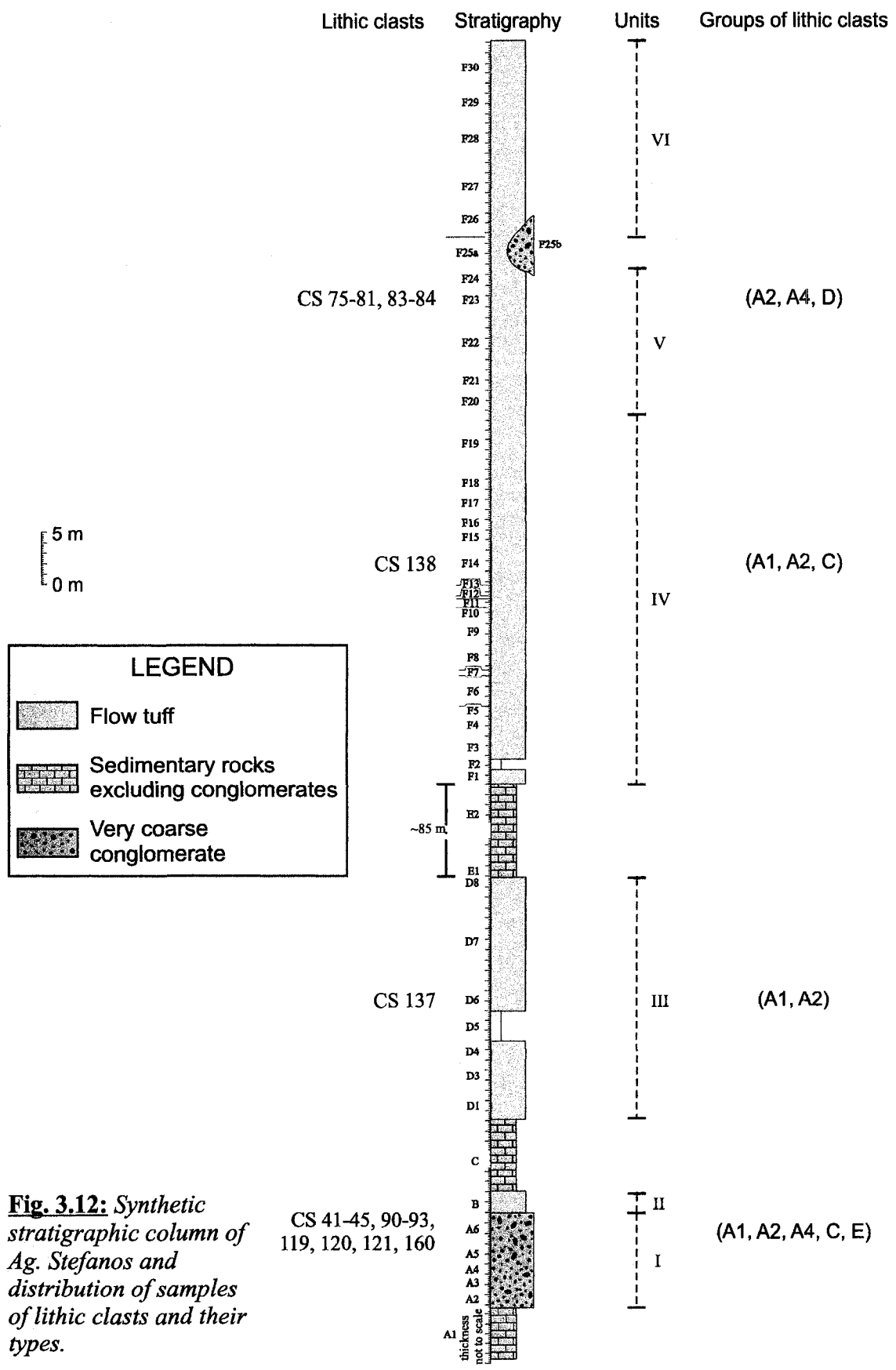


**Fig. 3.12:** Synthetic stratigraphic column of Ag. Stefanos and distribution of samples of lithic clasts and their types.

CS 41-45, 90-93, 119, 120, 121, 160

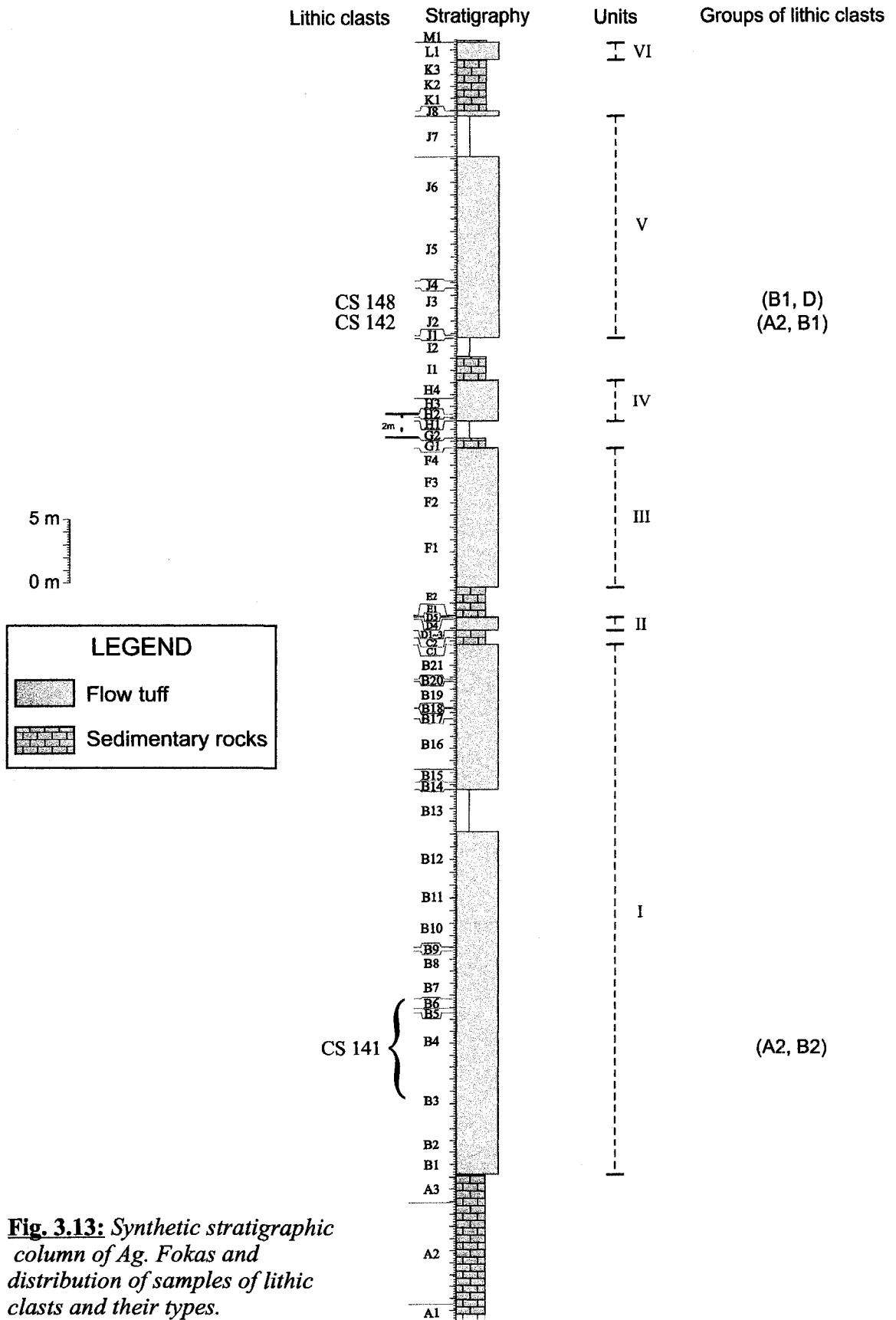


**Fig. 3.13:** Synthetic stratigraphic column of Ag. Fokas and distribution of samples of lithic clasts and their types.

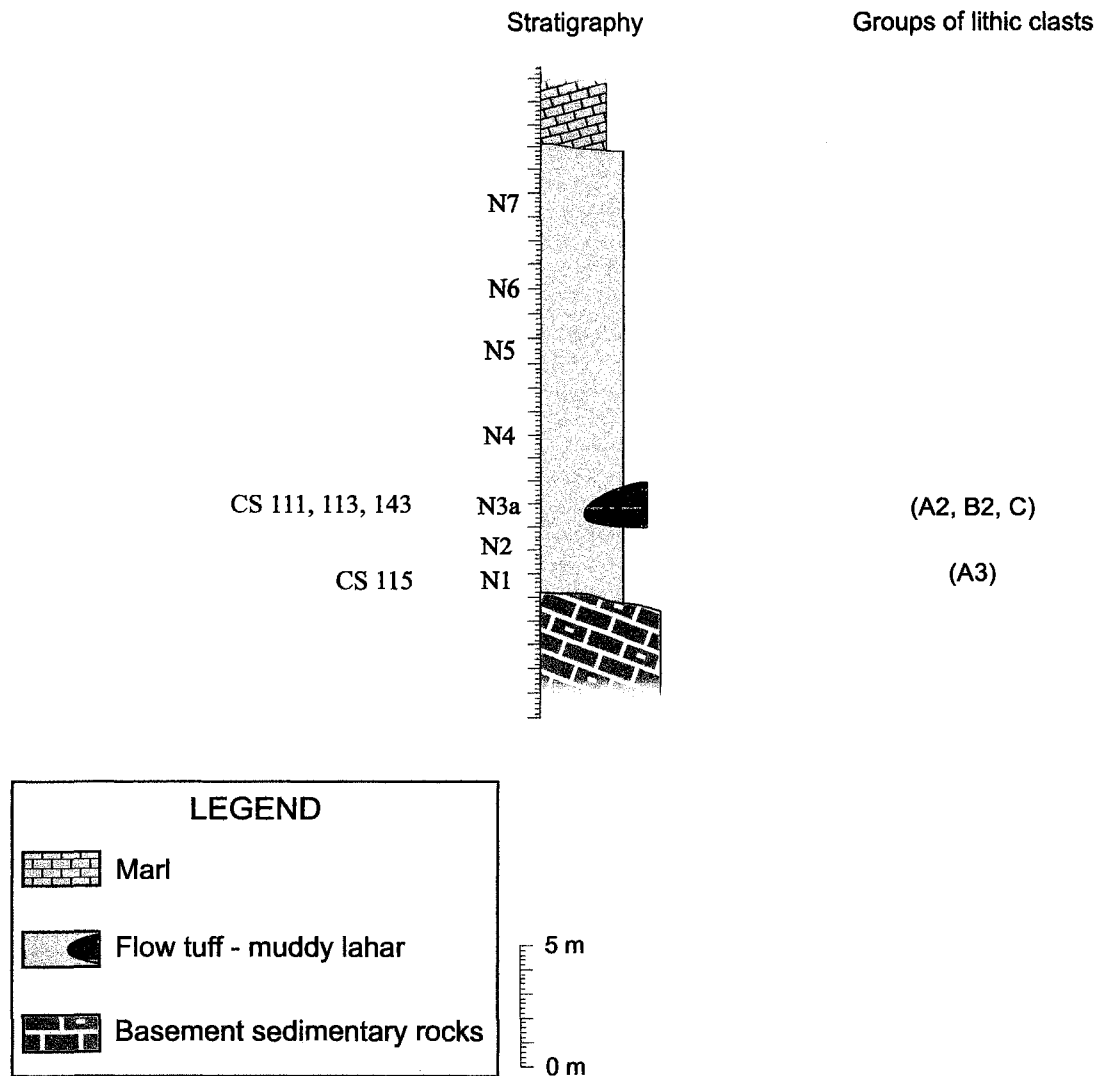


**Fig. 3.14:** Synthetic stratigraphic column of Ag. Fokas North and distribution of samples of lithic clasts and their types.

everywhere, except at the upper part of Ag. Fokas. A3 was identified only in Ag. Fokas North, and A4 only at the upper beds of Ag. Stefanos. Type B seems to be exclusively in eastern Kos. In Ag. Fokas, B2 was found at the lower beds, whereas B1 at the upper, but B2 was also present at Ag. Fokas North. Type C was recognized in Ag. Stefanos at two of the four stratigraphic levels, as well as in Ag. Fokas North. Type D is found only in the upper studied bed of Ag. Stefanos and Ag. Fokas.

In summary, a total of 503 clasts was collected from three stratigraphic horizons in Ag. Stefanos, three from Ag. Fokas and two from Ag. Fokas North (Table. 3.3). Pie diagrams of clast type abundance (Fig. 3.15) indicate that type A2 clasts are ubiquitous in the three areas, except the upper studied horizon of Ag. Fokas. In addition, it represents the majority of the clasts in both Ag. Stefanos and Ag. Fokas North, whereas in Ag. Fokas it is in the minority. Type A1 clasts are present in minor quantities only in Ag. Stefanos, decreasing upwards. Type B1 clasts were identified at the two upper studied horizons of Ag. Fokas only. The type B2 clast lithology is abundant at the lower stratigraphic horizons of Ag. Fokas, but is also present in minor amounts at Ag. Fokas North. Type C clasts are present in similar percentages in both the upper part of Ag. Stefanos and in Ag. Fokas North, and in minor amounts in lower horizons of Ag. Stefanos. Type D is found only in the upper part of Ag. Fokas. Type E, is present in significant amounts at the bottom of Ag. Stefanos.

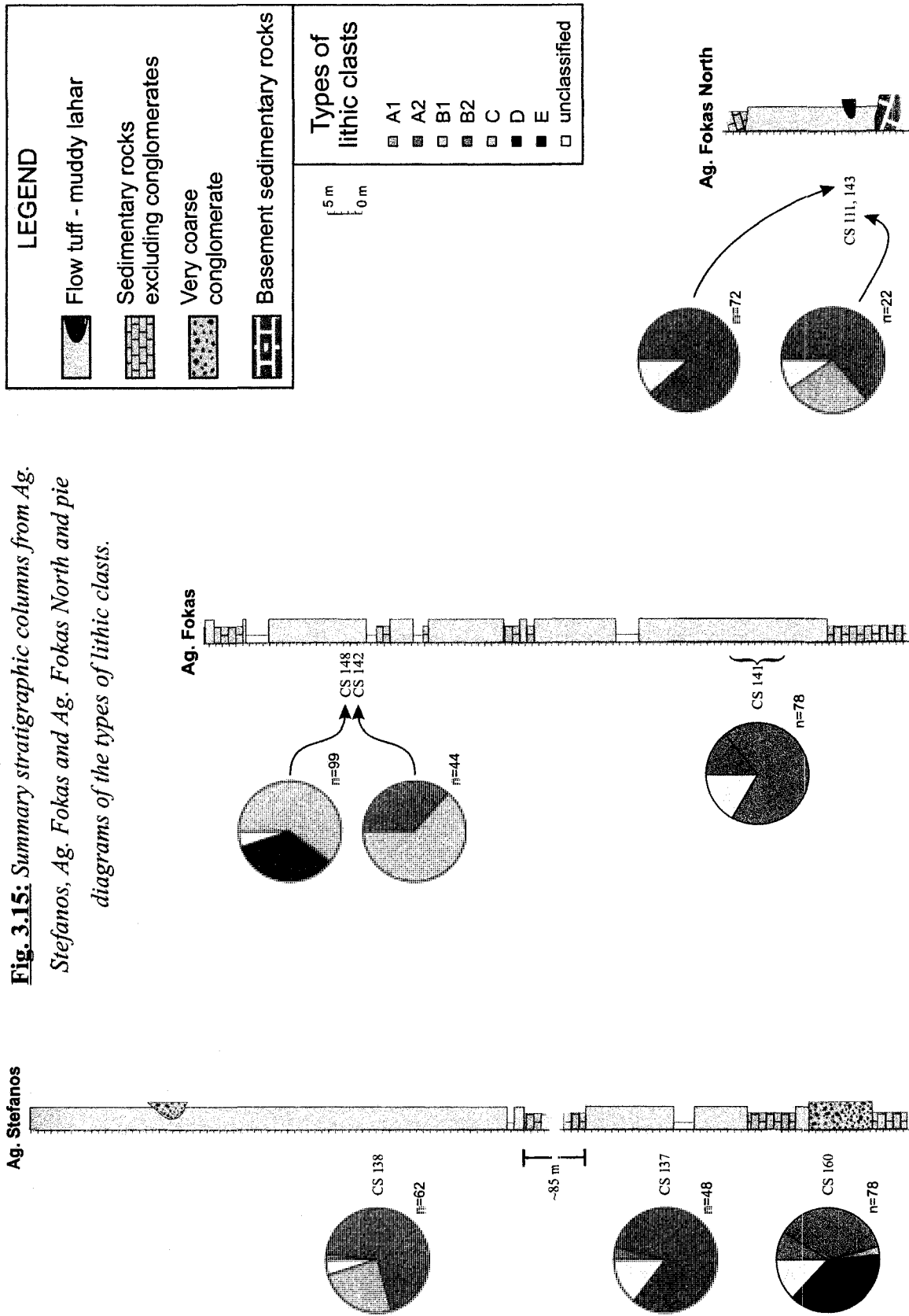


**Fig. 3.15:** Summary stratigraphic columns from Ag. Stefanos, Ag. Fokas and Ag. Fokas North and pie diagrams of the types of lithic clasts.

Unit	Types of clasts contained	Sample numbers
Ag. Fokas I	A2, B2	CS141(1), 141(2), 141(3), 141(4)
Ag. Fokas V	A2, B1, D	CS 142(1), 142(2), 142(3), 148(1), 148(2), 148(3)
Ag. Fokas North	A2, A3, B2, C	CS 111(1), 111(2), 111(5), 111(6), 111(7), 113, 115, 143(1), 143(4), 143(5), 143(6)
Ag. Stefanos I	A1, A2, A4, C, E, G	CS 41-45, 90-93, 119, 120, 121, 160
Ag. Stefanos III	A1, A2	137(1), 137(2), 137(3), 137(4)
Ag. Stefanos IV	A1, A2, C	CS 138(1), 138(2), 138(5), 138(6)
Ag. Stefanos V	A2, A4, D	CS 75, 76, 77, 78, 79, 80, 81, 83, 84
Prof. Ilias	-	-
Tripa	A2, A3, D, F	CS 61, 62, 63, 64, 66, 67, 68

**Table 3.2:** *Distribution of clast types by unit.*

Collection of lithic clast	Location	Bed	Type of clast	Size				Total no
				4-8mm	8-16mm	16-32mm	32-64mm	
CS 111	Ag. Fokas North	N3	A2		3	10	1	14
			C		2	2	2	6
			unclassified		1	1		2
CS 137	Ag. Stefanos	D6	A1		1	1	2	2
			A2		9	28	2	39
			unclassified		1	6		7
CS 138			A1			1	1	1
			A2	3	17	21	2	43
			C	4	8	2	1	15
			unclassified		1	2		3
CS 141	Ag. Fokas	B3-B6	A2		4	6	1	11
			B2	1	12	39	2	54
			unclassified		9	4		13
CS 142	Ag. Fokas	J2	A2		3	10	3	16
			B1	1	11	15	1	28
CS 143	Ag. Fokas North	N3	A2		5	41	16	62
			B2			1	1	2
			unclassified		4	4		8
			B1	4	30	26		60
CS 148	Ag. Fokas	J3	D	5	18	11		34
			unclassified		1	4		5
			A1	1	1	2	3	7
CS 160	Ag. Stefanos	A2-A6	A2		11	15	3	29
			C			2	2	2
			E		6	19	5	30
			unclassified		1	9		10

Total no of clasts: 503

**Table 3.3:** Summary of abundance and sizes of lithic clasts.

# CHAPTER 4

## *Geochemistry*

### **4.1. Introduction**

This chapter presents whole rock geochemical analyses for major, trace and rare earth elements (REE) of the Miocene lava flows and domes of Kos and from representative lithic clasts in the pyroclastic rocks. The goals of this analytical work were first to define the general geochemical character of the volcanic rocks of Kos, so that they can be compared with other Miocene volcanic rocks in the region and second, to define the geochemical character of lithic clasts in pyroclastic rocks and to relate them to the petrographical classification in Chapter 3. This information is used in Chapter 6 to help identify the source of the pyroclastic rocks. In this study, 23 samples were used: 7 represent lava flows and domes, 15 lithic clasts, and one sample is a crystal tuff (Table 4.1). Analyses from lithic clasts were limited by the availability of clasts of suitable size.

## **4.2 Analytical sample preparation**

Initially, fresh-looking samples were cut into slabs. Any saw marks from the trim saw blade were removed using sandpaper. A hydraulic crusher was used to break the slabs into small chips less than 1 cm in length. These chips were immersed in deionized water in a beaker and cleaned in an ultrasonic bath for about 1 minute to remove any loose material. The chips were finally washed with deionised water and left to dry. Finally, the samples were crushed for powder at the Minerals Engineering Centre of Dalhousie University, by using a shattererbox with an iron bowl. The powders were analysed for major and trace elements by Activation Laboratories according to their Code 4Lithoresearch and Code 4B1 packages , which combine lithium metaborate/tetraborate Fusion Inductively-Coupled Plasma (ICP) whole rock analyses with a trace element Inductively-Coupled Plasma Mass Spectrometry (ICP-MS) package. The precision of these data ranges from 0.01 % up to 1 ppm (Table 4.1). Minpet software was used to manipulate and plot the data.

## **4.3 Rock Nomenclature**

The rocks were classified using the standard IUGS system for volcanic rocks (LeBas et al., 1986), which uses the total alkalis (wt %  $K_2O + Na_2O$ ) versus silica (wt %  $SiO_2$ ). According to this nomenclature (Fig. 4.1), the ignimbrite sample collected from Ag. Fokas is a trachyte, and the only lithic clast analysed from the same area is a trachyandesite. The majority of the lithic clasts from Ag. Stefanos are also

Sample		CS41	CS42	CS43	CS44	CS45	
Rock unit		Lithic clast					
Locality		Ag. Stefanos					
Bed number		A2-A6	A2-A6	A2-A6	A2-A6	A2-A6	
Petrographical type		E	A4	A4	E	A2	
Symbol in Minpet		o	o	o	o	o	
Major Elements (wt %)	SiO <sub>2</sub>	(0.01)*	63.35	59.11	55.76	63.53	57.27
	TiO <sub>2</sub>	(0.001)	0.52	0.59	0.86	0.48	0.64
	Al <sub>2</sub> O <sub>3</sub>	(0.01)	16.35	16.77	17.04	15.91	16.23
	Fe <sub>2</sub> O <sub>3</sub> (T)	(0.01)	4.16	4.51	4.41	3.7	5.68
	MnO	(0.001)	0.05	0.08	0.07	0.09	0.11
	MgO	(0.01)	1.34	2.3	2.13	1.85	4.4
	CaO	(0.01)	4.28	5.4	6.82	4.37	7.29
	Na <sub>2</sub> O	(0.01)	3.77	3.69	3.59	3.8	3.35
	K <sub>2</sub> O	(0.01)	4.02	3.35	2.93	3.77	1.88
	P <sub>2</sub> O <sub>5</sub>	(0.01)	0.26	0.29	0.79	0.24	0.14
	L.O.I.	(0.01)	1.92	3.36	4.54	1.69	1.9
	Total		100.02	99.45	98.94	99.43	98.89
Trace Elements (ppm)	Ba	(3)	1180	1320	14000	1080	1550
	Rb	(1)	144	125	94	161	42
	Sr	(2)	780	876	1200	678	479
	Y	(0.5)	22.6	23	70.4	21.7	25.1
	Zr	(4)	218	239	269	213	121
	Nb	(0.2)	28.7	24.8	23.4	27.1	13.4
	Pb	(3)	65	74	73	80	9
	Ga	(1)	19	19	18	19	14
	Zn	(1)	80	80	87	72	59
	Cu	(1)	27	28	25	24	29
	Ni	(1)	16	12	14	10	66
	V	(5)	84	96	125	74	130
	Cr	(20)	26	b.d.	41	b.d.	104
	Co	(1)	7	10	10	7	18
	La	(0.05)	54.6	67.6	101	53.2	56.4
	Ce	(0.05)	94.9	116	155	89.8	55.7
	Pr	(0.01)	10.1	12.1	15.8	9.36	9.74
	Nd	(0.05)	37.5	44.3	58.6	32.7	35.2
	Sm	(0.01)	6.7	7.53	10.2	6.16	6.33
	Eu	(0.005)	1.62	1.82	2.27	1.49	1.46
	Gd	(0.01)	5.46	5.88	9.89	4.57	6.04
	Tb	(0.01)	0.79	0.81	1.41	0.69	0.82
	Dy	(0.01)	4.16	4.35	8.29	3.77	4.84
	Ho	(0.01)	0.76	0.76	1.73	0.69	0.91
	Er	(0.01)	2.31	2.3	5.71	2.04	2.72
	Tm	(0.005)	0.33	0.33	0.84	0.31	0.41
	Yb	(0.01)	2.1	2.04	5.12	1.91	2.51
	Lu	(0.002)	0.31	0.31	0.83	0.28	0.38
Cs	(0.1)	8.5	16.5	11.8	17.2	0.9	
Hf	(0.1)	6.4	6.7	7.2	6.2	3.4	
Sb	(0.2)	2.2	2.1	2.5	2	0.4	
Sc	(1)	8	10	12	8	18	
Ta	(0.01)	2.02	1.77	1.61	1.97	0.69	
Th	(0.05)	44.5	50	46.6	43.6	8.55	
U	(0.01)	15.2	17.2	46.9	19	2.53	

\*: Detection limit. For major elements as % and for trace elements as ppm.

**Table 4.1:** Whole rock geochemical analyses of representative samples from the studied rocks.

Sample		CS46	CS47	CS49	CS50	CS51	
Rock unit		Mioc. vol. rock	Mioc. vol. rock	Mioc. vol. rock	Mioc. vol. rock	Mioc. Ignimbrite	
Locality		Tripa	Tripa	Tripa	Prof. Ilas	Ag. Fokas	
Bed number		-	-	-	-	B2-B3	
Petrographical type		-	-	-	-	-	
Symbol in Minpet		▲	▲	▲	▼	■	
Major Elements (wt %)	SiO <sub>2</sub>	(0.01)*	53.85	54.27	62.64	56.56	57.08
	TiO <sub>2</sub>	(0.001)	0.86	0.91	0.48	0.64	0.47
	Al <sub>2</sub> O <sub>3</sub>	(0.01)	17.08	18.07	17.73	18.33	16.66
	Fe <sub>2</sub> O <sub>3</sub> (T)	(0.01)	6.3	6.34	4.2	5.61	3.9
	MnO	(0.001)	0.07	0.12	0.05	0.05	0.09
	MgO	(0.01)	1.57	1.85	1.2	1.41	1.43
	CaO	(0.01)	2.94	4.7	4.04	4.9	2.46
	Na <sub>2</sub> O	(0.01)	3.84	4.4	4.35	4.2	3.65
	K <sub>2</sub> O	(0.01)	5.94	4.62	4.8	3.94	3.31
	P <sub>2</sub> O <sub>5</sub>	(0.01)	0.46	0.47	0.19	0.27	0.21
	L.O.I.	(0.01)	5.97	3.52	0.62	3.78	10.69
	Total		98.88	99.27	100.30	99.69	99.95
Trace Elements (ppm)	Ba	(3)	1580	1680	1260	1310	1040
	Rb	(1)	214	117	210	166	215
	Sr	(2)	615	1030	858	1020	677
	Y	(0.5)	26.1	27.9	19.1	16.7	26.5
	Zr	(4)	408	431	262	257	519
	Nb	(0.2)	31.3	33.3	24.6	23	43.9
	Pb	(3)	56	60	62	45	105
	Ga	(1)	20	23	19	21	22
	Zn	(1)	82	95	51	82	109
	Cu	(1)	21	21	10	18	21
	Ni	(1)	2	3	4	9	4
	V	(5)	105	114	65	112	29
	Cr	(20)	b.d.	b.d.	b.d.	b.d.	b.d.
	Co	(1)	8	12	4	10	3
	La	(0.05)	108	110	83.6	88.7	127
	Ce	(0.05)	179	186	122	133	225
	Pr	(0.01)	19	19.9	11.7	13.1	22
	Nd	(0.05)	66.8	69.6	37.4	41.9	75.7
	Sm	(0.01)	11.1	11.7	5.78	6.01	11.2
	Eu	(0.005)	2.82	2.88	1.42	1.59	2.4
	Gd	(0.01)	7.54	7.88	3.94	3.88	7.7
	Tb	(0.01)	1.01	1.03	0.58	0.54	1
	Dy	(0.01)	5.38	5.63	3.41	3.17	5.2
	Ho	(0.01)	0.97	1.03	0.67	0.61	0.97
	Er	(0.01)	2.87	3.02	2.1	1.89	2.96
	Tm	(0.005)	0.4	0.43	0.33	0.28	0.47
	Yb	(0.01)	2.59	2.76	2.18	1.95	3.02
	Lu	(0.002)	0.39	0.4	0.33	0.29	0.45
Cs	(0.1)	42	17.9	11.5	5	28.8	
Hf	(0.1)	10.4	10.9	7.1	6.5	14.2	
Sb	(0.2)	1.1	0.3	2	1.6	2.2	
Sc	(1)	10	10	5	8	5	
Ta	(0.01)	1.86	1.93	1.43	1.3	2.67	
Th	(0.05)	50.1	51.8	49.1	42.1	60.9	
U	(0.01)	11.4	13.3	19.6	10.9	14.1	

\*: Detection limit. For major elements as % and for trace elements as ppm.

**Table 4.1:** *continued*

Sample		CS66	CS67	CS68	CS72	CS74	
Rock unit		Lithic clast	Lithic clast	Lithic clast	Mioc. vol. rock	Mioc. vol. rock	
Locality		Tripa	Tripa	Tripa	Prof. Ilas	Prof. Ilas	
Bed number		-	-	-	-	-	
Petrographical type		A3	F	A2	-	-	
Symbol in Minpet		Δ	Δ	Δ	▼	▼	
Major Elements (wt %)	SiO <sub>2</sub>	(0.01)*	55.18	53.35	53.83	71.63	49.55
	TiO <sub>2</sub>	(0.001)	0.995	1.168	1.117	0.337	0.929
	Al <sub>2</sub> O <sub>3</sub>	(0.01)	20.36	18.87	19.04	14.2	16.16
	Fe <sub>2</sub> O <sub>3</sub> (T)	(0.01)	5.05	7.32	5.61	2.26	5.95
	MnO	(0.001)	0.063	0.087	0.115	0.013	0.076
	MgO	(0.01)	1.21	2.02	1.92	0.29	3.37
	CaO	(0.01)	5.77	6.63	7.37	1.66	8.8
	Na <sub>2</sub> O	(0.01)	4.65	4.12	4.08	3.81	4.2
	K <sub>2</sub> O	(0.01)	3.8	2.45	3.88	5.05	1.04
	P <sub>2</sub> O <sub>5</sub>	(0.01)	0.6	0.87	0.85	0.17	1.18
	L.O.I.	(0.01)	1.98	3.6	2.05	1.43	8.29
	Total		99.66	100.49	99.86	100.85	99.55
	Trace Elements (ppm)	Ba	(3)	1829	2330	1686	666
Rb		(1)	85	63	87	229	250
Sr		(2)	1388	1663	1461	336	2745
Y		(0.5)	40.7	33	28.1	18	40.5
Zr		(4)	424	375	346	236	283
Nb		(0.2)	47.3	48.3	30.2	29.5	53.4
Pb		(3)	55	61	57	66	20
Ga		(1)	22	21	22	20	18
Zn		(1)	42	46	58	29	54
Cu		(1)	23	27	17	11	61
Ni		(1)	2	8	7	6	40
V		(5)	131	143	156	33	180
Cr		(20)	b.d.	b.d.	b.d.	b.d.	130
Co		(1)	5	11	7	2	24
La		(0.05)	104	106	97	43	135
Ce		(0.05)	181	189	183	70.8	245
Pr		(0.01)	20.8	21.8	20.5	8.04	29.7
Nd		(0.05)	72.3	75.6	72.5	26.8	110
Sm		(0.01)	13.1	13.1	12.2	4.87	18.6
Eu		(0.005)	3.28	3.08	3.01	0.976	4.9
Gd		(0.01)	10.2	9.62	8.7	3.82	14.5
Tb		(0.01)	1.41	1.25	1.11	0.56	1.69
Dy		(0.01)	7.1	6.14	5.52	2.87	7.77
Ho		(0.01)	1.33	1.12	0.97	0.55	1.34
Er		(0.01)	3.79	3.24	2.72	1.64	3.58
Tm		(0.005)	0.537	0.458	0.391	0.252	0.489
Yb		(0.01)	3.48	2.88	2.5	1.71	2.9
Lu		(0.002)	0.519	0.411	0.351	0.248	0.387
Cs	(0.1)	66.5	53.1	31	10	11.9	
Hf	(0.1)	10.3	8.7	8.5	6.7	7	
Sb	(0.2)	3.3	0.8	2.1	0.3	b.d.	
Sc	(1)	12	19	16	3	23	
Ta	(0.01)	2	1.52	1.69	2.2	2.41	
Th	(0.05)	48.1	36	34.9	49.7	26.8	
U	(0.01)	11.6	14.7	13.6	16.5	6.37	

\*: Detection limit. For major elements as % and for trace elements as ppm.

**Table 4.1: continued**

Sample		CS77	CS78	CS80	CS90	CS91	
Rock unit		Lithic clast					
Locality		Ag. Stefanos					
Bed number		F23	F23	F23	A2-A6	A2-A6	
Petrographical type		D	D	D	E	C	
Symbol in Minpet		o	o	o	o	o	
Major Elements (wt %)	SiO <sub>2</sub>	(0.01)*	53.41	55.57	57.91	59.69	58.99
	TiO <sub>2</sub>	(0.001)	0.906	0.809	0.553	0.641	0.667
	Al <sub>2</sub> O <sub>3</sub>	(0.01)	18.01	19.22	19.44	16.42	16.03
	Fe <sub>2</sub> O <sub>3</sub> (T)	(0.01)	18.01	5.72	4.56	3.7	3.72
	MnO	(0.001)	18.01	0.111	0.074	0.076	0.084
	MgO	(0.01)	18.01	1.24	0.52	2.73	2.75
	CaO	(0.01)	18.01	5.58	4.1	5.96	6.1
	Na <sub>2</sub> O	(0.01)	18.01	4.22	4.89	3.83	3.92
	K <sub>2</sub> O	(0.01)	18.01	4.69	5.44	3.45	3.42
	P <sub>2</sub> O <sub>5</sub>	(0.01)	18.01	0.57	0.35	0.3	0.3
	L.O.I.	(0.01)	18.01	2.07	1.08	3.03	3.99
Total		18.01	99.80	98.92	99.83	99.97	
Trace Elements (ppm)	Ba	(3)	1662	1629	1459	1241	1321
	Rb	(1)	91	152	181	129	135
	Sr	(2)	1407	1406	1286	837	968
	Y	(0.5)	28.7	22.2	22.6	43.2	25.6
	Zr	(4)	359	357	438	207	227
	Nb	(0.2)	31.6	34.4	35.7	18.2	18.1
	Pb	(3)	59	59	57	61	75
	Ga	(1)	23	22	24	21	21
	Zn	(1)	141	92	56	52	56
	Cu	(1)	21	8	9	12	19
	Ni	(1)	10	6	4	13	10
	V	(5)	167	143	67	95	87
	Cr	(20)	b.d.	b.d.	b.d.	70	50
	Co	(1)	15	9	5	11	11
	La	(0.05)	89.8	84.4	85.3	61.4	63.6
	Ce	(0.05)	164	146	152	119	115
	Pr	(0.01)	18.2	15.7	16	14.3	12.8
	Nd	(0.05)	63.6	52.9	52.2	55.2	45.3
	Sm	(0.01)	10.9	8.63	8.52	11.1	8.58
	Eu	(0.005)	2.82	2.54	2.45	2.35	1.95
	Gd	(0.01)	8	6.24	6.08	10	6.65
	Tb	(0.01)	1.04	0.83	0.82	1.39	0.94
	Dy	(0.01)	5.18	3.97	3.9	6.95	4.66
	Ho	(0.01)	0.92	0.72	0.72	1.27	0.85
	Er	(0.01)	2.53	2.07	2.09	3.62	2.41
	Tm	(0.005)	0.366	0.295	0.31	0.513	0.353
	Yb	(0.01)	2.27	1.84	2.08	3.33	2.32
	Lu	(0.002)	0.321	0.257	0.307	0.482	0.341
Cs	(0.1)	11.1	5.9	5.9	12.8	13.6	
Hf	(0.1)	9.2	9.1	11.1	5.6	6	
Sb	(0.2)	b.d.	0.6	0.4	0.2	0.3	
Sc	(1)	12	10	4	13	12	
Ta	(0.01)	1.6	1.71	2.09	1.35	1.38	
Th	(0.05)	39.1	46.5	59.1	39.6	40.9	
U	(0.01)	9.91	11.1	15.2	12.7	13.6	

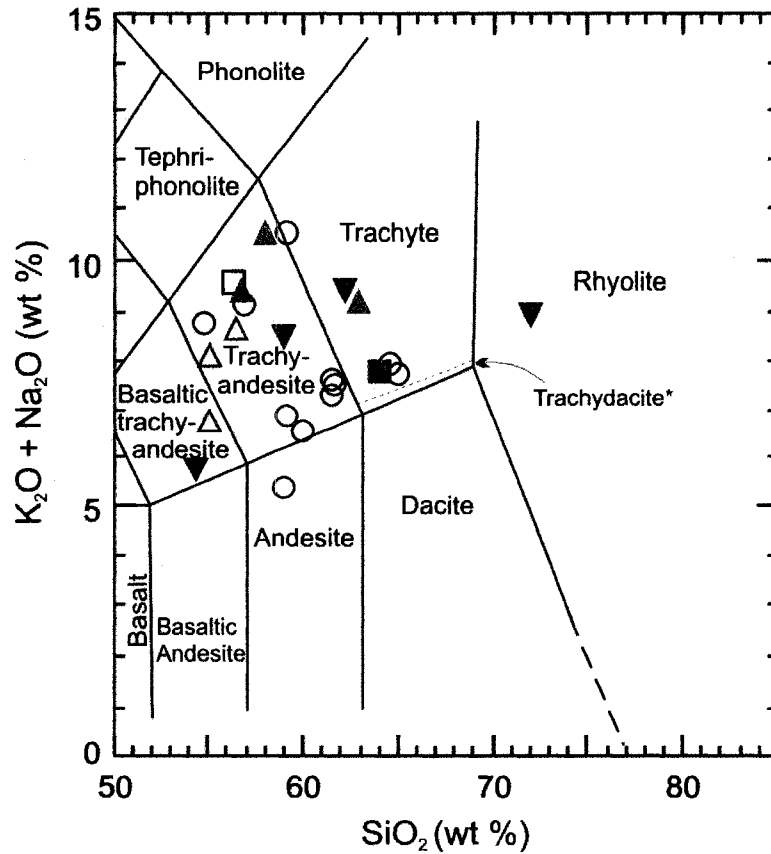
\*: Detection limit. For major elements as % and for trace elements as ppm.

**Table 4.1: continued**

Sample		CS93	CS101	CS115	
Rock unit		Lithic clast	Mioc. vol. rock	Lithic clast	
Locality		Ag. Stefanos	Prof. Ilas	Ag. Fokas North	
Bed number		A2-A6	-	N1	
Petrographical type		C	-	A3	
Symbol in Minpet		○	▼	□	
Major Elements (wt %)	SiO <sub>2</sub>	(0.01)*	57.19	59.53	53.72
	TiO <sub>2</sub>	(0.001)	0.684	0.406	1.037
	Al <sub>2</sub> O <sub>3</sub>	(0.01)	16.88	16.93	17.08
	Fe <sub>2</sub> O <sub>3</sub> (T)	(0.01)	5.28	3.76	5.88
	MnO	(0.001)	0.103	0.082	0.116
	MgO	(0.01)	2.82	0.94	2.86
	CaO	(0.01)	5.83	4.91	5.18
	Na <sub>2</sub> O	(0.01)	3.33	4.09	7.75
	K <sub>2</sub> O	(0.01)	2.93	4.93	1.37
	P <sub>2</sub> O <sub>5</sub>	(0.01)	0.38	0.19	0.5
	L.O.I.	(0.01)	4.66	3.63	5.24
	Total		100.09	99.40	100.73
Trace Elements (ppm)	Ba	(3)	1166	1096	93
	Rb	(1)	120	225	32
	Sr	(2)	923	825	382
	Y	(0.5)	26.3	18.3	28.4
	Zr	(4)	259	251	91
	Nb	(0.2)	16.7	21.5	24.2
	Pb	(3)	73	63	b.d.
	Ga	(1)	19	20	13
	Zn	(1)	72	55	60
	Cu	(1)	14	8	28
	Ni	(1)	12	7	15
	V	(5)	122	57	70
	Cr	(20)	30	b.d.	b.d.
	Co	(1)	10	7	16
	La	(0.05)	60.4	68	25.1
	Ce	(0.05)	110	110	51.5
	Pr	(0.01)	12.5	10.5	6.86
	Nd	(0.05)	44.2	32.8	29.3
	Sm	(0.01)	8.43	5.09	7.42
	Eu	(0.005)	2.04	1.24	2.32
	Gd	(0.01)	6.97	3.68	7.15
	Tb	(0.01)	0.98	0.53	1.1
	Dy	(0.01)	4.8	2.91	5.51
	Ho	(0.01)	0.88	0.57	0.95
	Er	(0.01)	2.46	1.78	2.52
	Tm	(0.005)	0.355	0.283	0.351
	Yb	(0.01)	2.34	1.95	2.17
	Lu	(0.002)	0.344	0.297	0.309
Cs	(0.1)	13.5	6	1.5	
Hf	(0.1)	6.5	6	2.4	
Sb	(0.2)	0.4	1.8	b.d.	
Sc	(1)	13	5	14	
Ta	(0.01)	1.28	1.53	1.25	
Th	(0.05)	38.6	38.7	5.19	
U	(0.01)	11.6	12.2	1.19	

\*: Detection limit. For major elements as % and for trace elements as ppm.

**Table 4.1: continued**



Volcanic rocks	Lithic clasts
■ Ag. Fokas	□ Ag. Fokas
▲ Tripa	△ Tripa
▼ Prof. Ilias	○ Ag. Stefanos

**Fig. 4.1:** *Geochemical nomenclature of representative volcanic rocks and lithic clasts from the Miocene of Kos, by IUGS system for volcanic rocks (LeBas et al., 1986).*

trachyandesites, but a few plot in the trachyte and andesite fields. The Prof. Ilias volcanic rocks show the greatest variation, ranging from 54 to 72 % in SiO<sub>2</sub>. They correspond to basaltic trachyandesite to rhyolite. Lastly, the Tripa volcanic rocks are trachyandesite and trachyte, whereas the analyzed lithic clasts are basaltic trachyandesite and trachyandesite.

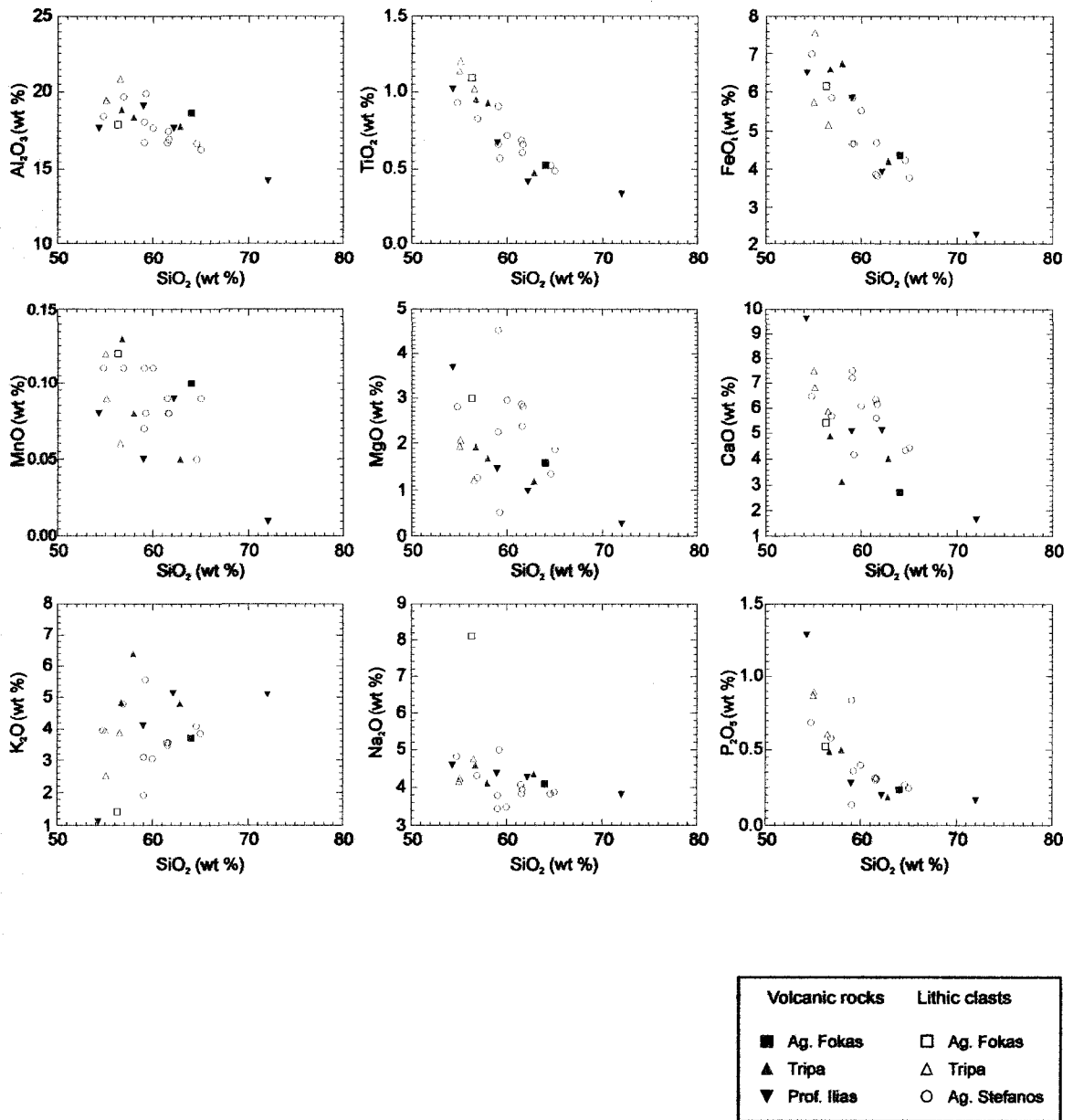


**Fig. 4.2:** Harker diagrams showing variations in major elements versus  $\text{SiO}_2$  for the Kos Upper Miocene volcanic rocks and the clasts from the pyroclastic rocks.

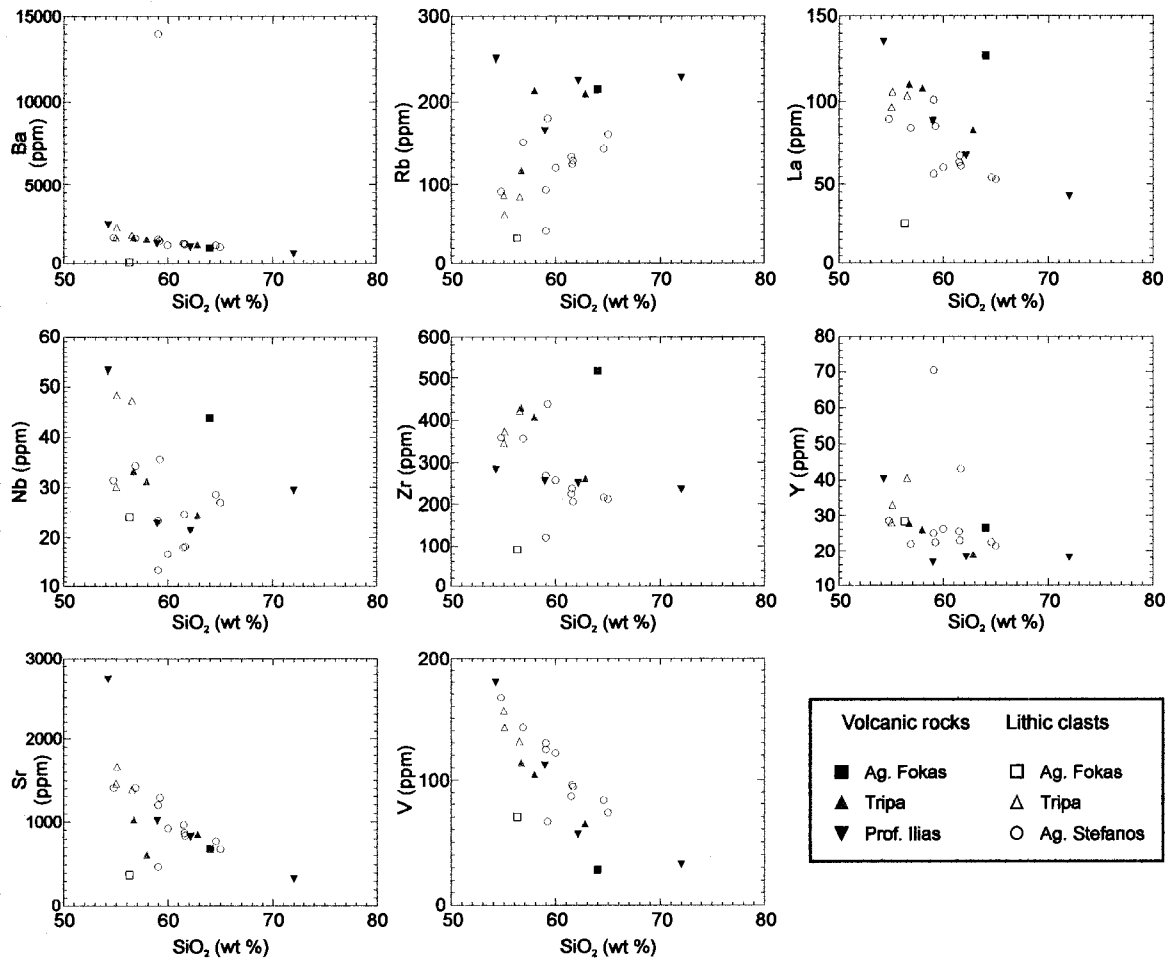


**Fig. 4.3:** Harker diagrams showing variations in selected trace elements versus  $\text{SiO}_2$  for the Kos Upper Miocene volcanic rocks and the clasts from the pyroclastic rocks.

#### **4.6 Rare Earth Element Patterns**

Chondrite-normalized rare earth element (REE) patterns for the volcanic rocks and lithic clasts tend to resemble one another (Fig. 4.4). Most rocks and clasts have  $La_N$  values between 300–500, and show a linear decrease in the normalized abundances of light and middle REE from La to Dy. The  $La_N/Eu_N$  ratio ranges between 7 and 13, with most values around 10 to 12. A weak negative Eu anomaly is visible in a minority of the 23 analyzed samples. The heavy rare earth elements (HREE) from Ho to Lu show little fractionation, with  $Ho_N/Lu_N$  ratios varying between 1.3 and 1. Unusual REE patterns are shown by three samples: the trachyandesite lithic clast CS 43, with unfractionated MREE and HREE; trachyandesite lithic clast CS115 from Ag. Fokas, with low LREE; and basaltic trachyandesite lava CS74 from Prof. Ilias, with high REE, particularly the MREE.

#### **4.7 Multi-Element Patterns**

Primitive mantle (Sun & McDonough, 1989)-normalized multi-element diagrams (Fig. 4.5), show that the analysed samples display an overall decrease in large ion lithophile elements (LILE) on the left such as Rb, Ba, Th and U, to the high field strength elements (HFSE) on the right such as Nb, Ti and Y. Those with unusual REE patterns also have unusual multi-element patterns. Most samples show the highest enrichment in U and the second highest in Th. All the samples are depleted in Nb, Ta, and Ti, some are in Ba and P.

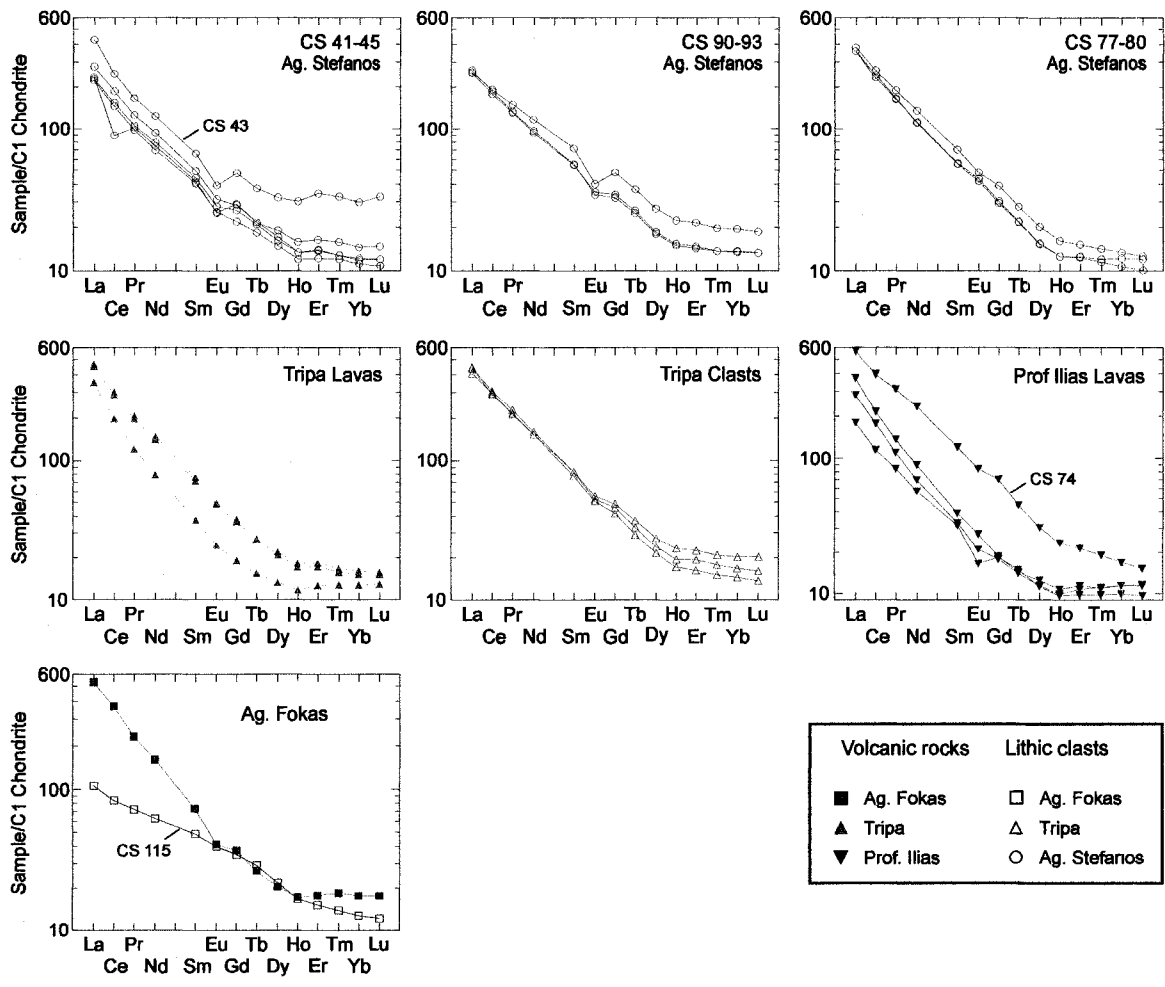


**Fig. 4.4:** Variations in REE for the Kos Upper Miocene volcanic rocks and the clasts from the pyroclastic rocks.

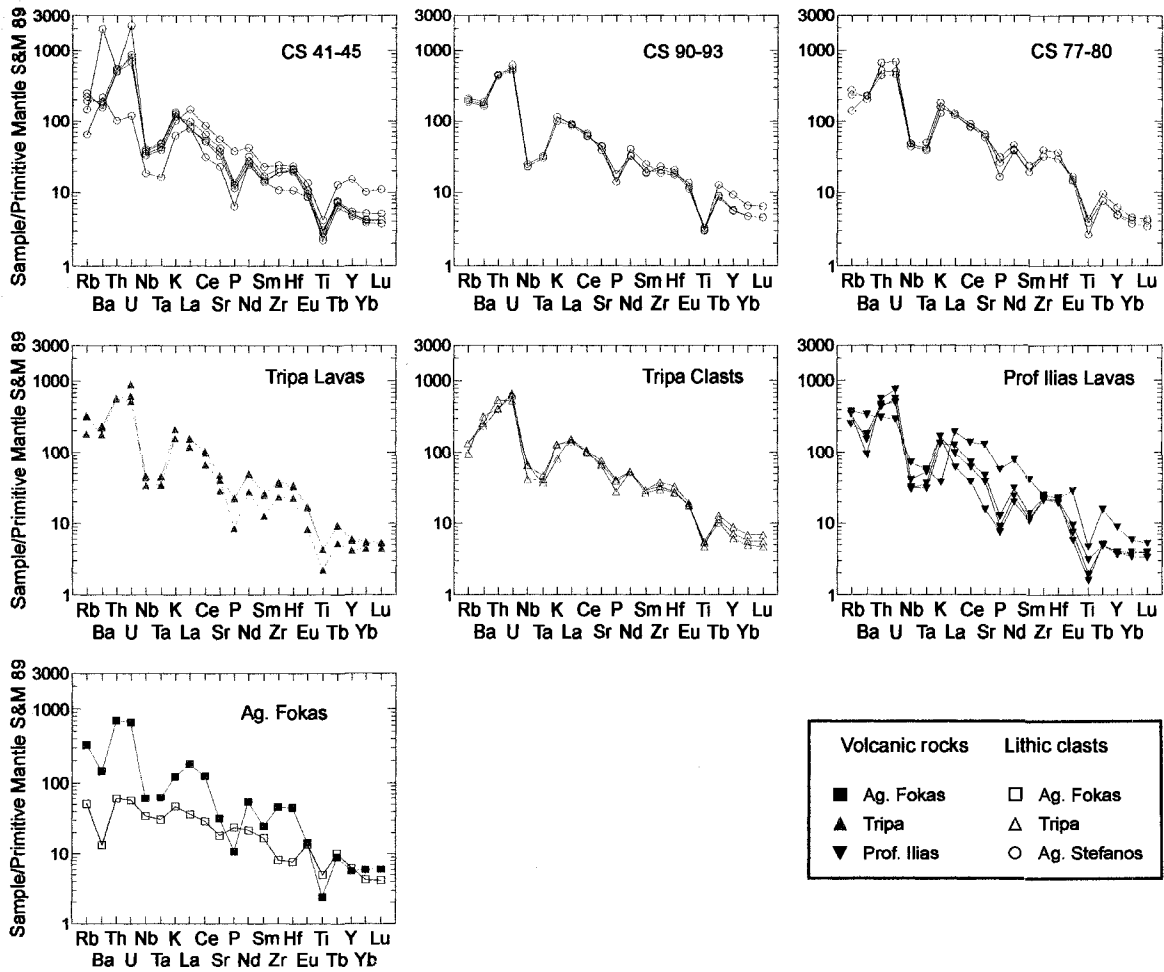


**Fig. 4.5:** Variations in selected trace elements, normalized to the primitive mantle (Sun & McDonough, 1989) for the Kos Upper Miocene volcanic rocks and the clasts from the pyroclastic rocks.

#### 4.8 Relation between clast petrography and geochemistry

The analyzed lithic clasts belong to particular types that were defined in the previous chapter according to petrographical criteria. These samples were plotted regarding to their petrographical type on the IUGS classification diagram (Fig. 4.6). This plot shows good correspondence between petrography and composition in the lithic clasts. Type E, however, plots as a trachyte and trachyandesite, which is something reasonable because this type contains clasts characterized by the presence of hornblende. In addition, petrographical types A2, A3 and D are geochemically distinct, as are types A4, C and E.

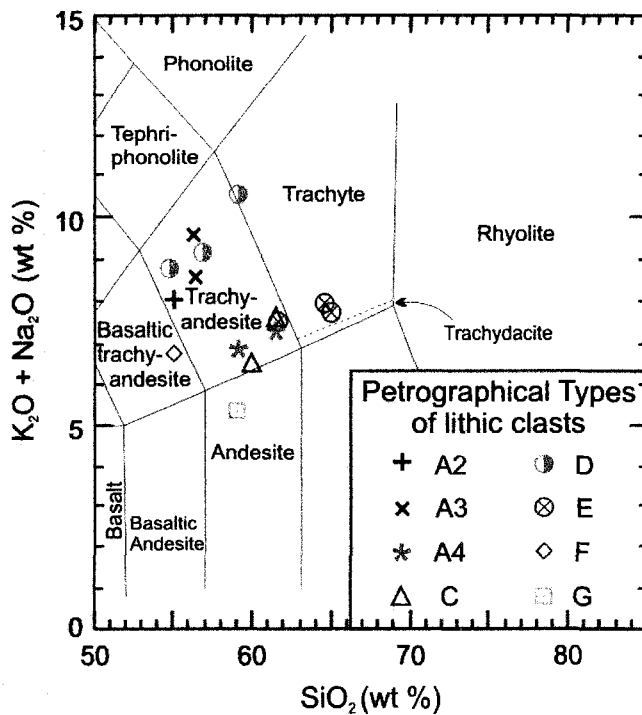
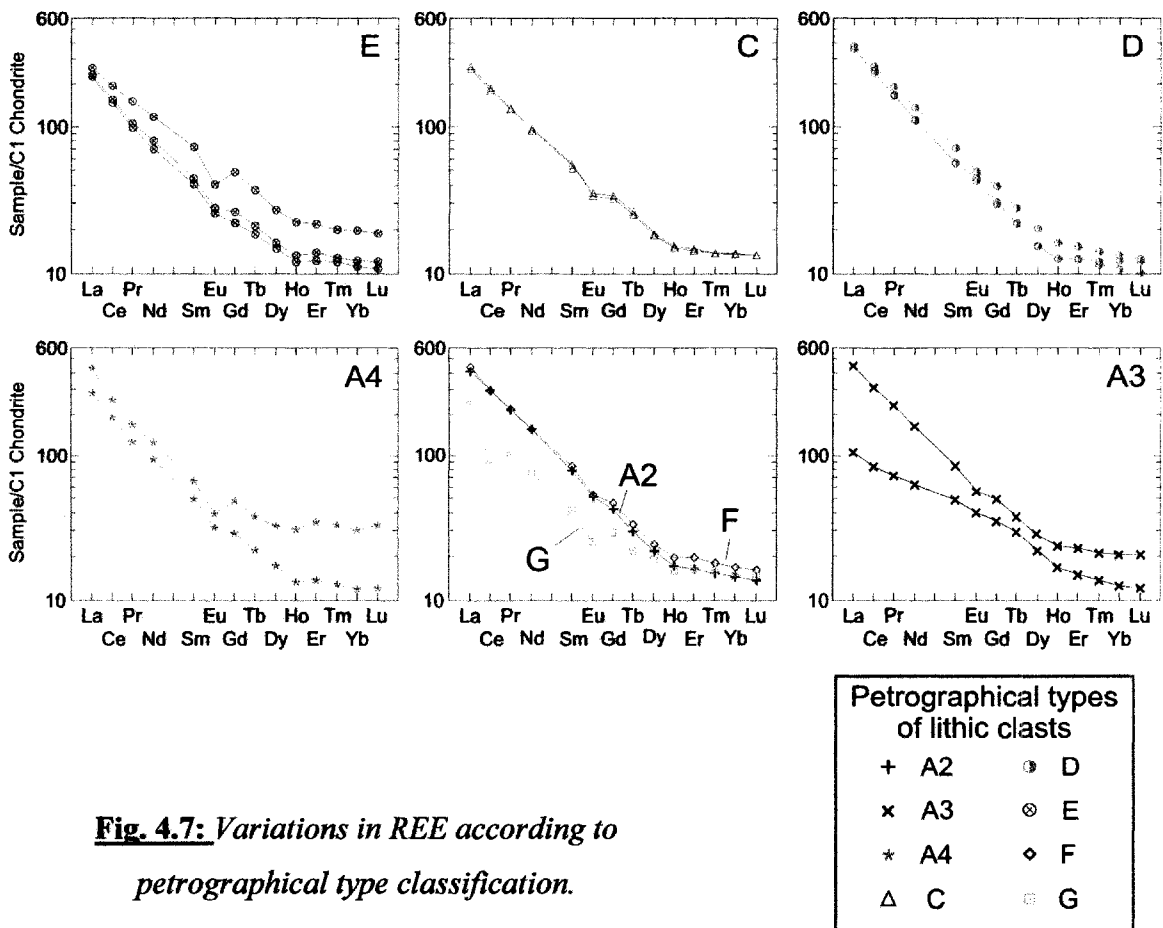


**Fig. 4.6:** *Geochemical nomenclature of the petrographical types of lithic clasts from the Miocene of Kos, by IUGS system for volcanic rocks (LeBas et al., 1986).*

The REE patterns show considerable variability (Fig. 4.7). The three analyzed samples of type E have the same trend but sample CS 90 has higher values as well as a stronger negative Eu anomaly. The two samples from type C are identical. The same can

be said for the three samples of type D which do not have Eu anomaly. In petrographical type A4, sample CS 43 has higher values and a negative Eu anomaly, and shows little fractionation from Tb to Lu, whereas sample CS 42 shows little fractionation from Ho to Lu. In type A3, the samples have the same general trend but sample CS 115 is less fractionated than CS 66. The other three types are represented by only one sample. Types A2 and F have the same REE pattern with D. The petrographical type G shows two negative anomalies in Eu and Ce, which is something unique compared to the rest of the patterns. Overall, the REE do not provide good discrimination of petrographical types. This is probably because the REE patterns are strongly controlled by accessory minerals.



#### **4.9 Comparison with other volcanic rocks of the Aegean Sea**

In this section the geochemistry of volcanic centres of late Miocene age in the southeastern Aegean Sea (Fig. 1.3) is compared with coeval volcanic rocks from Kos.

These volcanic centres are briefly described below:

1. **Patmos.** Volcanism on Patmos is of latest Miocene to early Pliocene age (7.4 – 4 Ma) (Fytikas et al., 1976; Robert & Cantagrel, 1979). Most rocks are trachyte to rhyolite. Minor basalt is present.

2. **Samos.** Volcanic rocks on Samos include trachyte of similar age (10 Ma) to those on Kos and latest Miocene bimodal basalt and rhyolite (Pe-Piper and Piper, 2007). These basalt and rhyolite are geochemically unlike the rocks on Kos.

3. **Bodrum.** On the Bodrum peninsula there is a volcanic centre with radiometric ages of 7.95 to 12 Ma (mostly ~10 Ma) (Fytikas et al., 1984; Robert & Cantagrel, 1979). However, the only published chemical analyses are for potassic mafic dykes (Robert et al., 1992). Therefore, geochemical comparisons of the volcanic rocks from Kos and Bodrum is not possible.

All of the trachytic volcanic rocks discussed above have been interpreted to result from small volume partial melts of enriched sub-continental lithospheric mantle (Robert et al., 1992; Pe-Piper and Piper, 2007). In addition, comparison is made with Lower Miocene K-rich volcanic rocks of the northeastern Aegean, represented by trachyandesite – trachyte – dacite of the island of Limnos. These rocks have been dated for 18 – 21 Ma (Innocenti et al., 1994; Fytikas et al., 1984). Similar shoshonitic rocks are known from Lesbos (Pe-Piper & Piper, 2003; Borsi et al., 1972) and Samothraki (Eleftheriadis et al., 1994).

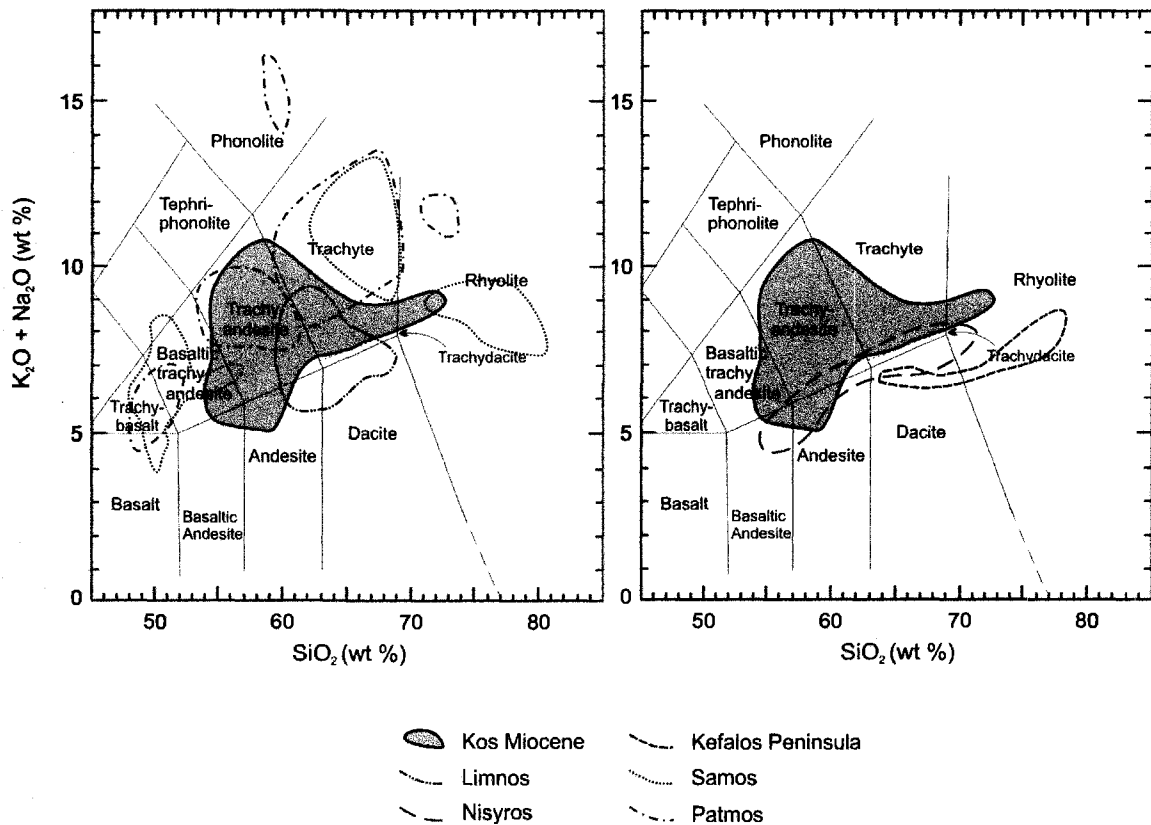


**Fig. 4.8:** IUGS plots for volcanic rocks showing fields for principal rocks of Samos, Patmos, Limnos, Kefalos Peninsula and Nisyros, compared to this of the Miocene of Kos.

The Kos Miocene samples plot in a field on an Alkali vs.  $\text{SiO}_2$  diagram (Fig. 4.8) that either overlaps or is geochemically distinct from those analyses representing Miocene volcanic rocks from the other volcanic centres. The overlap is most striking with the field where the trachyandesites of Patmos plot. However, the trachytes of both Samos and Patmos have higher wt. %  $\text{K}_2\text{O}$  and total alkalis than those of Kos. Furthermore, their REE patterns (Fig. 4.9) are less fractionated than those in Kos, with  $\text{La}_N = 200\text{-}300$ . The shoshonitic rocks from Limnos include dacites, but otherwise are similar to the Kos with

regard to major elements including  $K_2O$  and similar multi-element plots (including troughs at Rb and Ba).

REE patterns from other volcanic centres from the Aegean are were plotted in order to compare them with the Kos Miocene patterns (Fig. 4.9). One representative sample from each volcanic centre was plotted and notwithstanding the lack of values for some of the rare earth elements, the samples from Samos and Patmos are different. The Aegean volcanic rocks that most resemble those of Kos are the Lower Miocene trachyandesite and trachyte of the Romanou and Fakos units of Limnos, in the northeastern Aegean Sea (Pe-Piper et al. In press). The Limnos rocks have remarkably similar REE patterns with weak Eu anomaly and little fractionation for the heavy rare earth elements (HREE) from Ho to Lu (Figs. 4.4, 4.9). Pe-Piper et al. (In Press) argue that these distinctive characteristics, particularly the highly fractionated REE patterns, are the result of partial melting of enriched underplated mafic lower crust.

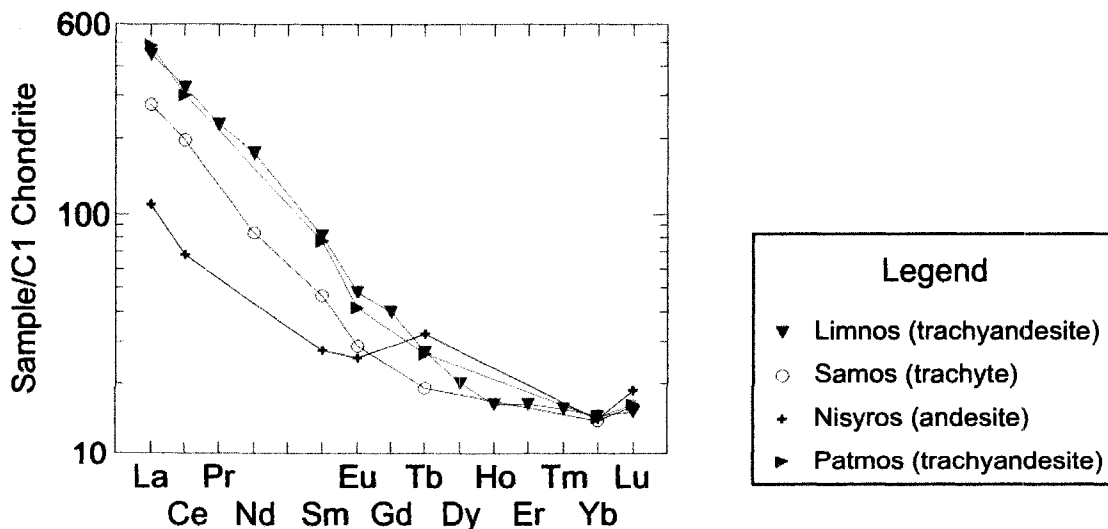


**Fig. 4.9:** REE plots for principal rocks of Limnos, Samos, Nisyros and Patmos.

It is also useful to compare the Kos Miocene volcanic rocks with Plio-Pleistocene volcanic rocks from the Kefalos Peninsula of Kos (Pe-Piper and Moulton, submitted) and with late Quaternary rocks from Nisyros (Vanderkluyzen et al. 2005). The Plio-Pleistocene rocks of the Kefalos Peninsula are rhyolite and dacite, with andesite enclaves. Compared with the Miocene rocks, they have quite different REE patterns ( $La_N = 100-200$ ) and multi-element plots (e.g., no troughs at Rb and Ba). The andesite from Nisyros has  $La_N$  of 100 and show a linear decrease in normalized abundance of light and middle REE, similar to the trachyandesite from Ag. Fokas (Fig. 4.4), but there is no increase in Tb. These rocks have been interpreted by Vanderkluyzen et al. (2005) to result principally from the fractionation of high-alumina basalt related to subduction processes and partial melting of base-of-crust amphibolite to form rhyolite melts. Late Quaternary volcanic rocks from Nisyros comprise basaltic andesite, andesite, dacite to trachydacite, and rhyolite. Geochemically, they are similar to the Kefalos Peninsula rocks and are thus quite unlike the Kos Miocene rocks.

In summary, the Miocene volcanic rocks of Kos show some geochemical features similar to trachytic rocks of Samos and Patmos, except that the REE are more fractionated and the  $K_2O$  content is lower in Kos. Their remarkable similarity to Early Miocene trachyandesite of Limnos suggests a similar petrogenetic origin. The Miocene rocks of Kos are quite different from the subduction-related andesites to rhyolites of Pliocene – Quaternary age in the Kefalos Peninsula and Nisyros.

#### **4.10 Geochemical constraints on the sources of the lithic clasts**

The lithic clasts from the pyroclastic rocks of Kos more closely resemble the volcanic rocks of Kos than those of any other Upper Miocene volcanic centres of the southeastern Aegean.

Clasts from Tripa pyroclastic rocks closely resemble Tripa trachyandesite lava in their major elements, trace elements, and REE patterns. They differ from clasts from the Ag. Stefanos pyroclastic rocks in having higher  $\text{TiO}_2$  and  $\text{La}_N$ . They could be derived from a local volcanic source geochemically similar to Tripa.

The clasts from the Ag. Stefanos pyroclastics were derived from a volcanic centre that was not geochemically very different from Tripa and Prof. Ilias. The slightly less fractionated REE patterns may indicate a larger trachyandesite volcano, with magma formed from a higher degree of partial melting of enriched mantle source rocks.

## CHAPTER 5

# *Directional analysis of pyroclastic rocks*

### **5.1. Introduction**

The unravelling of the stratigraphy, the petrology and the geochemistry of the studied pyroclastic rocks in the previous chapters leads to the next step which is the assessment of the spatial distribution of the potential volcanic centre(s). Thus, chapter 5 considers all the characteristics that were captured in the pyroclastic deposits and are related to the flow direction of pyroclastic currents. In addition, in order to better understand the paleotopography of the area during the pyroclastic accumulations, the paleocurrent indicators of the interbedded sediments were also studied.

### **5.2. Paleoflow Indicators in Pyroclastic Rocks**

Techniques based on the similar research that has been done in other pyroclastic successions in Greece (Pe-Piper, 1980; Dalabakis & Vougioukalakis, 1993), were applied to the pyroclastic flow deposits. Moreover, Branney & Kokelaar (2002) describe and interpret explicitly paleoflow indicators in ignimbrites. Those used are:

### **5.2.1 Orientation of elongate clasts on bedding planes**

This method requires observations on exposed bedding planes. Thus, the studied lithofacies have to be well-bedded. Measurements were made on elongated clasts with an aspect ratio of at least 1.5. The orientation of the long axis of these elongated clasts was either measured directly in the field or the bedding plane was photographed, so measurements can be taken later in the lab. These measurements were projected on rose diagrams. The preferred orientation of the clasts indicates flow direction. However, since the results are bidirectional, a unique flow direction cannot be determined by this method.

### **5.2.2 Imbrication of elongate clasts**

Once the bidirectional data of the flow direction has been established, the next step is to document the imbrication of the elongated clasts in sections orthogonal to bedding and parallel to the preferred orientation of the clasts. The first requirement is an outcrop with well-defined and clear bedding. This method involves searching for elongate clasts with the long axis oblique rather than parallel to the inferred bedding, creating an inclined dipping fabric. The imbricated clasts dip in the up-flow direction. This can be measured either directly in the field or from oriented field photographs.

### **5.2.3 Elutriation sheets and pipes**

These sheets and pipes are characterized by areas of concentrate coarse lithic clasts, which usually are up to 10 cm in size. The dimensions of these sheets can reach more than 3 m in length and 1 m in width. The occurrence of elutriation sheets and pipes in the massive ignimbrites of Ag. Stefanos and Ag. Fokas is rare overall, but common in some

stratigraphic horizons. According to Branney & Kokelaar (2002), these structures are created when the substrate is wet and unstable and a layer of lithic clasts is accumulated. The escaping gasses from the substrate in conjunction with the gravitational collapse of the relatively heavier lithic clasts, leads to their sinking across the degassing channels, creating these sheets. During the deposition of rapidly accreted ignimbrites, the flow currents cause shear deformation that rotates the original vertical alignment of the pipes and sheets. The sheets and pipes thus become inclined up-flow. Often, the elutriation sheets appear convex towards the origin of the current. In the field, elutriation sheets that are not perpendicular to bedding were used for measuring their orientation and that of bedding. Due to regional tectonic tilting, the orientation and dip direction of these sheets requires correction to an original horizontal orientation. This was calculated by using Schmidt net projections.

#### **5.2.4 Erosional grooves**

Grooves formed on erosional surfaces occur as parallel depressions and crests along the contact of two different lithofacies. As with elongated clasts, the axis of these grooves is bidirectional.

### **5.3. Paleoflow Indicators in Sedimentary Rocks**

The voluminous pyroclastic successions in both Ag. Stefanos and Ag. Fokas contain interbedded clastic sediments. Paleocurrent directions were measured on single sets of planar **cross-bedding** in medium to coarse grained sandstones (bar margins or lake-margin deltas) and on ripple **cross-lamination**. In the case of the volcaniclastic

conglomerates, blocking effects of boulders were identified in the field, and the general orientation of channels filled with coarse volcanoclastic conglomerate was measured. The other directional structure recognized in lacustrine rocks was the orientation of syn-sedimentary slump folds, which eventually formed close to the boundaries of the sedimentary basin.

The paleoflow indicators identified in the field are described below. These are presented in stratigraphical order in both Ag. Stefanos and Ag. Fokas.

#### **5.4 Ag. Stefanos**

In Ag. Stefanos, the thick coarse-grained volcanoclastic conglomerates of units A2-A6 in the Lower Sedimentary Unit were investigated for possible paleocurrent indicators. In particular, structures around large boulders were examined. In several cases, concentrations of cobbles were found on the down-dip side of boulders and in one case a scour was found on the down-dip side of boulders. These features were identified at localities 134, 215, 217, 299 and 304. The interpretation of these observations is ambiguous. In more turbulent hyperconcentrated flows, "tails" of cobbles are found on the down-flow sides of boulders, with scour on the up-flow side (Kim et al., 1995). On the other hand, in less turbulent hyperconcentrated flows, including many pyroclastic flows (Elston & Smith, 1970) and debris flow, large clasts move more slowly than the surrounding fluid and smaller clasts concentrate on the up-flow side of the large clast, the so-called "blocking effect". The one observation of scour implies a flow to north; the observations of cobbles on the down-dip side of boulders imply flow to the north if this is a blocking effect or flow to the south, if it is a "tail" from a turbulent flow. No

sedimentary structures were found in the thin interbedded sandstones, so that the paleocurrent significance of structures in the conglomerates remains ambiguous. There are no measured paleocurrent data from the Lower Pyroclastic Unit.

Stratigraphically upwards, medium to coarse grained sandstones as well as granule conglomerates of the Middle Sedimentary Unit were studied in the field (Fig. 5.1), The interpreted paleoflows are multidirectional, ranging from the S, SW, W, NW, N, NE and E (Fig. 5.2). They show no systematic pattern according to either spatial or stratigraphic distribution, so that even in cases where the measurements were made in nearby outcrops, there are significant differences in current direction.

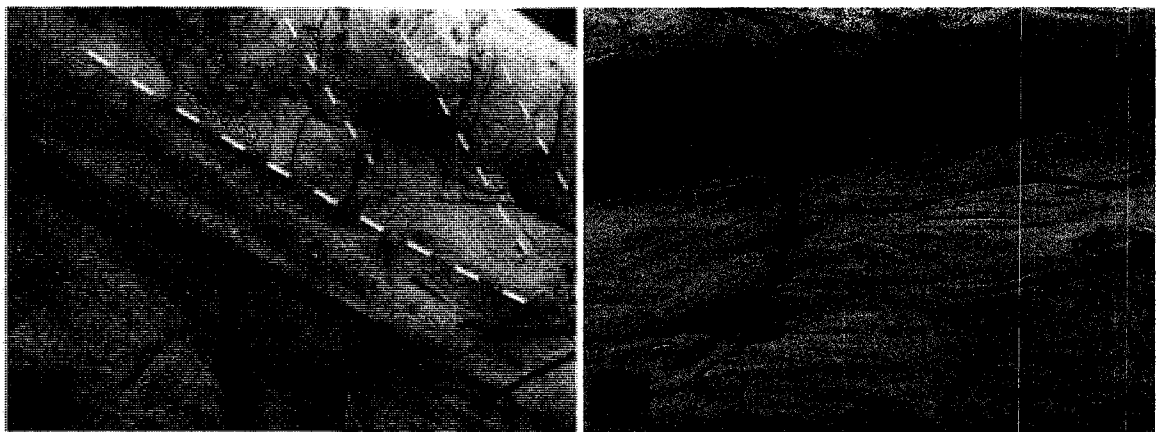


**Fig. 5.1:** a) *Typical dune x-bedding in sandstone at locality 156.*

b) *Ripple x-lamination in medium-grained sandstone (locality 262).*

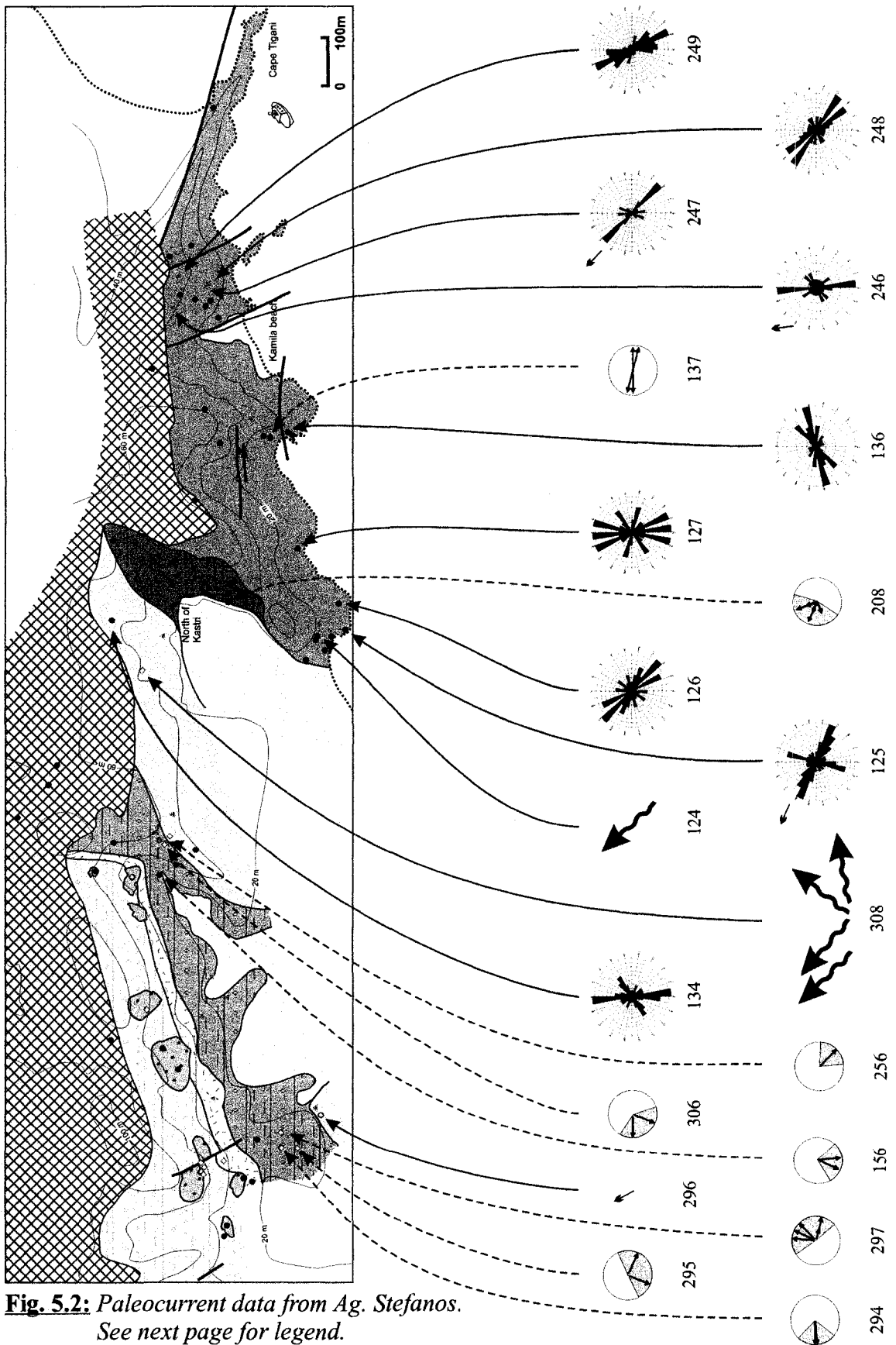


**Fig. 5.2:** Paleocurrent data from Ag. Stefanos.  
 See next page for legend.

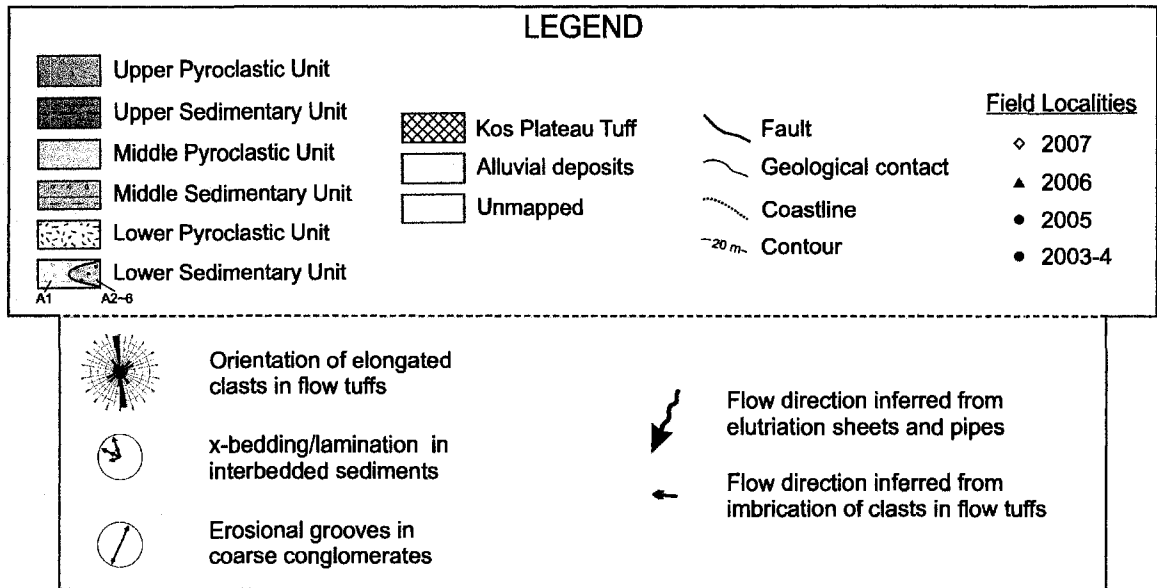


**Fig. 5.2:** *(continued)*

In one locality (134) of the Middle Pyroclastic Unit, elongated lithic clasts were measured and plotted in rose diagram showing preferred orientation of N-S. In addition, in locality 308 four elutriation sheets were measured showing paleoflow from SE through SW to W.

In the Upper Sedimentary Unit, cross-bedding in medium to coarse grained sandstone shows flow directions to WSW, WNW and NNW. The upper part of the succession (Upper Pyroclastic Unit) was studied intensively. Tens of elongated clasts were measured and 8 rose diagrams were created (Fig. 5.3). The rose diagrams from the localities 125, 126, 247, 248 and 249 show a general NW-SE orientation of clasts. In localities 127 and 246 this direction is N-S and only the diagram from locality 136 shows a preferred orientation of WSW-ESE (Fig. 5.2). The imbrication direction was identified in three of the localities (125, 246 and 247), suggesting a paleoflow direction to the N or NW (Fig. 5.4). At locality 137, erosional grooves and crests are present on the contact

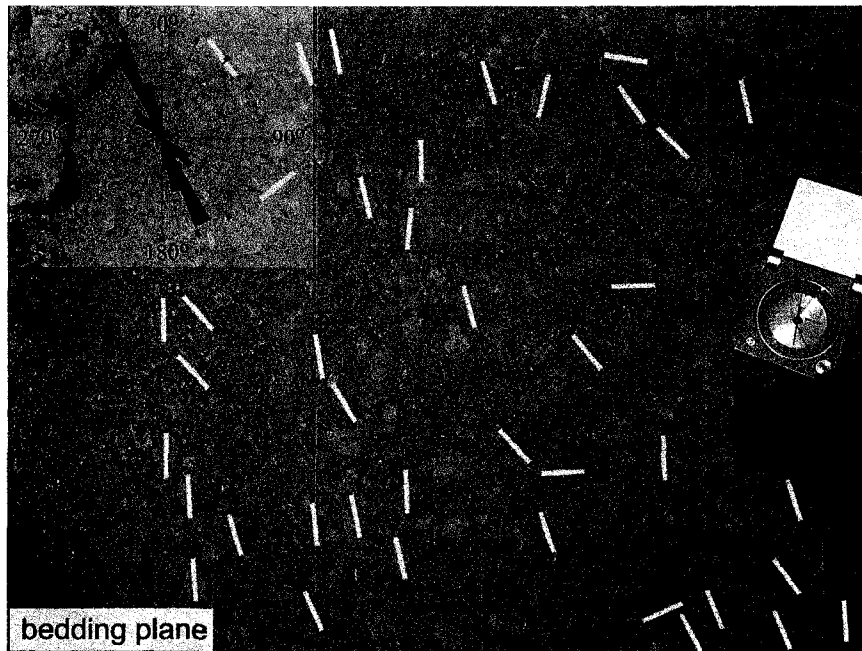


**Fig. 5.3:** *Elongated clast orientations. The yellow line corresponds to the long axis of the elongated clast. On the upper left side, the rose diagram shows the preferred orientation of the measured clasts.*

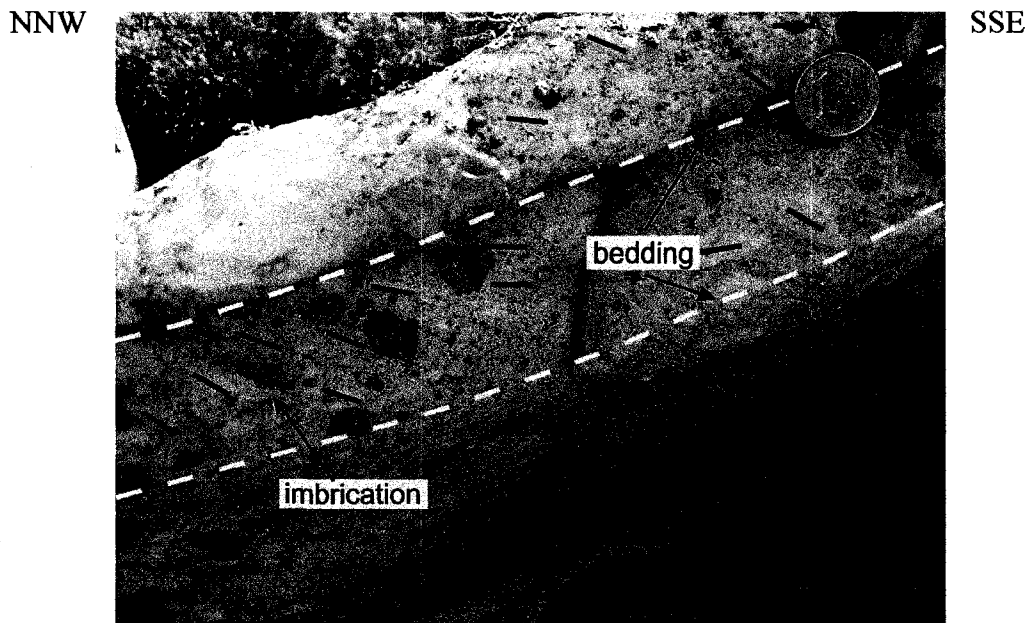


**Fig. 5.4:** *Vitric-lithic ignimbrite from the Upper Pyroclastic Unit. Imbrication dips to SSE and flow direction from the right to the left.*

between the flow tuffs and the superjacent clast-supported volcanoclastic conglomerate (bed F25b) (Fig. 5.5). These are oriented E-W. The only curved elutriation sheet was found at locality 251, implying flow direction towards NW (Fig. 5.6).

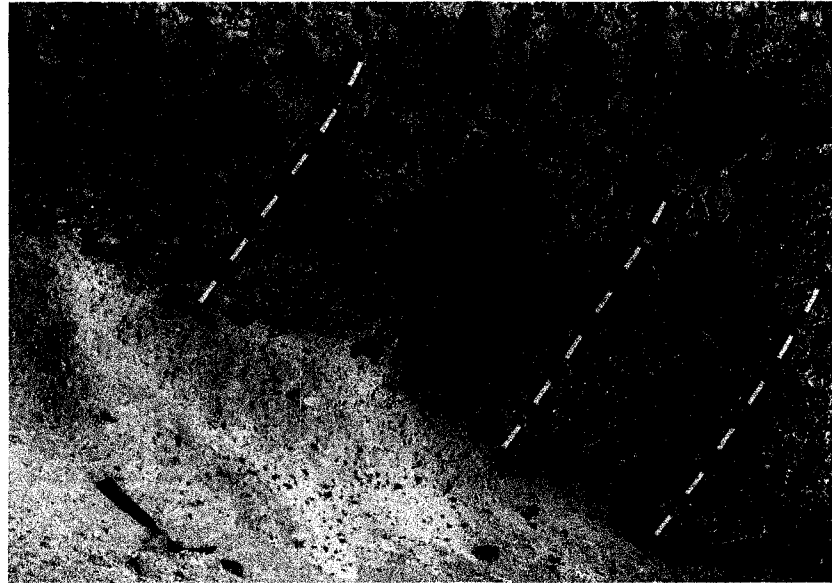


**Fig. 5.5:** *Erosional grooves at the bottom of a clast supported volcanoclastic conglomerate.*

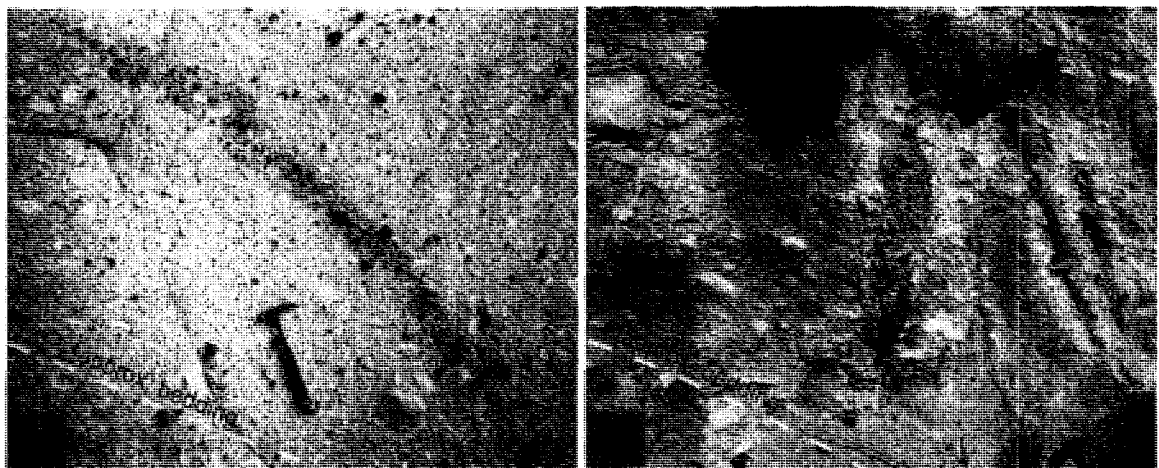


**Fig. 5.6:** a) *Curved elutriation sheet shows flow direction towards NW.*  
b) *Concentration of lithic clasts in an elutriation sheet.*

## **5.5 Ag. Fokas**

Across the cliffed coastline of Ag. Fokas, where the sedimentary rocks of the Lower Sedimentary Unit crop out, paleoflow indicators were identified in thick medium grained sandstones and granule conglomerates. The dune sets and ripple cross-laminations of locality 281 show sediment transportation towards SW to NNW (Fig. 5.8).

Stratigraphically upwards and approximately 100 m to the SW, airfall tuff beds, interbedded with marls, appear to be slump folded with the fold facing to the NNE. This fold is reversely faulted with strike direction WNW – SSE (Fig. 5.7). This is evidence for a palaeoslope dip direction toward the NNE. The elongated clasts identified few decimetres above are oriented to N – S and NNW – SSE. However, imbrication in those beds was not identified.



**Fig. 5.7:** *Slump of marls and airfall tuff beds. Brittle deformation with synchronous reverse faults is also present (red lines and arrows).*

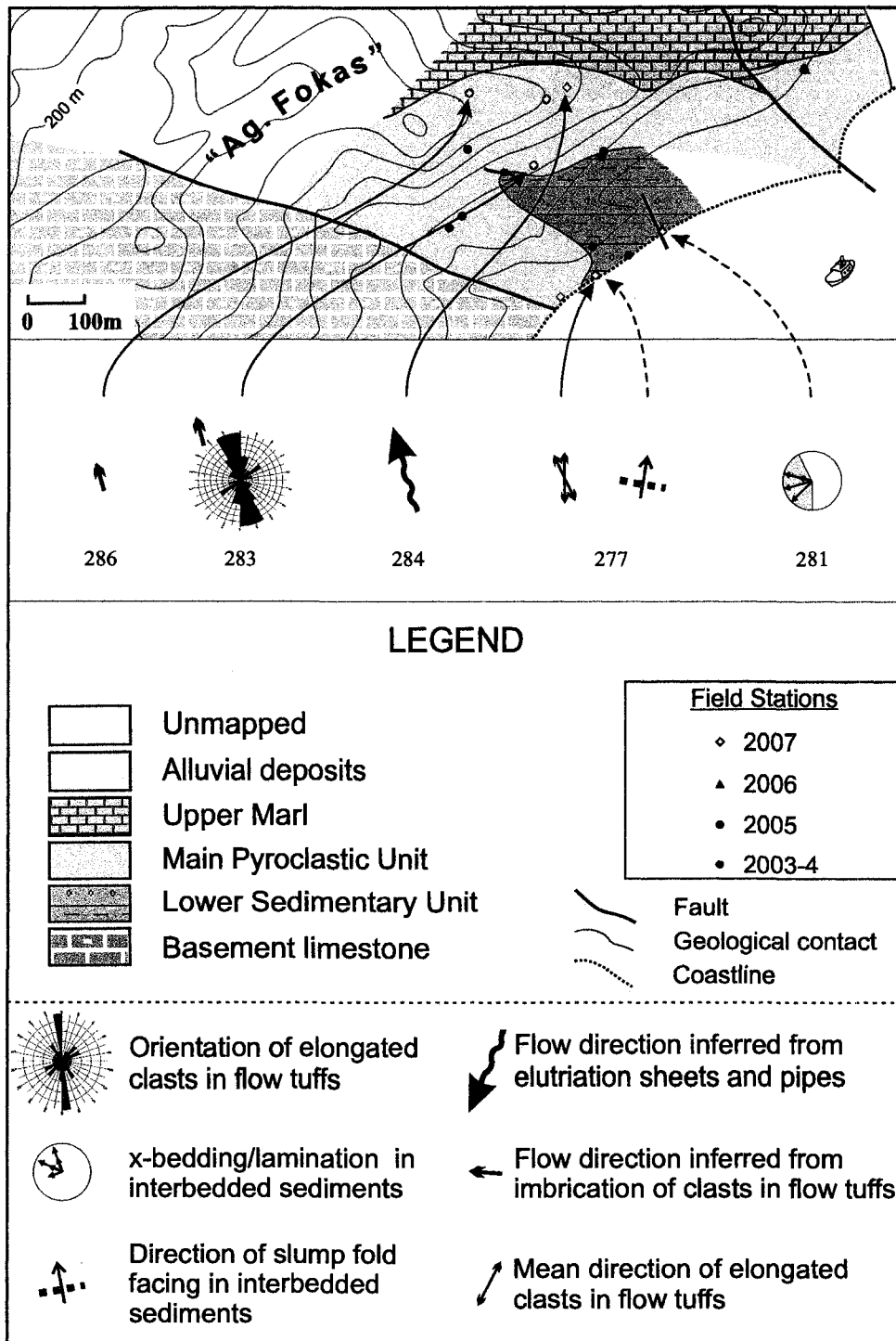


**Fig. 5.8:** Paleocurrent data from Ag. Fokas.

At locality 283, a surface parallel to bedding plane was used for measuring the elongated lithic clasts of bed J6. These clasts show a general NNW-SSE orientation, with the imbrication of pumice clasts indicating a flow direction to NNW (Fig. 5.8). Imbrication direction almost the same was also determined at locality 286. Elutriation sheets were found in a few localities, but bedding was uncertain except at locality 284, where a 2 m long sheet suggests a flow direction to NNW.

## **5.6 Synthesis**

In Ag. Stefanos, the flow direction for the thick coarse-grained volcanoclastic conglomerates is uncertain. Flow directions in sandstones interbedded with the pyroclastic succession are highly variable, with no preferred orientation. This suggests that above the Lower Pyroclastic Unit, there was no strong paleotopographic control in the depositional area. On the contrary, reliable interpretation of flow directions from the pyroclastic rocks is based on the orientation of lithic clasts, their imbrication and the orientation of elutriation sheets, all suggest that they originated from the SE (Fig. 5.9).

In Ag. Fokas, the Miocene sandstones underlying the pyroclastic succession has been derived from the NE to SE. However, the slumped marls and the overlain airfall tuffs which are a few decimetres stratigraphically above show a direction of slope vergence to the NNE. Although paleocurrent data are sparse in the pyroclastic rocks, they are consistent with flow from the SSE (Fig. 5.9).

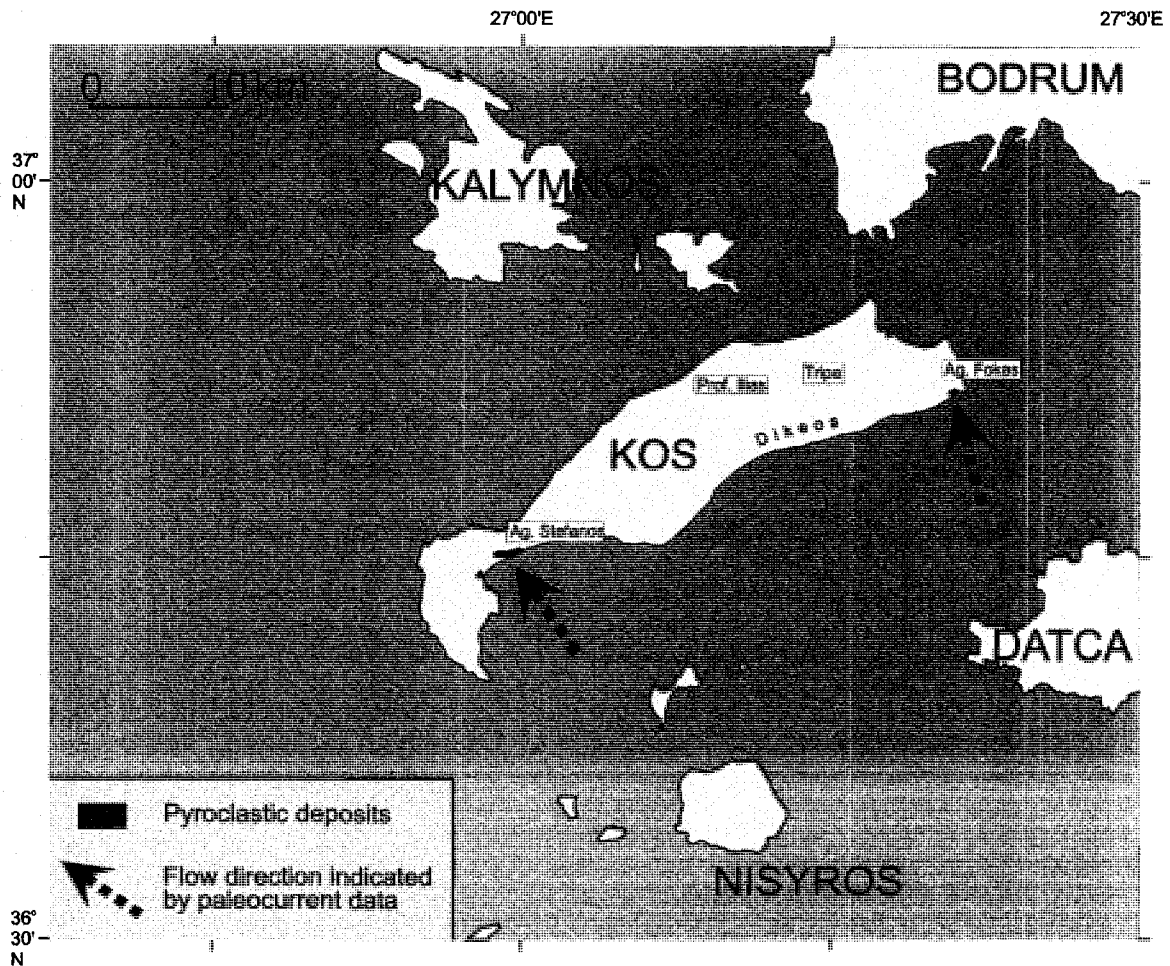


**Fig. 5.9:** Suggested flow direction for the pyroclastic deposits of Ag. Stefanos and Ag. Fokas according to interpretations regarding the orientation of lithic clasts, their imbrication and the elutriation sheets.

## CHAPTER 6

### *Discussion - Conclusions*

#### **6.1 Stratigraphic position of the Upper Miocene pyroclastic rocks**

Radiometric dating at Ag. Stefanos (Bellon & Jarriège, 1979), Tripa (Besang et al., 1977) and Ag. Fokas (Altherr et al., 1982) shows that the volcanic or pyroclastic rocks at these localities are of the same age of ~10.7 Ma to within the error limits of the dating (generally  $\pm 0.5$  Ma or better). This corresponds to the early part of the Tortonian Stage of the Upper Miocene.

The volcanic rocks at Prof. Ilias have not been radiometrically dated. However, they appear to be the same age as the other volcanism on the basis of (a) geochemical similarity; (b) their stratigraphic position which directly overlies the Mesozoic basement, as is also the case for Tripa; and (c) their stratigraphic position beneath the Pliocene conglomerates of the Konstantinos Formation of Willman (1983).

The volcanic stratigraphy of Ag. Fokas starts with air-fall tuffs interbedded with lacustrine marls of the Vasilios Formation of Boger et al. (1974) and Willman (1983), of Late Miocene age. These air-fall tuffs pass upward into flow tuffs with minor interbedded

marls. The 80 m thick succession of tuff is interrupted by two thin intervals of sediment, one marl and the other sandstone. The upper pyroclastic section is interbedded with volcanoclastic sandstone and conglomerate containing some extrabasinal clasts and appears to be overlain conformably by marl of the Palioskala Formation of Boger et al. (1974), of Late Miocene age.

At Ag. Stefanos, the lowest volcanic rocks are volcanoclastic conglomerates that occupy channels cutting lacustrine marls of Protocaravo member of Besenecker and Otte (1978), that they interpreted as Middle to Late Miocene in age. It is then followed by a pyroclastic unit rich in limestone clasts. This is overlain by 50-60 m of marls and clastic sediments, a 10-20 m pyroclastic succession, a further 80 m of more sedimentary rocks and finally 60 m of pyroclastic rocks. Sedimentary rocks immediately overlying the Upper Pyroclastic Unit are not preserved.

Basinal sediments north of Tripa consist of the Middle Miocene marine Askklupi Formation, consisting of bioclastic limestone and siliciclastic rocks, followed by lacustrine sedimentation of the Upper Miocene Vasilios Formation (Boger et al., 1974). The Vasilios Formation consists of marls, in places with slump structures, that are interbedded with a few air-fall tuff beds and a few lithic-vitric flow-tuff beds at least 30 cm thick.

There is thus evidence that the Middle Miocene marine sediments pass up into thick Upper Miocene lacustrine sediments in two basins. The first one is north of the Dikeos massif, including the area north of Tripa and northeast of Prof. Ilias. The other one is south of the Dikeos massif, including both the areas of Ag. Fokas and the thick Miocene sedimentary rocks of Kefalos peninsula. At the southern edge of the northern basin, thin

volcanic rocks outcrop at Prof. Ilias and Tripa and in some fault slices southwest of Tripa, and directly overlie the alpine basement. The Prof. Ilias volcanic succession is overlain by the Pliocene Konstantinos Formation, whereas at Tripa and Ag. Fokas North both the basement and the volcanic succession are apparently overlapped by lacustrine marls of the Vasilios Formation.

In summary, in the Middle to Late Miocene, the basins (grabens) of northern and southern Kos were separated by the Dikeos horst. Subsidence of the northeastern part of the horst led to onlap of the upper Vasilios Formation over thin volcanic successions. The widespread lack of Lower Pliocene rocks is the result of renewed uplift of the Dikeos horst, probably at the same time, causing shedding of the eroded coarse clastic sediments which belong to the Konstantinos Formation.

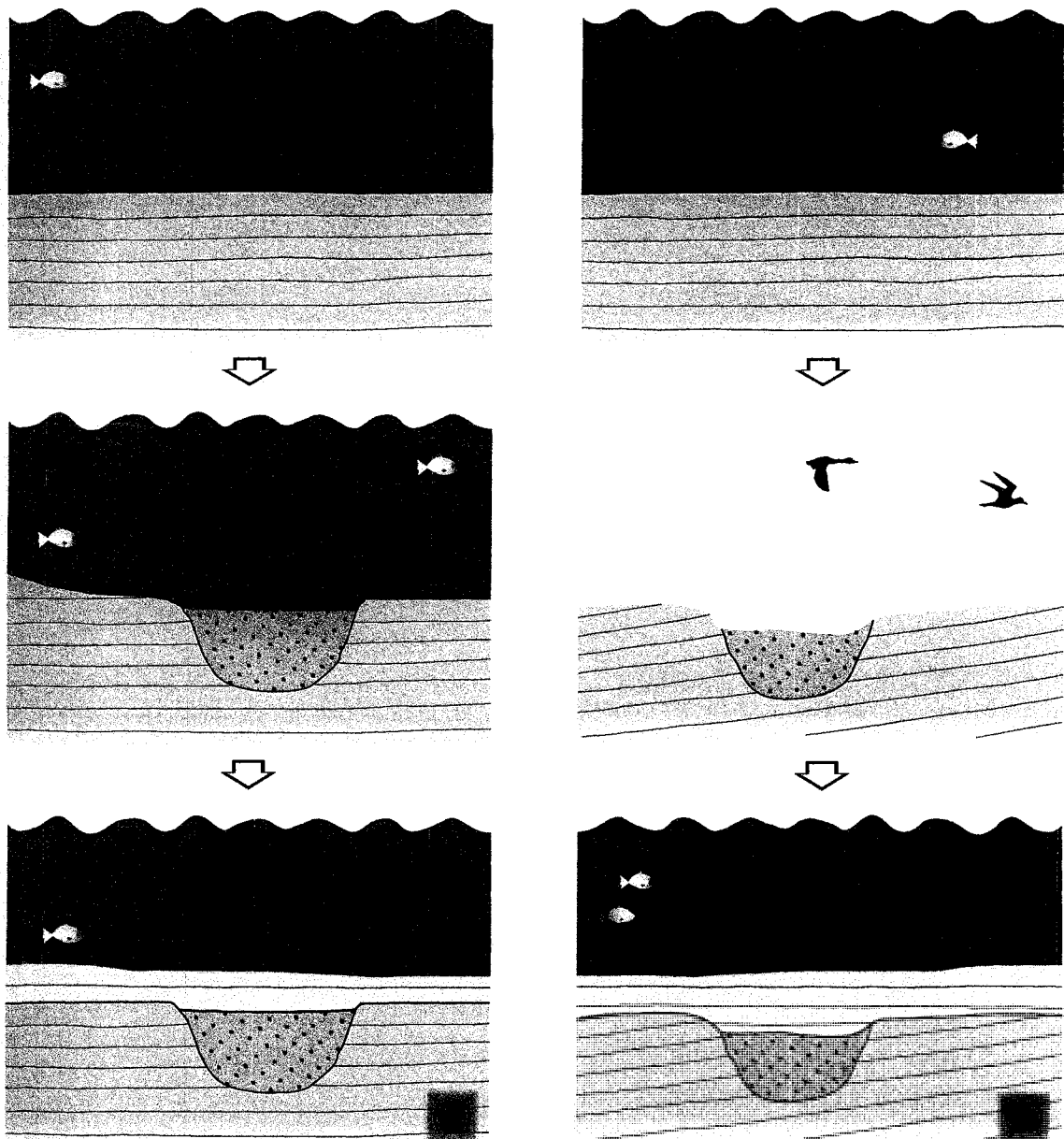
## **6.2 Volcanology of the Upper Miocene volcanic rocks**

The section at Ag. Fokas starts with air-fall tuffs interbedded with lacustrine marls. The air-fall tuffs become more abundant upward. The stratigraphically highest air-fall tuffs and their host marl show slumping to the NNE. These are overlain by 12 m of flow tuffs, with a large raft of marl 2 m above the base of the flow tuffs and then by a thin marl. The architecture of this succession suggests that some of the pyroclastic flows entered the lake in which the marls were accumulated, causing the erosion and deformation of some of the underlying marls. Comparable direction of the pyroclastic flows into the sea has been recently described by Hart et al. (2004) and inferred by Anastasakis and Pe-Piper (2006).

In the Ag. Stefanos succession, the basal volcanoclastic conglomerates appear to occupy channels, cutting lacustrine marls. It is not known if the channels are sub-lacustrine or subaerial. In the first case the sediments that host the conglomerates and the overlying sediments would be conformable (Fig. 6.1a), whereas in the second case sediments which overlie the conglomerates and related sediments might be unconformable due to transgression and subsidence (Fig. 6.1b). However, the angle of the unconformity would be small and consequently difficult to identify in the field. By analogy with Ag. Fokas, the conglomerate-filled channels may be sub-lacustrine.

The sandstones interbedded with the pyroclastic successions contain extra-basinal clasts, pointing to an alpine basement source, but deposition of the ignimbrites resulted in a flat fluvial or shallow lacustrine plain in which the sedimentary rocks were deposited with highly variable paleocurrent directions.

The interbedded sedimentary rocks at both Ag. Stefanos and Ag. Fokas allow eruptive cycles to be identified, followed by quiescent periods when sedimentary rocks accumulated. An individual eruptive cycle, emplaced perhaps over a few only days, may show less indurated tuffs at the base and more welded, cliff-forming tuffs towards the top. The basal flow tuffs can overlie thin air-fall tuffs. Crystal-rich air-fall tuffs can also characterize the top of the eruptive cycle. Individual pyroclastic flow units within the eruptive cycle generally have a basal lithic-rich breccia overlain by a thicker vitric-rich tuff, as seen in the Pleistocene Kos Plateau Tuff (Allen et al., 1999). In general, lithic clasts are rather similar throughout an eruptive cycle. In Ag. Stefanos, the three pyroclastic units give the evidence for six to seven eruptive cycles; one for the Lower



- Alternating marls, sandstones and shales
- Volcanoclastic conglomerates

**Fig. 6.1:** Schematic sections showing the three stages of the two proposed depositional environments for the channelised volcanoclastic conglomerates, before the arrival of the Lower Pyroclastic Succession.

- a) The case of sub-lacustrine deposition.
- b) The case of subaerial deposition.

Sedimentary Unit, one for the Middle Sedimentary Unit and four to five for the Upper Pyroclastic Unit. The Ag. Fokas succession consists of 7 to 9 eruptive cycles.

Petrographic data shows that some types of lithic clasts are ubiquitous across the same section (types A1, A2 in Ag. Stefanos), as well as in the localities of Ag. Stefanos, Ag. Fokas and Ag. Fokas North (types A2, C). This suggests that Ag. Stefanos and Ag. Fokas might have come from the same source, but do not record all the same eruptive cycles. The occurrence of different petrologic types in particular localities, for instance type E only in Ag. Stefanos or type D only in Ag. Fokas, may be the result of a particular petrological type being common in only one eruptive cycle. The geochemical data show that the voluminous pyroclastic accumulations were derived from a volcanic centre that geochemically was not very different from Tripa and Prof. Ilias, but did not resemble any of the other Upper Miocene volcanic centres of the southeastern Aegean.

The regional topography would have controlled not only the paths of the interbedded sediments but also the route of the pyroclastic deposition. The lack of thick flow tuffs at Ag. Fokas North, only 450 m from Ag. Fokas, suggests that there may have been an important topographic control on the distribution of flow tuffs. Likewise, thick flow tuffs are absent at Tripa and Prof. Ilias where possibly the horst at Dikeos Mt., which is located between the two basins, obstructed further transportation northwards (Fig. 5.9). The presence of extrabasinal, granule to fine pebble size clasts in interbedded sandstones at both Ag. Stefanos and Ag. Fokas indicates considerable relief at the time the pyroclastic successions were accumulated.

Plinian fall-out lapilli tuffs have nowhere been seen in the Miocene of Kos. This suggests that all the pyroclastic rocks are relatively distal (i.e., more than few kilometres

from the source vent). The small volume of volcanic products and the lack of Plinian deposits rules out Tripa and Prof. Ilias as sources of the major pyroclastic successions.

### **6.3 The volcanic source of the thick pyroclastic successions**

We have already argued that the lack of Plinian deposits and the small size of the Tripa and Prof. Ilias volcanism make it unlikely that the source volcano for the pyroclastic successions at Ag. Stefanos and Ag. Fokas was on the island of Kos. Likewise, the geochemical constrains indicate that the lavas from Tripa differ from clasts from the Ag. Stefanos pyroclastic rocks in having higher  $\text{TiO}_2$  and  $\text{La}_N$ . Multiple pyroclastic eruptive cycles tens of meters thick with abundant trachy-andesite and trachyte lithic clasts, imply a major source volcano likely with complex successions of lava flows, dykes and pyroclastic rocks, as seen in the modern volcano of Santorini (Druitt et al., 1999) and the late Miocene Bodrum volcanic complex (Robert et al., 1992).

The maximum size of lithic and pumiceous clasts at Ag. Stefanos and Ag. Fokas can be used as an approximate indicator of the distance from a major source vent, using the clast size distribution from the Pleistocene Kos Plateau Tuff (KPT) (Allen et al., 1999) as a guide. The typical maximum size of pumice at Ag. Stefanos is 8 cm, with the largest clast seen measuring 35 cm, whereas the equivalent data for the lithic clasts are 3 cm and 12 cm. For Ag. Fokas, the normal maximum size of vitric clasts is 4 cm with the largest ones to be around 12 cm, and 2 and 15 cm for the lithic clasts. In the KPT eruption Allen (2001) recorded lithic clasts up to 1-2 m in diameter at one horizon, with the typical maximum clast size of 20 cm. In both the KPT and the Miocene tuffs, different units have different clast sizes in the same area, which probably reflects

differences in the dynamics of each eruptive episode. It seems that the source of the Miocene pyroclastic rocks, if the source volcano had the eruption style of the KPT, would have been a little more distal.

The Bodrum volcanic complex is unlikely to be the source of the Ag. Fokas and Ag. Stefanos pyroclastic successions, although radiometric dating reported by Fytikas et al. (1984) suggests that it may be of similar age. Bodrum is situated northeast of Kos and can be excluded as the source for the following reasons:

- (a) Thick pyroclastic accumulations are found on the south side of the Dikeos horst, which as has been demonstrated acted as a topographic barrier. Even in basinal settings on the north side of the horst, there are only a few thin flow tuffs within the Vasilios Formation.
- (b) Paleoflow directions in the pyroclastic succession of Ag. Fokas are from the south (Fig. 5.8), whereas Bodrum lies almost due to north (Fig. 5.9). Topographic influences on flow are unlikely to have caused complete reversal of flow direction.
- (c) Ag. Fokas is more proximal than Ag. Stefanos with respect to Bodrum, being ~23 km compared with ~42 km distant. However, the grain size of the coarsest lithic and vitric clasts at Ag. Stefanos (Fig. 2.26) is greater than Ag. Fokas. The Ag. Fokas succession was deposited in a basinal setting, perhaps with more accommodation than at Ag. Stefanos, indicated by the greater proportion of interbedded lacustrine marl. It therefore cannot be argued that the pyroclastic flows derived from Bodrum bypassed Ag. Fokas on their way to Ag. Stefanos.

The paleoflow directions at Ag. Stefanos and Ag. Fokas indicate that the source volcano was located south of Kos and the size of clasts suggests that Ag. Stefanos was

more proximal than Ag. Fokas. This is also indicated by the presence of the coarse volcanoclastic conglomerate facies underlying the Pyroclastic Succession at Ag. Stefanos. The size of clasts suggests that the source volcano was not more than a few tens of kilometres distant. The area south of Kos is now largely submerged beneath the sea, but the most likely source would be a volcano on the site of the present island of Nisyros and the Pleistocene Kos Plateau Tuff caldera between Yali and Nisyros (Fig. 6.2). Such a source would account for the observed variation in maximum size of pumice and lithic clasts and the observed paleoflow direction at Ag. Stefanos (Fig. 5.2). The sparse paleoflow indicators at Ag. Fokas indicate flow from the south; this is consistent with the source in Nisyros (to the southeast of Ag. Fokas), if there were minor topographic control on flow, perhaps by the western end of the Datca horst. An alternative source due to south of Ag. Fokas and southeast of Ag. Stefanos would not explain the more proximal facies at Ag. Stefanos compared with Ag. Fokas.

An additional line of evidence supporting a Nisyros source is that the modern Nisyros volcano is underlain by alpine limestones (St. Seymour & Vlassopoulos, 1989). The Lower Pyroclastic Unit at Ag. Stefanos includes abundant large lithic clasts of limestone (Fig. 2.20).

#### **4.4 Major Element variation**

Harker diagrams show a negative correlation between  $\text{SiO}_2$  and  $\text{Al}_2\text{O}_3$ ,  $\text{TiO}_2$ ,  $\text{FeO}_t$ ,  $\text{CaO}$ ,  $\text{MgO}$ ,  $\text{MnO}$ ,  $\text{P}_2\text{O}_5$  and a positive correlation with  $\text{K}_2\text{O}$ .  $\text{Na}_2\text{O}$  shows considerable scatter (Fig. 4.2).

#### **4.5 Trace Element variation**

Variation diagrams of eight trace elements versus  $\text{SiO}_2$  are illustrated in Fig. 4.3. The rocks show the expected decrease in most incompatible trace elements with increasing  $\text{SiO}_2$ . One clast from Ag. Stefanos shows an extremely high concentration of Ba (14,000 ppm), probably due to hydrothermal alteration. Rb shows similar behaviour to  $\text{K}_2\text{O}$  in having relatively positive correlation with  $\text{SiO}_2$ . The  $\text{La}/\text{SiO}_2$  ratio is higher for the volcanic rocks ( $\text{La}/\text{SiO}_2 = 1.67$ ) compared with the lithic clasts ( $\text{La}/\text{SiO}_2 = 1$ ). A similar trend is seen less clearly for Zr and Rb, but no other systematic differences between volcanic, rocks and lithic clasts were noted.

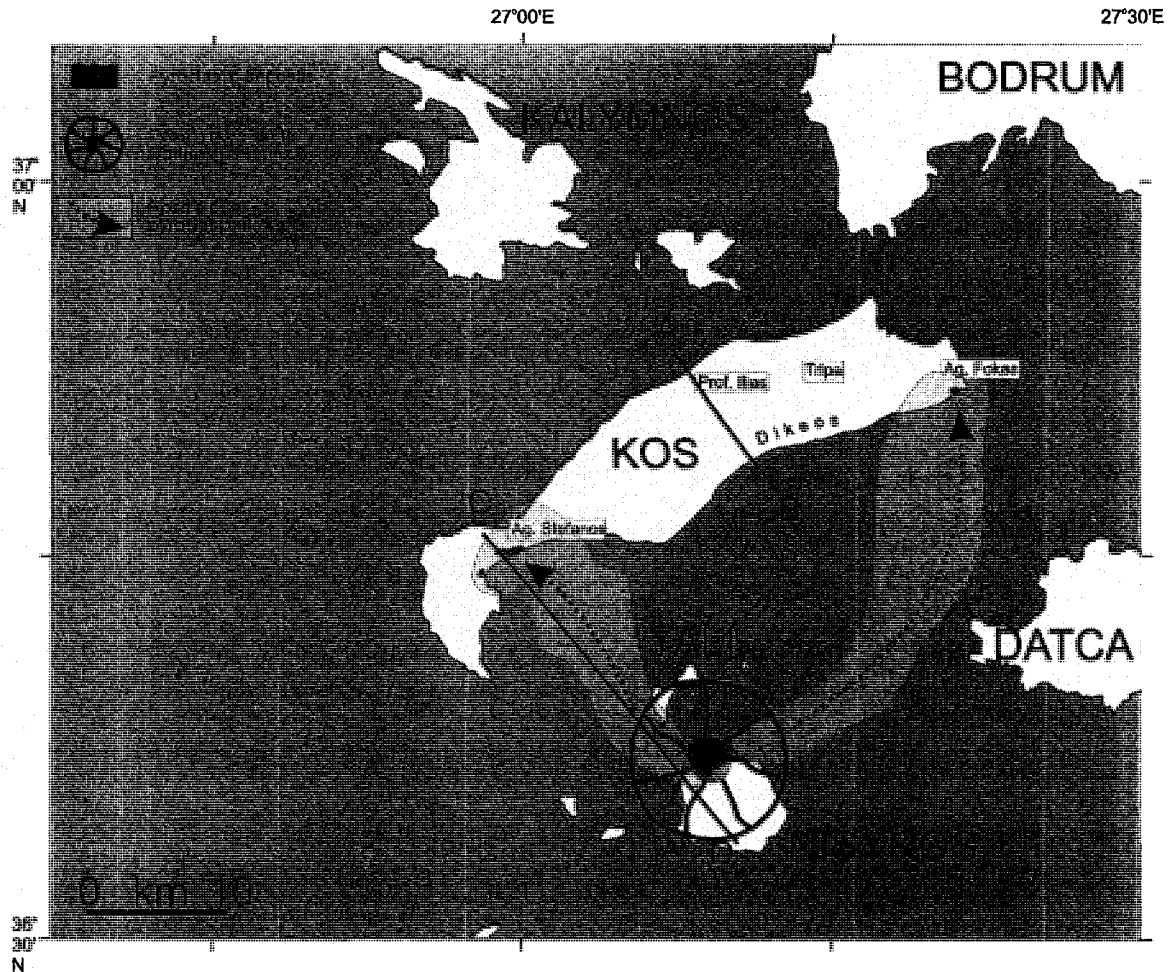


**Fig. 6.2:** Map that shows the possible source volcano for the Miocene pyroclastic rocks of Ag. Stefanos and Ag. Fokas. The cross sections along A – B and C – D are shown in Fig. 6.3.

The Miocene volcanic centre of proto-Nisyros volcano had trachyandesitic composition with back-arc character (Pe-Piper & Piper, 2002), which in the Quaternary had transformed to a subduction-related volcano. This indicates that the magma pathway remained energetic for long period, even when the geodynamic setting of the area changed, keeping the volcano active for more than 10 Ma. Analogous examples are widespread in the Aegean Sea such as in Patmos (back-arc to alkaline through perhaps 4

Ma) (Wyers & Barton, 1986), in Lesbos (calc-alkaline to shoshonitic, 5 Ma) (Pe-Piper & Piper, 1992), and in Samothraki (10 Ma) (Pe-Piper & Piper, 2002).

## **6.4 Conclusions**

Miocene volcanic rocks on Kos were recognized in four localities. In northern Kos, thin andesite flows and dacite domes are overlain by thin pyroclastic rocks near Prof. Ilias and at Tripa. In southern Kos and particularly in Ag. Stefanos, the lowest volcanic rocks are volcanoclastic conglomerates, overlain by an ignimbrite rich in limestone clasts. This is overlain by 50-60 m of marls and clastic sediments, a 10-20 m thick ignimbrite succession, a further 80 m of marls and clastic sediments, and finally 60 m of ignimbrite. In the southeast, the Ag. Fokas succession is made up of 80 m of pyroclastic rocks, which overlie thin airfall tuff over marls, sandstones and conglomerates. The pyroclastic stratigraphy is interrupted by two thin intervals of sediment, one marl and the other sandstone. At North of Ag. Fokas, a thin pyroclastic succession includes lahars and rests directly on the basement.

Geochemically, the majority of the lithic clasts of the Miocene volcanic rocks on Kos correspond to trachyandesites, whereas the lavas from Prof. Ilias and Tripa are basaltic trachyandesites to rhyolites. The geochemical characteristics of the lithic clasts do not provide a good means of discriminating between petrographical types. They show some geochemical features similar to trachytic rocks of Samos and Patmos, but the lithic clasts from Kos more closely resemble the volcanic rocks of Kos than those of any other Upper Miocene volcanic centre of the southeastern Aegean.

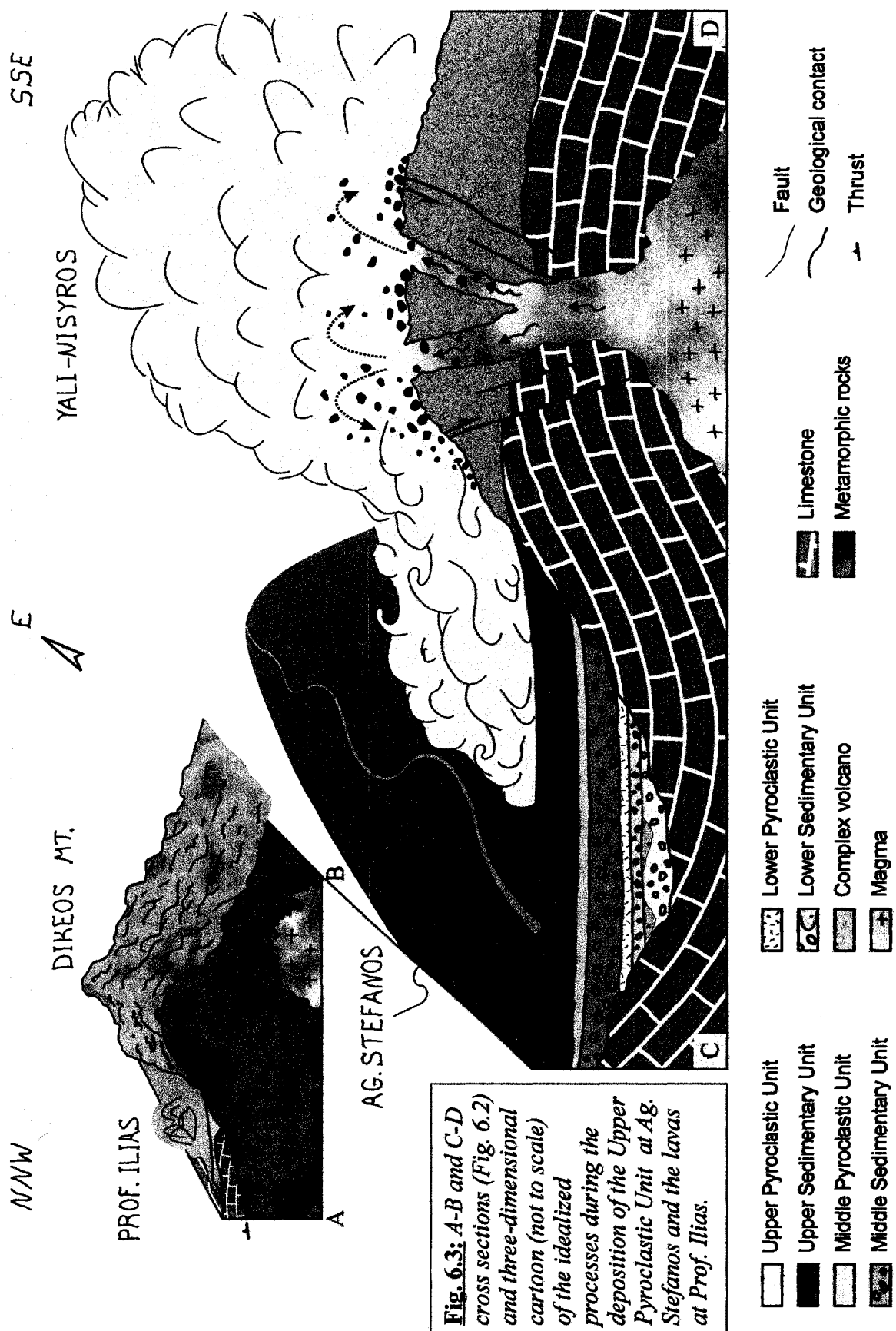
Paleocurrent indicators based on the orientation of elongated clasts on bedding planes, the imbrication of elongated clasts, and the direction of elutriation sheets and pipes, erosional grooves and slump folds in the pyroclastic rocks, suggest that the Ag. Stefanos section was derived from a source to the southeast and Ag. Fokas from a source to the south.

The geochemical features of the analysed lithic clasts, as well as the petrographical data from the pyroclastic rocks of Ag. Stefanos and Ag. Fokas, indicate affinity with regard to their origin. Moreover, these thick pyroclastic accumulations, in agreement with their coarse clast-size, suggest a relatively proximal volcano source. The volcanoes at Tripa and Prof. Ilias are close enough to be suitable candidates for the rocks, but although they have similar geochemical patterns as the tuffs at Ag. Stefanos and at Ag. Fokas, they do not seem to have the dynamics to produce such voluminous pyroclastic accumulations. Furthermore, the directional analysis in the pyroclastic rocks does not support an origin from these localities, but reversely, suggest derivation from the southeast for Ag. Stefanos and south for Ag. Fokas. It is unlikely that the Bodrum volcanic complex was the source of any of the Kos pyroclastic rocks since: (a) the thick pyroclastic successions are found on the south side of the Dikeos horst, a topographic barrier, (b) the paleoflow indicators are inconsistent with a Bodrum source, and (c) the clast size of the lithic and vitric clasts is coarser in Ag. Stefanos rather than in Ag. Fokas, which is nearer to Bodrum. The available data therefore suggest that the Ag. Stefanos and Ag. Fokas pyroclastic successions most probably originated from a Miocene precursor of the modern volcanic centre of Nisyros – Yali (Fig. 6.3).

The proto-Nisyros – Yali volcano was a back-arc trachyandesite volcano during the Miocene, which continued to be a magma pathway changing in the Quaternary to a subduction-related volcano. Thus, Nisyros was active for more than 10 Ma, providing extrusives with a magma supply that evolved overtime.

This is a field based study of the Miocene volcanic stratigraphy of Kos, which with the contribution of petrographical and geochemical analyses of the lava flows and the lithic clasts contained in the pyroclastic rocks, as well as the directional analysis of the pyroclastic flows, was able to bring out the Miocene precursor of the modern volcanic centre of Yali – Nisyros, and to reconstruct the geodynamic evolution of the area.

\* \* \*



SSE

YALI-MISYROS

E  
A

DIKEOS MT.

PROF. ILIAS

A

B

AG. STEFAMOS

C

D

**Fig. 6.3:** A-B and C-D cross sections (Fig. 6.2) and three-dimensional cartoon (not to scale) of the idealized processes during the deposition of the Upper Pyroclastic Unit at Ag. Stefanos and the lavas at Prof. Ilias.

- Upper Pyroclastic Unit
- Upper Sedimentary Unit
- Middle Pyroclastic Unit
- Middle Sedimentary Unit
- Lower Pyroclastic Unit
- Lower Sedimentary Unit
- Complex volcano
- Magma
- Limestone
- Metamorphic rocks
- Fault
- Geological contact
- Thrust

# References

- Allen, S.R. & McPhie, J. (2001). Syn-eruptive chaotic breccia on Kos, Greece, associated with an energetic pyroclastic flow. *Bull. Volcanol*, v. 63, 421-432.
- Allen, S.R. (2001). Reconstruction of a major caldera-forming eruption from pyroclastic deposit characteristics: Kos Plateau Tuff, eastern Aegean Sea. *J. Volcanol. Geotherm. Res.* v. 105, p. 141- 162.
- Allen, S.R. & Cas, R.A.F. (1998). Rhyolitic fallout and pyroclastic density current deposits from a phreatoplinian eruption in the eastern Aegean Sea. *J. Volcanol. Geotherm. Res.* v. 86, 219- 251.
- Allen, S.R. & Cas, R.A.F. (2001). Transport of pyroclastic flows across the sea during the explosive, rhyolitic eruption of the Kos Plateau Tuff, Greece. *Bull. Volcanol.* v. 62, p. 441-456.
- Allen, S.R., Stadlbauer, E. & Keller, J. (1999). Stratigraphy of the Kos Plateau Tuff: product of a major Quaternary rhyolitic eruption in the eastern Aegean, Greece. *International Journal of Earth Sciences*, v. 88, p. 132-156.
- Altherr, R. & Siebel, W. (2002). I-type plutonism in a continental back-arc setting: Miocene granitoids and monzonites from the central Aegean Sea, Greece. *Contrib. Mineral Petrol.* v. 143, p. 397-415.

- Altherr, R. (1972). Die Kontaktmetamorphose des Dicheo-Intrusivkörpers auf Insel Ko, Griechenland: Metapelitische und metabasische Paragenesen. *Dipl. Arb. Miner. Inst. Freiburg*, 85 S.
- Altherr, R., Keller, J. & Kott, K. (1976). Der jungtertiäre Monzonit von Kos und sein Kontakthof (Ägäis, Griechenland). *Bull. Soc. Géol. France*, v. XVIII/2, p. 403-412.
- Altherr, R., Kreuzer, H., Wendt, I., Lenz, H., Wagner, G. A., Keller, J., Harre, W. & Hohndorf, A. (1982). A Late Oligocene/Early Miocene High Temperature Belt in the Attic-Cycladic Crystalline Complex (SE Pelagonian, Greece). *Geologisches Jahrbuch*, E23, p. 97-164.
- Anastasakis, G. & Pe-Piper, G. (2006). An 18 m thick volcanoclastic bed in Pantelleria Trough, Sicily Channel, deposited from a mega-gravitational flow during the Green Tuff eruption. *Marine Geology*, v. 231, p. 391-403.
- Bellon, H. & Jarrige, J. J. (1979). Le magmatisme néogène et quaternaire de l'île de Kos (Grèce): données géochronologiques. *C.R. Acad. Sci. Paris, D*, v. 228, p. 1359-1362.
- Besang, C., Eckhardt, F.J., Harre, W., Kreuzer, G. & Müller, P. (1977). Radiometrische Altersbestimmungen an neogenen Eruptivgesteinen der Türkei. *Geol. Jb.*, v. 25, p. 3-36.
- Besenecker, H. & Otte, O. (1978). Late Cenozoic sedimentary history and paleogeography of Kos, Aegean Sea. Proceedings of VIth Colloquium on the Geology of the Aegean Region, v.1, p. 451-457.

- Bignot, G. & Guernet, C. (1976). Sur la présence de *Borelis curdica* (Reichel) dans le Miocène de l'île de Kos (Grèce). *Géologie méditerranéenne*, v. 3, p. 15-26.
- Blondeau, A., Fleury, J.J. & Guernet, C. (1975). Sur l'existence, dans l'île de Kos (Dodécanèse, Grèce), d'une série néritique surmontée d'un flysch d'âge Cuisien supérieur ou Lutétien inférieur à sa base. *Comptes Rendus de l'Académie des Sciences*, v. 280. p. 817-819.
- Böger, H. (1978). Sedimentary History and Tectonic Movements during the Late Neogene. – in Closs et al. (Edit.), Alps, Apennines, Hellenides. *I.U.C.G. Sc. Rept.* v. 38, p. 510–512, Stuttgart.
- Böger, H., Gersonde, R. & Willmann, R. (1974). Das Neogen in Osten der Insel Kos (Ägäis, Dodekanes) – Stratigraphie und Tektonik. *N. Jb. Geol. Paläontol. Abh.* v. 145, p. 129-152.
- Borsi, S., Ferrara, G., Innocenti, F. & Mazzuoli, R. (1972). Geochronology and petrology of recent volcanics in the eastern Aegean Sea (West Anatolia and Lesbos Island). *Bull. Volcanol.* v. 36, p. 473–496.
- Branney, M.J. & Kokelaar, P. (2002). *Pyroclastic Density Currents and the Sedimentation of Ignimbrites*. Geol. Soc., London, Memoir, v. 27. p. 143.
- Dalabakis, P. & Vougioukalakis, G. (1993). The Kefalos Tuff Ring (W. Kos): Depositional Mechanisms, Vent Position and Model of the Evolution of the Eruptive Activity. *Bull. Geol. Soc. Greece*. vol. XXVIII/2, p. 259-273.
- Druitt, T.H., Edwards, L., Mellors, R.M., Pyle, D.M., Sparks, R.S.J., Lanphere, M., Davis, M. & Barriero, B. (1999). *Santorini Volcano*. Geol. Soc., London, Memoir, v. 19. p.165.

- Eleftheriadis, G., Pe-Piper, G., Christofides, G., Soldatos, T. & Esson, J. (1994). K-Ar dating of the Samothraki volcanic rocks, Thrace, northeastern Aegean (Greece). *Bulletin of the Geological Society of Greece*. v. 30/1, p. 205-212.
- Elston, W.E. & Smith, E.I. (1970). Determination of flow direction from rhyolitic ash-flow tuffs from fluidal textures. *Bulletin of the Geological Society of America*, v. 81, p. 3393-3406.
- Fytikas, M., Innocenti, F., Manetti, P., Mazzuoli, R., Peccerillo, A. & Villari L. (1984). Tertiary to Quaternary evolution of volcanism in the Aegean region. *Geol. Soc. London, Special Publication*, v.17, p. 687-699.
- Fytikas, M.D., Giuliani, O., Innocenti, F., Marinelli, G. & Mazzuoli, R. (1976). Geochronological data on recent magmatism of the Aegean Sea. *Tectonophysics*, v. 31, p. 29-34.
- Gralla, P. (1982). Das Präneogen der Insel Kos (Dodekanes, Griechenland). Ph.D. Thesis, University of Braunschweig, 182 pp.
- Hart, K., Carey, S., Sigurdsson, H., Sparks, R.S.J., & Robertson, R.E.A. (2004). Discharge of pyroclastic flows into the sea during the 1996-1998 eruptions of the Soufriere Hills volcano, Montserrat, *Bulletin of Volcanology*, v. 66, p. 599-614.
- Innocenti, F., Manetti, O., Mazzuoli, R., Pertusati, P., Fytikas, M. & Kolios, N. (1994). The geology and geodynamic significance of the island of Limnos, North Aegean Sea, Greece. *N. Jb. Geol. Paläont. Mh.* v. 11, p. 661-691.

- Kim, S.B., Chough, S.K., & Chun, S.S., 1995. Bouldery deposits in the lowermost part of the Cretaceous Kyokpori Formation, SW Korea: cohesionless debris flows and debris falls on a steep-gradient delta slope. *Sedimentary Geology*, v. 98, 97-119.
- Klein, C. (1989). *Minerals and Rocks: Exercises in Crystallography, Mineralogy, and Hand Specimen Petrology*. John Wiley and Sons, Toronto, 405 pages.
- Maeno, F. & Taniguchi, H. (2006). Silicic lava dome growth in the 1934-1935 Showa Iwo-jima eruption, Kikai caldera, south of Kyushu, Japan. *Bull. of Volcanol.*, v. 68, p. 673-688.
- Mariolakos, I., Fountoulis, I., & Kranis, H. (2001). Geology and Tectonics: Sterea Hellas area. *Engineering Geology and the Environment*, Marinos, Koukis, Tsiambaos & Stournaras (Eds.) 2001 Swets & Zeitinger, Lisse, ISBN 90 5410 8827, p. 3971-3986.
- Montigny, R. & Robert, U. (1991).  $^{39}\text{Ar}$ - $^{40}\text{Ar}$  dating igneous rocks from the Bodrum volcanic complex (SW Turkey). *Terra Abstract* 3, p. 500.
- Pe-Piper, G. (1980). The Cenozoic Volcanic Sequence of Lesbos, Greece. *Z. dt. geol. Ges.* v. 131, p. 889-901.
- Pe-Piper, G. (2000). Origin of S-type granites coeval with I-type granites in the Hellenic subduction system, Miocene of Naxos, Greece. *Eur. J. Mineral.* v. 12, p. 859-875.
- Pe-Piper, G. & Moulton, B. (Submitted). Magma evolution in the Plio-Pleistocene succession of Kos (South Aegean Arc), Greece. *Lithos*.

- Pe-Piper, G. & Piper, D.J.W. (1993). Revised stratigraphy of the Miocene volcanic rocks of Lesbos, Greece. *Neues Jahrbuch für Geologie und Paläontologie Monatshefte*. v. 2, p. 97–110.
- Pe-Piper, G. & Piper, D.J.W. (2007). Upper-Miocene igneous rocks of Samos: the role of tectonism in petrogenesis in the southeastern Aegean. *Geological Society of London, Special Publication*. v. 291, p. 75-97.
- Pe-Piper, G. & Piper, D.J.W., 2002: *The Igneous rocks of Greece: the anatomy of an orogen*. Gebrüder Borntraeger, Stuttgart, 573 p.
- Pe-Piper, G., Piper, D.J.W., Koukouvelas, I., Dolansky, L.M. & Kokkalas, S. (In Press). The Miocene volcanic rocks of Limnos, Greece: origin of shoshonitic rocks from dehydration melting of metadiorite underplating continental crust. *Geological Society of America Bulletin*.
- Pe-Piper, G., Piper, D.J.W. & Perissoratis, C. (2004). Neotectonics and the Kos Plateau Tuff eruption of 161 ka, South Aegean arc. *Journal of Volcanology and Geothermal Research*. v. 139, p. 315-338.
- Robert, U., Foden, J. & Varne, R. 1992. The Dodecanese Province, SE Aegean: a model for tectonic control on potassic magmatism. *Lithos*. v. 28. p. 241-260.
- Robert, U. & Cantagrel, J. M., (1979). Le volcanisme basaltique dans le Sud-Est de la Mer Egée. Données géochronologiques et relations avec la tectonique. Proc. VI Conf. Geol. Aegean Region, Athens, v. 3, p. 961-967.
- Robert, U., Foden, J. & Varne, R. (1992). The Dodecanese Province, SE Aegean: a model for tectonic control on potassic magmatism. *Lithos*, v. 28, p. 241-260.

- St. Seymour, K. & Vlassopoulos, D. (1989). The potential for future explosive volcanism associated with dome growth at Nisyros, Aegean volcanic arc, Greece, *Journal of Volcanology and Geothermal Research*, v. 37, p. 351–364.
- Triantaphyllis, M. (1994). Western Kos Sheet (Kefalos), 1:50,000 geological map. IGME, Athens.
- Triantaphyllis, M. (1998). Eastern Kos Sheet, 1:50,000 geological map. IGME, Athens.
- Ulusoy, I., Cubukcu, E., Aydar, E., Labazuy, P., Gourgaud, A. & Vincent, P. M. (2004). Volcanic and deformation history of the Bodrum resurgent caldera system southwestern Turkey). *Journal of Volcanology and Geothermal Research*, v. 136, iss. 1-2, p. 71-96.
- Van Hinsbergen, D.J.J., Langereis, C.G., & Meulenkaamp, J.E. (2005). Revision of the timing, magnitude and distribution of Neogene rotations in the western Aegean region. *Tectonophysics*, v. 396, p. 1-34.
- Vanderkluyzen, L., Volentik, A., Hernandez, J., Hunzicker, J.C., Bussy, F. & Principe, C. (2005). The petrology and geochemistry of lavas and tephras of Nisyros Volcano (Greece). *Memoires de Géologie (Lausanne)*, no 44, p. 79-99.
- Willmann, R. (1983). Neogen und juntertiären Entwicklung de Insel Kos (Ägäis, Griechenland). *Geologische Rundschau*, v. 72, p. 815-860.
- Wimmenauer, W. (1977). Lamprophyres and associated rocks in the dyke suite of the Dikeos monzonite, Kos (Greece). *Ann. geol. Pays hellen.* XXVIII, p. 427-435.
- Wyers, G.P. & Barton, M. (1986). Petrology and evolution of transitional alkaline-subalkaline lavas from Patmos, Dodecanesos, Greece: evidence for fractional

crystallization, magma mixing and assimilation. *Contributions to Mineralogy and Petrology*, v. 93, p. 297–311.